

**The RNA-binding protein and tumour marker IMP3:
Functional analysis and development of therapeutic
circular RNA sponges**

Dissertation

vorgelegt von

Corinna Jessica Ulshöfer

(M. Sc. Biochemie)

Zur Erlangung des akademischen Grades

doctor rerum naturalium

(Dr. rer. nat.)

Institut für Biochemie, Fachbereich 08 Biologie und Chemie
Justus-Liebig-Universität Gießen

Gießen, November 2021

Die vorliegende Arbeit wurde am Institut für Biochemie des Fachbereichs 08 der Justus-Liebig-Universität Gießen in der Zeit von September 2017 bis November 2021 unter der Leitung von Prof. Dr. Albrecht Bindereif angefertigt.

Dekan:

Prof. Dr. Thomas Wilke

Institut für Tierökologie und spezielle Ökologie

Fachbereich für Biologie und Chemie

Justus-Liebig-Universität Gießen

1. Gutachter:

Prof. Dr. Albrecht Bindereif

Institut für Biochemie

Fachbereich für Biologie und Chemie

Justus-Liebig-Universität Gießen

2. Gutachter:

Prof. Dr. Elena Evguenieva-Hackenberg

Institut für Mikro- und Molekularbiologie

Fachbereich für Biologie und Chemie

Justus-Liebig-Universität Gießen

Table of contents

Table of contents	i
Abstract	v
Zusammenfassung	vi
1 Introduction	1
1.1 IMP3, a classical multidomain RNA-binding protein and tumour marker	1
1.1.1 RNA-binding proteins	1
1.1.2 The IMP family	2
1.1.3 RNA-binding preferences	3
1.1.4 Biological functions	7
1.1.5 Function of IMP3 in cancer	11
1.2 ER targeting – secretory pathway and the role of RBPs	13
1.3 Circular RNAs – a novel class of noncoding RNAs	16
1.3.1 Discovery and history	16
1.3.2 Biogenesis and function	18
1.3.3 Interactions with proteins and microRNAs	20
1.3.4 Methods of circRNA synthesis and expression	22
1.3.5 Design and application of circRNAs in molecular medicine	25
1.4 Aims of this work	26
2 Material	28
2.1 Bacterial and eukaryotic cells	28
2.2 Antibodies	28
2.3 Enzymes	29
2.4 Plasmids	29
2.5 Oligonucleotides	30
2.6 Markers	35
2.7 Commercial kits	35

2.8	Chemicals and reagents	35
2.9	Laboratory equipment	37
2.10	Consumables.....	38
3	Methods.....	40
3.1	Cloning of DNA fragments into <i>E. coli</i>	40
3.1.1	Preparation of plasmid DNA	40
3.1.2	Enzymatic restriction digest.....	40
3.1.3	Agarose gel extraction	40
3.1.4	Ligation.....	40
3.1.5	Transformation.....	40
3.1.6	Screening and analysis of bacterial clones	40
3.2	Design and generation of constructs	41
3.2.1	<i>In vitro</i> circRNA sponge T7 templates.....	41
3.2.2	Design of IMP3 sponges for stable <i>in vivo</i> expression	41
3.2.3	Cloning of Tornado sponge constructs.....	42
3.2.4	Cloning of FLAG-IMP3 for transient expression in ES-2 cells	42
3.3	Eukaryotic cell culture methods.....	43
3.3.1	Cultivation	43
3.3.2	Transfection of cells with plasmid DNA	43
3.3.3	Transfection of cells with RNA	43
3.3.4	Generation of HeLa Flp-In T-REx stable cell lines	44
3.4	General RNA-related methods.....	45
3.4.1	Analysis by denaturing polyacrylamide gel electrophoresis	45
3.4.2	Isolation of cellular RNA	45
3.4.3	Quantification	46
3.4.4	Reverse transcription (RT)	46
3.4.5	PCR	46
3.4.6	Agarose gel electrophoresis	47

3.4.7	Quantitative PCR	47
3.4.8	RNase R digestion.....	47
3.5	RNA <i>in vitro</i> transcription and circularisation.....	48
3.5.1	Transcription of unlabelled RNA.....	48
3.5.2	Transcription of ³² P-labelled RNA.....	48
3.5.3	Purification of transcripts	48
3.5.4	CircRNA generation by ligation	48
3.5.5	CircRNA purification by gel extraction	48
3.6	General protein-related methods.....	49
3.6.1	SDS-PAGE	49
3.6.2	Coomassie staining.....	49
3.6.3	Western blot.....	49
3.6.4	Purification of recombinant IMP3	50
3.7	Subcellular fractionation of eukaryotic cells	51
3.7.1	Cytoplasm/nucleus fractionation of Tornado-transfected HeLa cells.....	51
3.7.2	Cytoplasm/membrane organelle fractionation of ES-2 cells	51
3.8	Electrophoretic mobility shift assay (EMSA).....	52
3.9	RNA immunoprecipitation (RIP).....	53
3.10	Library preparation for RNA-seq	54
3.11	Individual-nucleotide resolution crosslinking and immunoprecipitation (iCLIP) ..	54
3.12	Bioinformatic analyses of high-throughput sequencing data.....	61
4	Results.....	62
4.1	IMP3 circRNA sponges.....	62
4.1.1	IMP3 binds to circRNA sponges with high affinity <i>in vitro</i>	63
4.1.2	Stable expression of circRNA sponges <i>in vivo</i>	67
4.1.3	Transient expression of Tornado circRNA sponges	71
4.2	Function of IMP3 in RNA localisation	76
4.2.1	Establishment of the subcellular fractionation procedure	77

4.2.2	Combined analysis of RNA-seq and iCLIP data reveals target mRNAs	78
4.2.3	Experimental validation of target mRNAs	85
4.2.4	Functional analysis of IMP3 circRNA sponges on target mRNAs	90
5	Discussion	92
5.1	Designer circRNAs function as IMP3 sponges.....	92
5.1.1	<i>In vitro</i> interaction of IMP3 with circRNA sponges	92
5.1.2	<i>In vivo</i> sponging of IMP3	93
5.2	IMP3 functions in RNA localisation	96
5.2.1	RNA-seq and iCLIP experiments reveal a subset of target mRNAs.....	96
5.2.2	Biochemical validation of target mRNAs	98
5.2.3	Effect of circRNA sponges on target mRNA localisation.....	100
5.3	Future perspectives.....	103
6	References	104
7	Abbreviations	124
8	Eidesstattliche Erklärung	128

Abstract

RNA-binding proteins (RBPs) are involved in many cellular processes and thereby contribute to the regulation of gene expression. As a consequence, mutation or altered expression of RBPs can cause diseases such as cancer. Members of the insulin-like growth factor 2 mRNA binding protein (IMP, IGF2BP) family are recognised tumour markers as they are upregulated or *de novo* expressed in a variety of cancer types. They are known to regulate RNAs in terms of stability, translation and localisation. However, the overall picture of their biological function is still unclear. Developing strategies to inhibit these proteins could thus promote new anti-cancer therapies, but requires also a better understanding of the underlying biological functions.

This thesis focusses on the tumour marker and multidomain RBP IMP3. In a first step, IMP3 was targeted by designer circRNAs, which should functionally inhibit IMP3 by competing with endogenous RNA for its binding. Initial *in vitro* experiments revealed high binding affinities for IMP3 to circRNA sponges. To examine if this holds also true *in vivo*, two different circRNA expression systems were tested: circRNAs were either stably integrated into the genome and could be inducibly expressed, or circRNA expression was plasmid-driven and mediated by the so-called Tornado ribozyme system. Interactions of IMP3 with circRNAs were then captured *in vivo* by RNA-immunoprecipitation assays. This way, binding of our designer circRNAs could be confirmed in cell culture and represents a new strategy for inhibiting RBPs in the context of anti-cancer therapies.

Concerning the biological function of IMP3, we had preliminary evidence that it might operate in the secretory pathway. Thereby, mRNAs are guided to the endoplasmic reticulum (ER) for local translation, and the resulting protein is translocated into the ER lumen. To obtain more insight on a global transcriptome level, subcellular fractionation was combined with next-generation RNA-sequencing (RNA-seq) and individual-nucleotide resolution crosslinking and immunoprecipitation (iCLIP) in human ES-2 cells. We focussed on mRNAs with IMP3-dependent changes of gene expression levels in the membrane organelle fraction. A subset of direct mRNA targets was identified to be downregulated upon IMP3 knockdown. Biochemical validation by IMP3 RIP experiments and RT-qPCR of subcellular extracts confirmed our results and revealed certain mRNAs of the secretory pathway to be additionally regulated by IMP3. In a last step, the effect of our designer circRNA sponges on target mRNA localisation was tested. In sum, our results support a model in which IMP3 interactions with the mRNA 3'-UTR provide an additional localisation signal to direct specific mRNAs into the secretory pathway.

Zusammenfassung

RNA-Bindeproteine (RBPs) sind an vielen zellulären Prozessen beteiligt und tragen so zur Regulierung der Genexpression bei. Folglich können Mutationen oder die veränderte Expression von RBPs Krankheiten verursachen, wie beispielsweise Krebs. Mitglieder der *insulin-like growth factor 2 mRNA binding protein* (IMP, IGF2BP) Familie sind bekannte Tumormarker, da sie in einer Vielzahl an Krebsarten hochreguliert oder re-exprimiert werden. Sie regulieren RNAs in Bezug auf Stabilität, Translation und Lokalisation. Das Gesamtbild ihrer biologischen Funktion ist jedoch noch unklar. Die Entwicklung von Strategien zur Hemmung dieser Proteine könnte somit neue Krebstherapien fördern, erfordert aber auch ein besseres Verständnis der zugrundeliegenden biologischen Funktionen.

Die vorliegende Thesis fokussiert sich auf den Tumormarker und Multidomänen-RBP IMP3. Im ersten Schritt wurden „Designer“-circRNAs entwickelt, die durch zielgerichtete Bindung an IMP3 mit endogenen RNAs konkurrieren und so IMP3 funktionell hemmen sollten. Erste In-vitro-Experimente zeigten eine hohe IMP3-Bindungsaffinität zu den circRNAs. Um zu prüfen, ob dies auch *in vivo* zutrifft, wurden zwei verschiedene circRNA-Expressionssysteme getestet: circRNAs wurden entweder stabil ins Genom integriert und konnten induzierbar exprimiert werden, oder die circRNA-Expression war Plasmid-gesteuert und erfolgte durch das sogenannte Tornado-Ribozymsystem. Interaktionen von IMP3 mit circRNAs wurden dann *in vivo* durch RNA-Immunpräzipitation (RIP) Analysen erfasst. Auf diese Weise konnte die Bindung unserer „Designer“-circRNAs in Zellkultur bestätigt werden und stellt eine neue Strategie zur Inhibierung von RBPs im Rahmen von Krebstherapien dar.

Hinsichtlich der biologischen Funktionen von IMP3 hatten wir vorläufige Hinweise darauf, dass es im sekretorischen Weg agieren könnte. Dabei werden mRNAs zum endoplasmatischem Retikulum (ER) geführt und lokal translatiert, sodass das entstehende Protein direkt in das ER-Lumen transloziert wird. Um tiefere Einblicke auf globaler Transkriptomebene zu erhalten, wurde subzelluläre Fraktionierung mit Hochdurchsatz-RNA-Sequenzierung (RNA-seq) und *individual-nucleotide resolution crosslinking and immunoprecipitation* (iCLIP) in humanen ES-2 Zellen kombiniert. Wir konzentrierten uns auf mRNAs mit IMP3-abhängiger Veränderung des Genexpressionslevels in der Membranorganell-Fraktion. Eine Gruppe direkter Ziel-mRNAs wurde identifiziert, welche bei IMP3-*knockdown* herunterreguliert waren. Biochemische Validierung durch IMP3 RIP-Experimente und RT-qPCR mit subzellulären Extrakten bestätigten unsere Ergebnisse und zeigten, dass bestimmte mRNAs des sekretorischen Wegs zusätzlich durch IMP3 reguliert werden. Als letzter Schritt wurde der

Effekt unserer „Designer“-circRNAs auf die Lokalisation der Ziel-mRNAs getestet. Zusammenfassend unterstützen unsere Ergebnisse ein Modell, in dem IMP3-Interaktionen mit der mRNA 3'UTR ein zusätzliches Lokalisierungssignal darstellen, um spezifische mRNAs in den sekretorischen Weg zu leiten.

1 Introduction

1.1 IMP3, a classical multidomain RNA-binding protein and tumour marker

1.1.1 RNA-binding proteins

Gene expression needs to be carefully controlled in organisms to maintain functioning cells. This can be achieved through gene-specific transcription or post-transcriptional processes, the latter being largely mediated by RNA-binding proteins (RBPs). RBPs have been shown to regulate gene expression in a variety of contexts, such as splicing, nuclear export, cellular localisation, stability, translation and degradation. During the last decade, RNA-interactome capture studies have increased the number of human RBPs to about 800 (Baltz *et al.*, 2012; Castello *et al.*, 2012), while a bioinformatic approach even predicted around 1500 RBPs corresponding to 7.5% of the human proteome (Gerstberger *et al.*, 2014). In all three studies, hundreds of the found RBPs do not relate to the classical view of an RBP as they do not possess any common RNA-binding domains (RBDs). Further research will clarify how they engage with RNA and shed light on their biological functions (for more detailed information see Hentze *et al.*, 2018).

For the conventional RBPs, however, different well-defined RBDs explain their binding to RNA and the formation of ribonucleoprotein complexes (RNPs). While some of them bind to double-stranded RNA (dsRNA), most of them engage with single-stranded RNA (ssRNA). Examples for ssRNA-recognising RBDs are the RNA-recognition motif (RRM) and the hnRNP K homology (KH) domains. RRM domains comprise about 90 amino acids (aa) and recognise 2 – 8 nucleotides (nt), whereas the smaller KH domains bind to 4 nt with a so-called GxxG-loop (Cléry *et al.*, 2008; Valverde *et al.*, 2008). Specificity and affinity of RNA binding can be increased by combining multiple domains (Lunde *et al.*, 2007). However, this is not sufficient to explain selective binding to RNAs for all RBPs, since also intrinsically unstructured regions are enriched in RBPs and participate in RNA binding, but remain structurally enigmatic (Järvelin *et al.*, 2016). Overall, protein and RNA structure as well as dynamics of their interaction need to be understood to fully unravel the recognition process (Corley *et al.*, 2020).

Besides their natural functions, RBPs play an increasing role in molecular medicine. Mutations in RBP genes cause diverse disease phenotypes, which are predominantly related to metabolism and nervous system development (Corbett, 2018; Gebauer *et al.*, 2021; Ravanidis *et al.*, 2018). Furthermore, a variety of cancers involves mutated or altered expressed RBPs, e.g. Hu antigen

R (HuR), the insulin-like growth factor 2 mRNA-binding protein (IGF2BP, IMP) family or the RNA-binding motif (RBM) family (Mohibi *et al.*, 2019). Different therapeutic strategies are currently available to target RBPs with further potential new application methods such as circular RNAs (circRNAs) or CRISPR-based strategies (Mohibi *et al.*, 2019). Hence, research on RBPs is not only important to get insights into basic cell biological processes, but also to develop new pharmaceutical approaches to combat diseases.

1.1.2 The IMP family

The insulin-like growth factor 2 mRNA-binding proteins (IGF2BPs, IMPs) represent an RBP family consisting of three paralogues in mammals. The nomenclature of these proteins is rather inconsistent due to their discovery in different contexts. For example, the chicken orthologue of IMP1 is often referred to as ZBP1 (zipcode-binding protein 1), whereas IMP3 was first named KOC (KH domain containing protein overexpressed in cancer) and its frog orthologue is termed Vg1RBP or Vera (Vg1 RNA-binding protein or VgLE binding and ER association, respectively). An attempt was made to summarise all members (Vg1RBP/Vera, IMP1-3, CRD-BP, KOC, ZBP1) in the so-called VICKZ group based on the first letters of the founding members (Yaniv and Yisraeli, 2002), but practically this acronym is rarely used.

The IMP family is highly conserved across species with *Drosophila* IMP (dIMP) being atypical due to the lack of one RRM domain (Fig. 1.1A). All other main isoforms contain two RRM- and four KH-domains, clustered in tandems (Fig. 1.1B). In humans, the three paralogues possess a sequence identity of around 70%, with IMP1 and IMP3 being most similar.

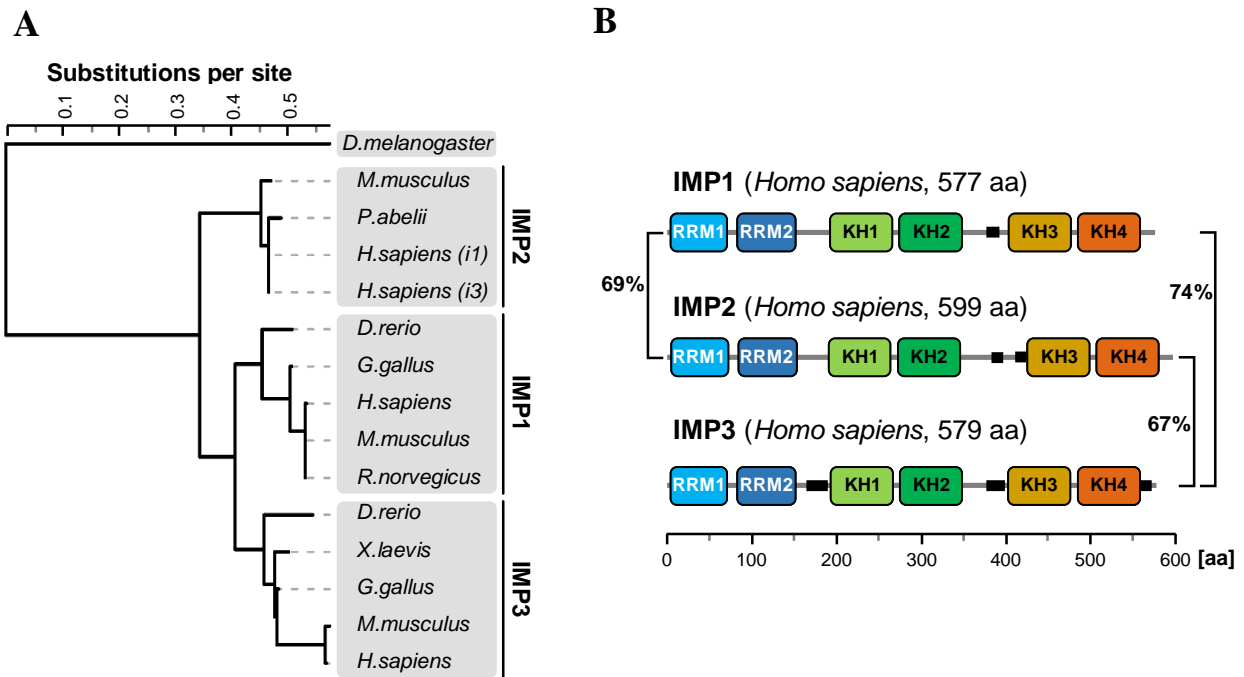


Figure 1.1: The IMP family of RNA-binding proteins.

(A) Phylogenetic tree of selected IMP paralogs from different species. Amino acid substitutions per site are indicated.

(B) Domain structure of human IMPs. The six RNA binding domains comprising two RRM (blue boxes) and four KH domains (green and orange boxes) are depicted for all three members. Black rectangles represent low-complexity regions. Sequence identities between paralogs are indicated.

Modified from Korn *et al.*, 2021.

All IMPs are highly expressed during embryogenesis, but expression declines after birth for IMP1 and IMP3 (Hammer *et al.*, 2005; Hansen *et al.*, 2004; Mori *et al.*, 2001; Mueller-Pillasch *et al.*, 1999; Nielsen *et al.*, 1999). IMP3 is expressed in brain, testis and ovaries of human adults, whereas human IMP1 expression occurs in adult kidney, prostate, testis and trachea (Hammer *et al.*, 2005). By contrast, IMP2 is widely expressed in adult tissues (Bell *et al.*, 2013; Dai *et al.*, 2011; Hammer *et al.*, 2005). Interestingly, IMP2 is also the only paralogue with considerable expression of different isoforms (in particular isoform 2, also known as p62 (Zhang *et al.*, 1999)), highlighting further its exclusive role in the IMP family. Nevertheless, all three IMPs have been associated with cancer and are classified tumour markers. In cancer tissues, IMP1 and IMP3 are strongly upregulated or *de novo* synthesised, leading to poor patient survival (reviewed in Bell *et al.*, 2013; Lederer *et al.*, 2014; Mancarella and Scotlandi, 2020).

1.1.3 RNA-binding preferences

Given the high sequence identity of the IMP proteins, one wonders how diverse their RNA-binding specificity might be. Indeed, overlapping pools of target RNAs have been found for all

IMPs, but also a large set of distinct RNA targets has been mapped to each paralogue (Conway *et al.*, 2016; Hafner *et al.*, 2010; Huang *et al.*, 2018). Of note, all proteins bind preferably to the 3' untranslated regions (UTRs) of protein-coding transcripts, but only IMP3 binds additionally to coding exons with a similar preference (Conway *et al.*, 2016). This in turn provokes the question if they recognise different RNA sequence motifs. Numerous efforts have been made to shed light on this, including studies with full-length proteins or single domains. For full-length IMPs, high-throughput *in vitro* approaches such as RNAcompete or RNA Bind-n-Seq have been applied (Conway *et al.*, 2016; Dominguez *et al.*, 2018; Ray *et al.*, 2013), but also *in vivo* methods such as crosslinking and immunoprecipitation (CLIP) (Ennajdaoui *et al.*, 2016; Hafner *et al.*, 2010; Hansen *et al.*, 2015; Huang *et al.*, 2018; Palanichamy *et al.*, 2016). Except for Huang *et al.* (2018), who found a common UGGAC motif for all three human IMPs, CA-rich binding motifs were reported from other studies, independent of the paralogue and the method used. This cannot explain the different RNA target groups and might be due to the averaged motifs obtained by all six RBDs. Hence, RNA binding of individual domains was studied employing scaffold-independent analysis (SIA) (Dagil *et al.*, 2019) or systematic evolution of ligands by exponential enrichment (SELEX) approaches (Biswas *et al.*, 2019; Farina *et al.*, 2003; Jia *et al.*, 2018; Munro *et al.*, 2006; Patel *et al.*, 2012; Schneider *et al.*, 2019). Most of these studies focused on the KH tandem domains, especially on KH3-4, since they have been regarded to be primarily responsible for RNA binding for a long time (Farina *et al.*, 2003; Nielsen *et al.*, 2002; Wächter *et al.*, 2013).

RNA recognition by KH3-4 seems to be conserved throughout the IMP family, as several studies found KH3 to interact with a CA-rich motif and KH4 to recognise a motif containing a central GG di-nucleotide (Biswas *et al.*, 2019; Nicastro *et al.*, 2017; Patel *et al.*, 2012; Schneider *et al.*, 2019). Both motifs have to be appropriately spaced (~ 9 – 25 nt) and their exact nucleotide composition differs dependent on the paralogue. For KH1-2, the RNA recognition seems to be similar, as IMP3 KH1 interacts like KH4 with a CGGCA motif and KH2 binds to a CA-rich sequence as KH3 does (Schneider *et al.*, 2019). In agreement, SIA experiments revealed IMP1 KH1 binding to a CNG motif (Dagil *et al.*, 2019). Last but not least, the RRM domains were also shown to be involved in RNA binding and a CA-rich consensus motif for IMP3 RRM1-2 could be determined (Schneider *et al.*, 2019), in line with the available crystal structure for IMP3 RRM1-2 in complex with ACAC or CCCC (Jia *et al.*, 2018). The structure showed also that only RRM1 binds to RNA, since the canonical RNA-binding site of RRM2 was sterically blocked (Jia *et al.*, 2018). It would be interesting to see how the RRM domains of the other two IMP paralogues function, but since the role of these domains in RNA binding was

controversially discussed in the past years and mostly considered irrelevant, their contribution was neglected (Chao *et al.*, 2010; Farina *et al.*, 2003; Git and Standart, 2002; Nielsen *et al.*, 2004; Wächter *et al.*, 2013). Furthermore, the roles of the linkers connecting the domains need to be examined in more detail. The short conserved linkers between two domains within a tandem are responsible for proper orientation of the domains and thereby contribute to RNA binding (Chao *et al.*, 2010; Patel *et al.*, 2012). However, the role of the long linkers connecting the tandem domains (i.e. between RRM2 and KH1, or KH2 and KH3) is less clear. This is partly due to their exclusion from structural studies, based on their high flexibility and low-complexity regions (see Fig. 1.1B). In addition, phosphorylation of residues in the long linkers was shown for different IMP paralogues to affect RNA binding (Dai *et al.*, 2011; Dai *et al.*, 2013; Git *et al.*, 2009; Hüttelmaier *et al.*, 2005).

To sum up, a full RNA-recognition code could be unravelled for IMP3, determined by previous work from our lab and supported by other studies cited above (Fig. 1.2). In addition, the RNA sequence motif was found in several endogenous target RNAs of IMP3 and biochemically validated (Schneider *et al.*, 2019).

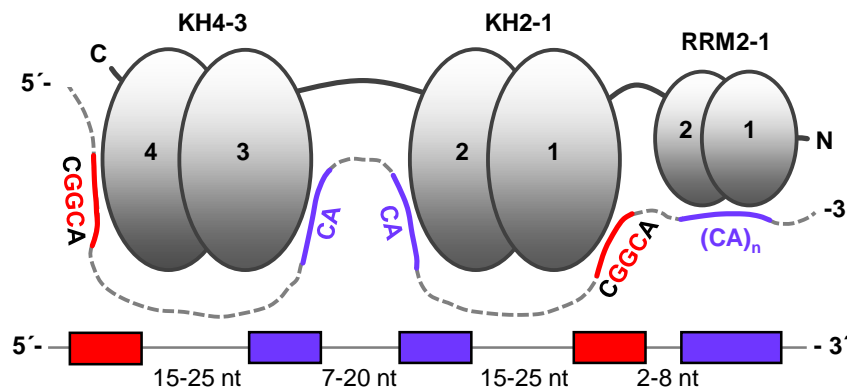


Figure 1.2: Model for RNA recognition by IMP3.

IMP3 is schematically depicted with its six RNA-binding domains (oval forms) organised in tandems. The RNA containing CA-rich (blue) or GGC-rich (red) sequences is bound by all domains; the spacing between motifs was derived from SELEX-seq analysis. Adapted from Schneider *et al.*, 2019.

Although detailed findings of RNA binding by the multidomain IMP proteins are available, a comprehensive picture and understanding is still missing of how they engage with RNA. For instance, the kinetics of the individual protein-RNA interactions are unclear. For IMP1, binding kinetics were examined for KH1-2 (Dagil *et al.*, 2019) and KH3-4 (Nicastro *et al.*, 2017). In both studies, the tandem domains were predicted to interact with the RNA with one KH domain first, followed by binding of the second KH domain, and thereby provoking RNA looping. This intramolecular binding was favoured over intermolecular binding to either another RNA

molecule, or of a second KH tandem domain to the same RNA. Moreover, it was suggested that the binding to RNA was dependent on the protein and not the RNA concentration, albeit the protein being present in excess. Despite the overall similar affinities for both KH tandems to their respective RNA elements, the kinetics were profoundly different, since KH1-2 displayed a fast complex formation, whereas KH3-4 showed a slower complex dissociation (Dagil *et al.*, 2019; Nicastro *et al.*, 2017). However, since both tandem KH domains were not examined together and the contribution of the RRM domains is also unclear, only speculations of how the full-length proteins finally engage with RNA can be made. In addition, the structure of the protein-RNA complex remains elusive. Taking only the protein structure into account, several possibilities of a complex formation exist (Fig. 1.3). In these models, the RNA loops around the tandem domains as has been described in studies examining single domains (Chao *et al.*, 2010; Dagil *et al.*, 2019; Nicastro *et al.*, 2017; Patel *et al.*, 2012; Schneider *et al.*, 2019).

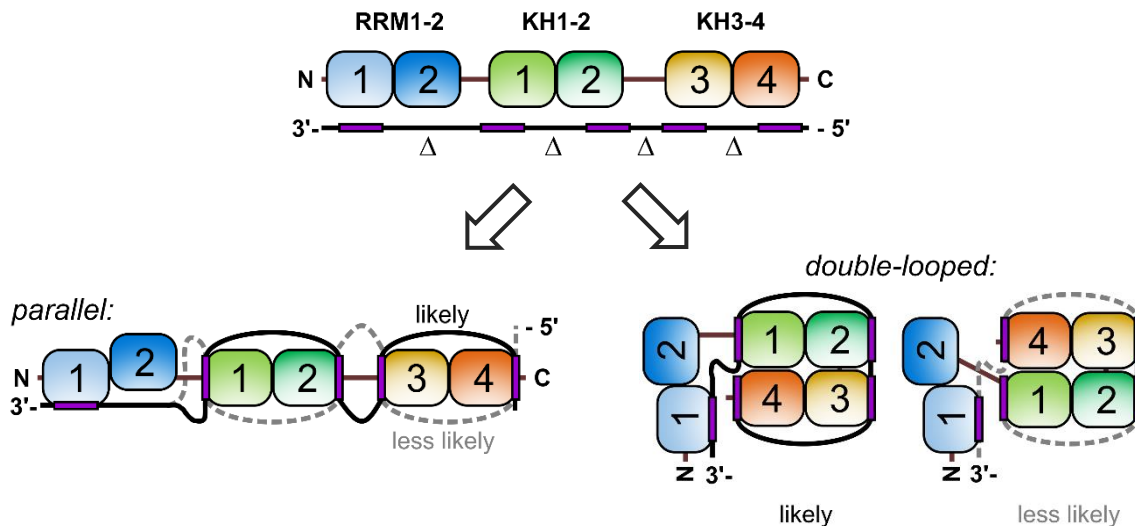


Figure 1.3: Model of IMP-RNA complex formation.

Binding of an IMP protein to RNA (black) is mediated by recognition of five short ssRNA motifs (purple) being appropriately spaced (Δ) with five of its six RBDs. The complex can be assembled in a simple parallel fashion (left) or in a compact, double-looped formation (right). Either way, the RNA loops around the KH tandem domains in two possible orientations (“likely” and “less likely”). Modified from Korn *et al.*, 2021.

The model gets significantly more complex if the RNA structure or the contribution of other RNA-binding proteins is taken into account. Based on their RNA sequence preferences, binding of IMPs to ssRNA regions, as e.g. present in loops or bulges, is expected. This requires a certain accessibility of motifs within structured RNAs, which is especially important considering their preference towards (often highly structured) 3' UTRs within target messenger RNAs (mRNAs) (Hafner *et al.*, 2010; Huang *et al.*, 2018). Furthermore, RNA modifications might influence IMP binding as it was recently reported for N⁶-methyladenosine (m⁶A)-modified RNAs (Chen

et al., 2019; Hu *et al.*, 2020; Huang *et al.*, 2018; Li *et al.*, 2019b; Müller *et al.*, 2019). Whether this is truly a direct binding or indirect interaction via other RBPs is not fully resolved. In the case of a direct binding, the interaction might not rely on the RNA modification itself, but rather on the local unfolding of RNA secondary structure induced by this modification, leading to accessible target motifs (Sun *et al.*, 2019).

In conclusion, much information regarding RNA-binding preferences has been assembled, especially during the past decade and mostly on isolated individual RBDs, but we are still missing the overall picture of how multidomain-IMP/RNA complexes are formed.

1.1.4 Biological functions

The classification as RNA-binding proteins already suggests that the IMP family is involved in post-transcriptional gene regulation. Indeed, they have been shown to regulate gene expression in terms of RNA localisation, stability and translation. IMPs are mainly present in the cytoplasm in the form of stable RNP granules (200 – 800 nm size) with a preference for lamellipodia and/or the perinuclear region, depending on the cell type (Eliscovich *et al.*, 2017; Jøanson *et al.*, 2007; Mateu-Regué *et al.*, 2019; Nielsen *et al.*, 1999; Oleynikov and Singer, 2003; Fig. 1.4).

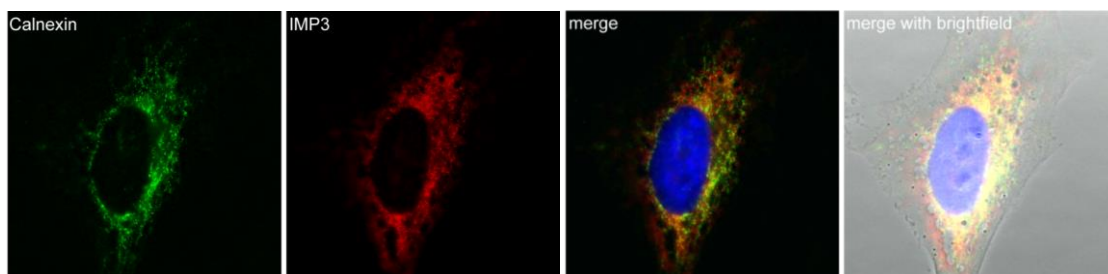


Figure 1.4: IMP3 localises in the perinuclear region.

HeLa cells were fixed and stained by immunofluorescence-coupled antibodies targeting the endoplasmic reticulum (ER) resident protein calnexin (green, left) or IMP3 (red, middle). The nucleus was visualised by staining with DAPI (blue). IMP3 is located in the cytoplasm with a preference for the perinuclear region and strongly overlaps with the ER (see merge). With permission of Dr. Christian Preußner and Silke Schreiner.

The by far best studied paralogue is IMP1 and its chicken orthologue ZBP1. ZBP1 was named after its ability to bind to the conserved zipcode motif within the 3'UTR of β -actin (*ACTB*) mRNA (Ross *et al.*, 1997). Together with the cytoskeleton, ZBP1 regulates the localisation of *ACTB* mRNA to the periphery in cells, thereby permitting localised translation of the mRNA and thus controlling cell migration (Farina *et al.*, 2003; Hüttelmaier *et al.*, 2005; Oleynikov and Singer, 2003). ZBP1/IMP1 has also been found to similarly regulate other RNAs as e.g. *TAU*

mRNA localisation and translation by binding to its 3'UTR (Atlas *et al.*, 2004; Atlas *et al.*, 2007) as well as localisation of the non-coding RNAs *H19* (Runge *et al.*, 2000) and *Y3* (Köhn *et al.*, 2010; Sim *et al.*, 2012). In line, dIMP controls localised expression of *gurken* and *oskar* mRNA together with other proteins during *Drosophila* oogenesis (Geng and Macdonald, 2006; Munro *et al.*, 2006). Apart from ZBP1 and β -actin mRNA, another well-studied example of mRNA localisation regulation concerns the IMP3 orthologue Vg1RBP/Vera in *Xenopus laevis* together with its target mRNA *Vg1*. Vg1RBP binds to a distinct region in the 3'UTR of *Vg1* (Deshler *et al.*, 1997; Deshler *et al.*, 1998; Kwon *et al.*, 2002). During mid and late oogenesis, Vg1RBP co-localises with *Vg1* mRNA to the vegetal ER subcompartment in a microtubule-dependent process (Chang *et al.*, 2004; Havin *et al.*, 1998; Kloc and Etkin, 1998). Injection of antibodies targeting Vg1RBP led to partial inhibition of *Vg1* localisation (Kwon *et al.*, 2002), supporting the role of Vg1RBP in *Vg1* regulation. Furthermore, release of *Vg1* mRNA from the vegetal cortex correlates with phosphorylation of a serine residue between KH2 and KH3 of Vg1RBP, with a proposed involvement of other mRNP components (Git *et al.*, 2009). The transport of translationally repressed *Vg1* mRNA by Vg1RBP and its release through phosphorylation of Vg1RBP with subsequent local translation in *Xenopus* follows the same principle as observed for chicken ZBP1 and β -actin mRNA. Possible differences include the involvement of the ER, since this has not been examined for ZBP1, although IMP1-containing RNP granules were reported to contain mRNAs encoding proteins of ER-associated quality control and the secretory pathway (Jøanson *et al.*, 2007). In addition, the initial engagement of IMP and its target RNA was described differently, since ZBP1 was proposed to already bind to the mRNA co-transcriptionally in the nucleus (Hüttelmaier *et al.*, 2005; Oleynikov and Singer, 2003). However, this is controversially discussed, and recent evidence suggests formation of mRNPs outside of the nucleus at the nuclear pore (Mateu-Regué *et al.*, 2019), in agreement with the enrichment of IMPs in the perinuclear region. Last but not least, how IMP-RNA complexes are transported within the cytoplasm is not fully elucidated as evidence for both actin-directed and microtubule-mediated localisation exist (Oleynikov and Singer, 2003; Song *et al.*, 2015; Taniuchi *et al.*, 2014b). Nevertheless, regulation of RNA localisation has been established as a common functional feature of the IMP family.

Another prominent role of the IMP family is their functioning in RNA stability. In human cells, transient knockdown of IMP1 and IMP3 was shown to decrease one of the transcripts of *CD44*, which is necessary for invadopodia formation (Vikesaa *et al.*, 2006). IMP proteins bind to multiple sites of the long 3'UTR of this transcript isoform and thereby enhance its stability, as demonstrated by a decreased half-life upon IMP1/3 knockdown and increased CD44 protein,

but not mRNA levels, upon IMP3 overexpression (Vikesaa *et al.*, 2006; Hu *et al.*, 2014). An additional well-studied example is the regulation of *MYC* mRNA. Here, IMPs bind to a sequence in the 3' terminus of the open reading frame, the so-called coding region stability determinant (CRD) (Bernstein *et al.*, 1992; Huang *et al.*, 2018). For IMP1 it was shown that the stability of *MYC* is enhanced through association with other distinct RBPs in IMP1-containing mRNP granules, thereby protecting the transcript from endonucleolytic attack at the CRD until constant translation occurs (Lemm and Ross, 2002; Sparanese and Lee, 2007; Weidensdorfer *et al.*, 2009). Recent studies suggest that m⁶A-modification of *MYC* as well as (de)phosphorylation of IMP1 fine-tune the regulation of *MYC* translation (Huang *et al.*, 2018; Lambrianidou *et al.*, 2021). Also other IMP family members, namely IMP2, IMP3 or dIMP, increase *MYC*'s half-life (Huang *et al.*, 2018; Samuels *et al.*, 2020), but biochemical details of this effect are not known. For the human IMPs, this was observed when they were overexpressed in HeLa cells stressed by heat shock (Huang *et al.*, 2018). The stabilisation of target mRNAs under different stress conditions (e.g. osmotic stress, oxidative stress or heat shock) is a common feature of the IMPs and the proteins are present in stress granules by associating with stress granule-associated protein markers (Huang *et al.*, 2018; Stöhr *et al.*, 2006; Stöhr *et al.*, 2012; Taniuchi *et al.*, 2014a; Wächter *et al.*, 2013; Zeng *et al.*, 2020). Nevertheless, this mRNA protection seems not to rely on the formation of stress granules, but alone on the IMP protein within small mRNP granules (Bley *et al.*, 2015). The described mRNA protection is therefore often referred to as stable “caging” of the mRNA. Similarly, IMP target mRNAs were shown to be stabilised by protecting them from microRNA-mediated decay. In this so-called “safe-housing” mechanism, e.g. the *HMG2* transcript is bound in its 3'UTR by an IMP protein, thereby making microRNA (miRNA) binding sites inaccessible (Busch *et al.*, 2016; Jønson *et al.*, 2014; Degrauwe *et al.*, 2016a; Schneider *et al.*, 2019). In conclusion, there are different ways how IMPs stabilise their target mRNAs.

Last but not least, the third most prominent role of IMPs is their influence on mRNA translation. IMPs were first identified as translational regulators of *IGF2* (insulin-like growth factor 2) and hence named after it (Nielsen *et al.*, 1999). They modulate *IGF2* expression by binding to the 5'UTR of one of the *IGF2* transcript isoforms. While IMP1 was first found to repress translation of *IGF2* (Nielsen *et al.*, 1999), more recent evidence suggests a promotion of *IGF2* translation in line with the reported enhancement of *IGF2* translation by IMP2 and IMP3 (Dai *et al.*, 2011; Dai *et al.*, 2013; Liao *et al.*, 2005). This function depends on phosphorylation in the linker connecting RRM2 and KH1 domains of the IMPs (Fig. 1.5) and is mediated by the mTOR (mammalian target of rapamycin) protein kinase complexes (Dai *et al.*, 2011; Dai *et al.*, 2013).

Since IGF2 promotes cellular growth, its regulation is crucial also in regard to tumour development (see section 1.1.5).

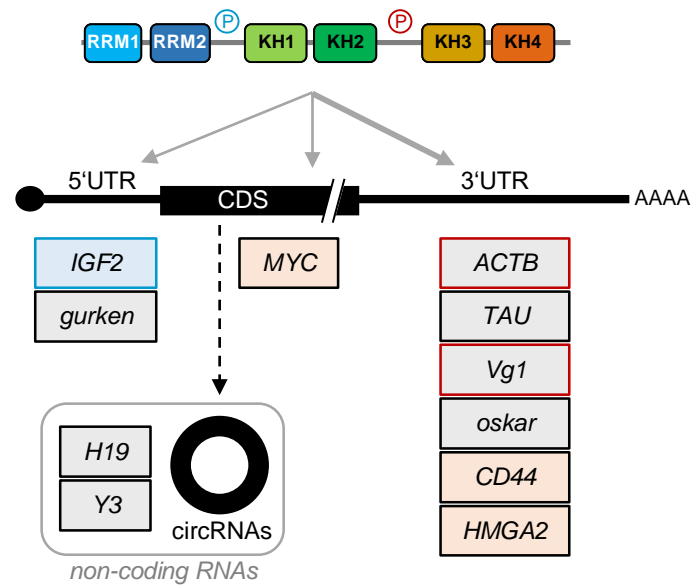


Figure 1.5: Function of IMP binding to target RNAs.

IMP proteins consisting of six RBDs bind to mRNAs (black) or non-coding RNAs (grey box). Capped (black circle) and polyadenylated mRNAs are bound by IMPs in their 5'UTR, coding sequence (CDS) or 3'UTR. Example mRNAs for each region are listed below and explained in the main text. Colour indicates functional regulation in terms of RNA translation (blue), stability (orange) or localisation (grey). For some RNA targets, functions are coupled (see main text). Phosphorylation of IMPs in linker regions has been reported to influence binding to *IGF2* (blue) or *ACTB/Vg1* (red). Binding to non-coding RNAs such as circRNAs, Y-RNAs (*Y3*) and *H19* has also been reported.

All in all, IMPs regulate genes in various ways on the post-transcriptional level, with some well-studied example targets (summarised in Fig. 1.5). However, several aspects in their biological functions remain unclear. For example, the role of the interaction with other RNA classes such as circular RNAs remains elusive. Previous work from our lab described the association of IMP3 with a set of 34 different circRNAs identified by RIP-seq analysis and biochemically validated the interaction with the top two candidates ANKRD17 and NFATC3 in detail (Schneider *et al.*, 2016). Since then, further publications also reported circRNAs to be associated with all IMP family members (Chen *et al.*, 2019; Hanniford *et al.*, 2020; Li *et al.*, 2021), but so far there is no clear common function of the observed interactions. Moreover, regulation of the IMP proteins themselves is largely unknown, with phosphorylation being currently the best-studied modification shown to influence IMP-RNA interactions. In general, association with other proteins has been reported, with probably most of them being RNA-mediated (summarised in Korn *et al.*, 2021). These interactions will also influence the paralogous specificity of RNA targets. Furthermore, the role of homo/hetero-oligomerisation of the IMPs on (some) RNAs remains elusive (Git and Standart, 2002; Hafner *et al.*, 2010; Nielsen *et al.*,

2004; Runge *et al.*, 2000; Wächter *et al.*, 2013). Hence, further research is needed to derive a clear picture of the biological functions of the IMP proteins.

1.1.5 Function of IMP3 in cancer

All IMP proteins have been associated with cancer, with a main reported function for IMP1 and IMP3. This is also due to their absence in normal adult tissues, but strong upregulation or *de novo* expression in cancer cells, classifying the IMPs as oncofetal proteins. IMP3 has been described in a variety of different cancer types and its expression leads to poor prognosis for the patients (Lederer *et al.*, 2014; Mancarella and Scotlandi, 2020; Fig. 1.6).

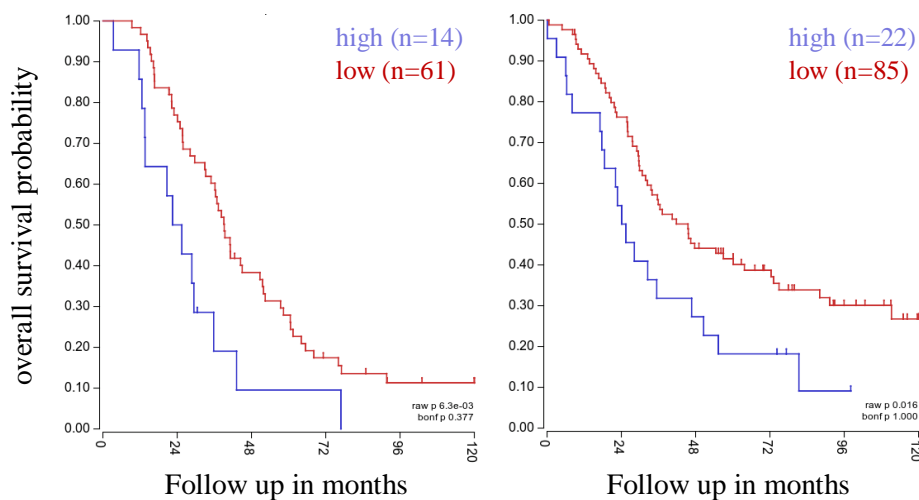


Figure 1.6: Survival rate in ovarian cancer upon IMP3 expression.

Kaplan-Meier estimates of the overall survival rate are depicted for the expression of IGF2BP3 (IMP3). Two different tumour ovarian datasets (Lisowska *et al.*, 2014; Mateescu *et al.*, 2011) were used for the prediction by the R2: Genomics Analysis and Visualization Platform (<http://r2.amc.nl>).

Enhanced IMP3 expression correlates with increased proliferation, motility, invadopodia formation, migration/invasion of cancer cells as well as increased aggressiveness by forming metastases and being resistant to cancer treatments (Ennajdaoui *et al.*, 2016; Liao *et al.*, 2011; Mancarella *et al.*, 2018; Samanta *et al.*, 2013; Vikesaa *et al.*, 2006; Zhao *et al.*, 2017). Recently, a phase II clinical trial, in which IMP3 and two other antigens were targeted by a peptide-based vaccine to treat head and neck squamous cell cancer, led to better prognosis for the patients (Yoshitake *et al.*, 2015). Also other potential vaccines contain a mixture of different peptides including the peptide targeting IMP3, and were tested in different cancer types (Daiko *et al.*, 2020; Murahashi *et al.*, 2016). This outlines the relevance of IMP3 as a tumour marker and target for cancer therapy.

On a molecular level, the described phenotypic effects reflect the operation of different networks within cancer cells. The peptide hormone IGF2 is normally expressed during embryogenesis and promotes cell proliferation, growth, migration, differentiation and survival (reviewed in Livingstone, 2013). In agreement, IMP3-mediated upregulation of *IGF2* translation in different cancers leads to enhanced tumour growth as well as increased cell survival after ionising radiation-induced apoptosis (Liao *et al.*, 2005; Liao *et al.*, 2011; Suvasini *et al.*, 2011). Since the IGF2 signalling cascade includes several downstream kinases, including mTOR which phosphorylates IMP3 and thereby enhances translation of *IGF2*, a positive feedback loop might exist (Dai *et al.*, 2013; Mancarella and Scotlandi, 2020; Suvasini *et al.*, 2011).

Cancer promotion by IMP3 is also associated with miRNAs. A well-studied example is the regulation of *HMGA2* mRNA, which encodes a fetal transcription factor re-expressed in human cancers (Zhang *et al.*, 2019). Several miRNAs can regulate *HMGA2* expression, among them the tumour suppressor let-7, which binds to several sites in the 3'UTR of *HMGA2* and promotes its degradation (Mayr *et al.*, 2007). In cancer cells, IMP3 binds to 3'UTR sites of *HMGA2* in proximity to let-7 binding sites, thereby preventing the miRNA-directed repression (Jønson *et al.*, 2014; Schneider *et al.*, 2019). In addition to *HMGA2*, also other let-7 repressed mRNAs were present in IMP3 granules, e.g. *LIN28B*, which encodes for an RBP inhibiting let-7 biogenesis (Balzeau *et al.*, 2017; Jønson *et al.*, 2014). IMP1 and IMP2 were also shown to stabilise *HMGA2* and in the case of IMP2, this stabilisation is also vice versa as *HMGA2* protein enhances transcription of the IMP2 gene (Busch *et al.*, 2016; Degrauwe *et al.*, 2016a; Li *et al.*, 2012). Thus, a complex regulatory network of the IMPs and let-7 results (Fig. 1.7), and it is likely that similar networks with other IMP3 target RNAs exist.

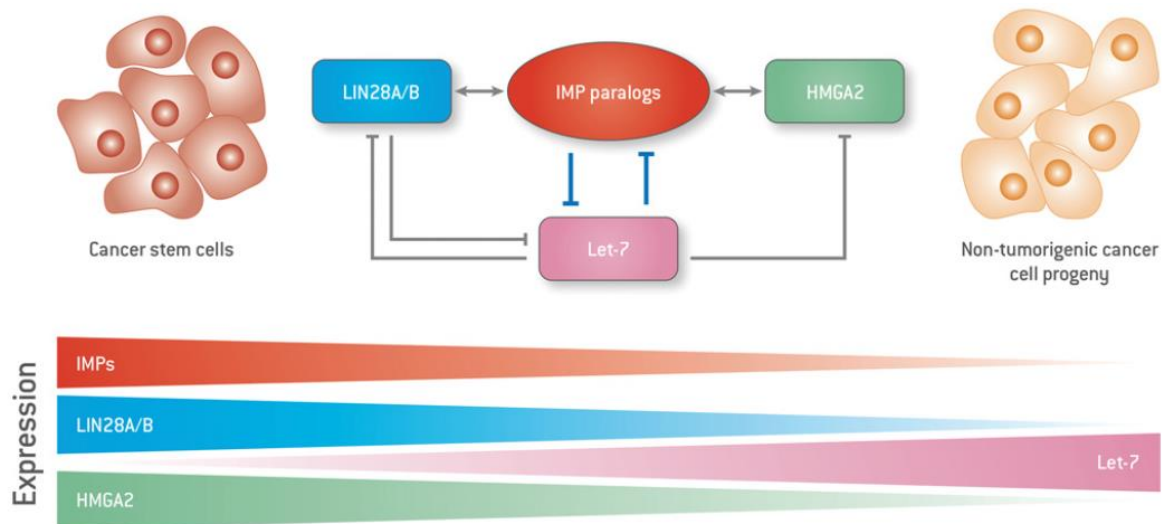


Figure 1.7: Schematic overview of the IMP/HMGA2/let-7/LIN28 network in cancer cells.

IMP proteins stabilise HMGA2 and LIN28 mRNAs by protecting them from let-7 mediated degradation. Additionally, IMP mRNA is also targeted by let-7. In turn, LIN28 RNA-binding proteins inhibit let-7 biogenesis. The complex interplay leads to opposing expression profiles of let-7 and the protein factors. Adapted from Degrauwe *et al.*, 2016b.

Taken together, IMP3 is a multifunctional post-transcriptional regulator normally expressed during embryogenesis but also present in a variety of different cancer types. A better understanding of its functions as well as a targeted inhibition of it will be beneficial for cancer therapy.

1.2 ER targeting – secretory pathway and the role of RBPs

The endoplasmic reticulum represents the largest membrane surface of the cell together with the outer nuclear membrane (Hermesh and Jansen, 2013). It is the entry site to the majority of endomembrane compartments, and about 30% of all eukaryotic genes encode proteins that target and translocate to it (Aviram and Schuldiner, 2017). Classically, a signal sequence within the protein is thought to mediate ER targeting in a co- or post-translational manner. The first factor found to recognise this signal sequence was the signal recognition particle (SRP; Walter *et al.*, 1981; Walter and Blobel, 1981). The SRP binds to a hydrophobic N-terminal signal sequence during ribosomal translation of an mRNA. This leads to stalling of translation and translocation of the ribosome-mRNA-SRP complex to the ER membrane, where SRP binds to the membraneous SRP receptor (Fig. 1.8; reviewed in Kellogg *et al.*, 2021; Reid and Nicchitta, 2015). Upon GTP hydrolysis, SRP dissociates from its receptor, and translation of the polypeptide chain continues directly into the ER via the Sec61 translocon. The resulting protein

is then released either into the ER lumen (most secreted proteins), or inserted in the ER membrane (membrane proteins), and can be further transported, e.g. to the Golgi apparatus, lysosomes or the plasma membrane.

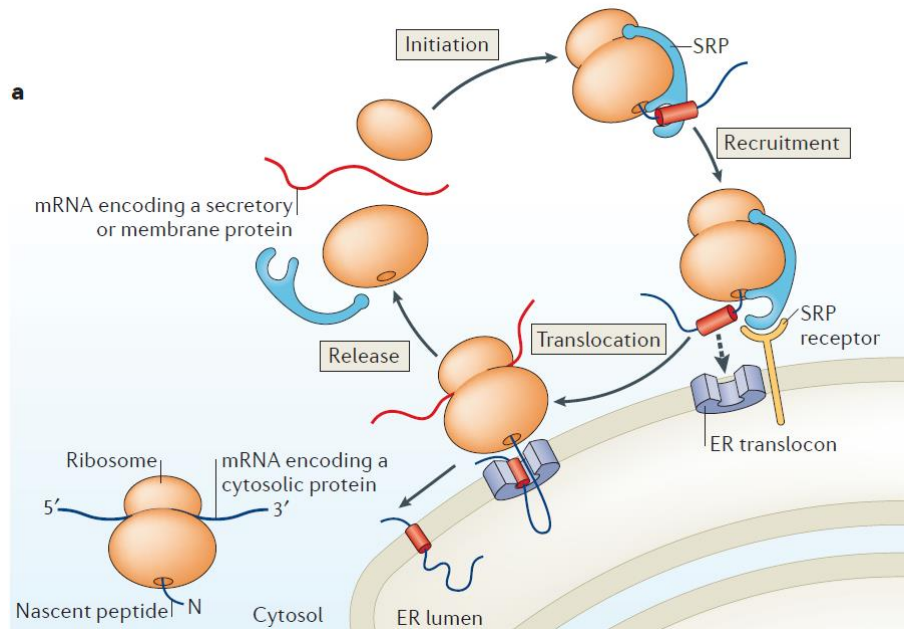


Figure 1.8: SRP-mediated mRNA translation on the ER.

Translation is initiated in the cytosol. The SRP recognises an N-terminal hydrophobic signal sequence in the nascent polypeptide chain and binds to it, thereby stalling translation. The complex is recruited to the ER membrane by the SRP receptor. Dissociation of the SRP and its receptor lead to translocation of the ribosome complex to the ER translocon, where translation continues into the ER lumen. In case of membrane proteins, the protein resides in the ER membrane after completed translation, whereas secreted proteins are released into the ER lumen. Adapted from Reid and Nicchitta, 2015.

Besides the well-studied SRP-dependent mechanism, other pathways for ER entering exist. This was first suggested by the observation that SRP components are not essential in yeast (Hann and Walter, 1991). It is now known that ER-targeting in mammals can also be facilitated by the Sec62/63 complex, which forms an SRP-independent translocon, the SND (SRP-independent) pathway or by using the cytosolic chaperone TRC40 (transmembrane recognition complex of 40 kDa) pathway (summarised in Aviram and Schuldiner, 2017). The latter is used for tail-anchored proteins containing a C-terminal signal sequence, but was also proposed to target short secretory proteins (Johnson *et al.*, 2012). All these pathways have a protein-based signal sequence in common. However, there is emerging evidence that mRNAs are targeted to the ER independent of their translation. This is facilitated by RNA-binding proteins, which recognise *cis*-acting localisation elements (also known as zipcodes) located within the mRNA.

Up to now, three different ways of how RBPs mediate RNA localisation to the ER have been reported (Fig. 1.9). In yeast, the localisation factor She2p was shown to tether mRNAs to ER

membranes in dividing cells (Schmid *et al.*, 2006; Fig. 1.9 ①). It recognises specific zipcode motifs in its target mRNAs containing a conserved CGA triplet within a loop-stem-loop structure (Jambhekar *et al.*, 2005; Olivier *et al.*, 2005). RNA localisation is then facilitated by binding simultaneously to its target mRNA and the ER membrane, probably by recognising the curvature of the latter (Genz *et al.*, 2013). Alternatively, integral ER membrane RBPs were shown to mediate RNA localisation (Fig. 1.9 ②). The abundant mammalian receptor p180 anchors mRNAs to the ER in a translation-independent manner (Cui *et al.*, 2012). The exact mechanism of this is unclear but partially relies on ionic interactions between a basic cytoplasmic region with the negatively charged RNA backbone. Similarly, the oncogenic protein AEG-1 (astrocyte elevated gene-1) was suggested to localise mRNAs to the ER membrane (Hsu *et al.*, 2018). Further research is needed to understand these associations and reveal other potentially involved proteins.

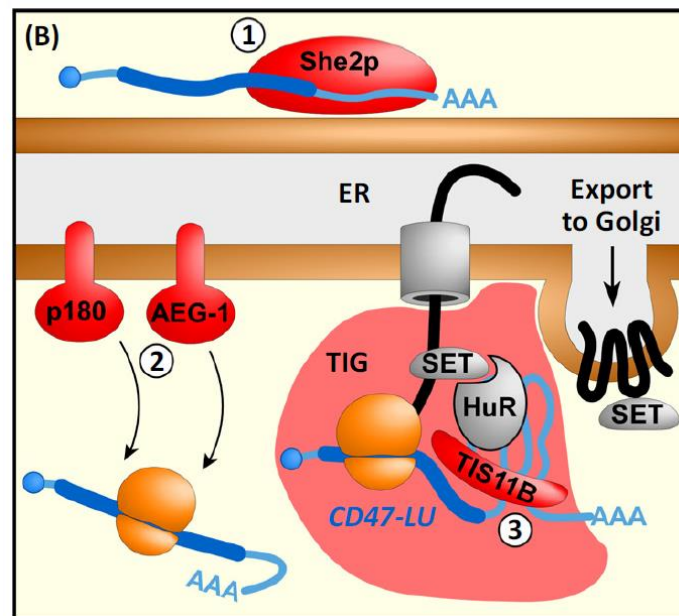


Figure 1.9: Overview of RBPs involved in ER-coupled translation.

Targeting of mRNAs to the ER is facilitated by RBPs associating with the ER-membrane (①), integral membrane receptors (②) or within TIS granules (③). For details, see main text. Adapted from Béthune *et al.*, 2019.

ER-targeting of mRNAs is not only facilitated by RBPs associating with membranes, but can be also mediated by cytosolic RBPs within granules (Fig. 1.9 ③). The human *CD47* gene was found to produce mRNAs with two alternative 3'UTR isoforms containing either a short or long 3'UTR (*CD47-SU* or *CD47-LU*, respectively; Berkovits and Mayr, 2015). *CD47* protein translated from *CD47-SU* localises predominantly to the ER, whereas the protein isoform resulting from *CD47-LU* translation is present at the cell surface. The differences in protein

localisation were partially due to the RBP HuR, which binds to the 3'UTR of the long, but not of the short isoform of *CD47*. HuR further recruits SET, which associates electrostatically with the cytoplasmic domain and C-terminus of CD47 protein and translocates it to the plasma membrane. All interactions between *CD47-LU*, HuR and SET at the ER membrane occur in so-called TIS granules, which are composed of the RBP TIS11B and form a reticular meshwork that intertwines with the ER (Ma and Mayr, 2018). These granules create a special environment with biophysical properties different than those from the cytoplasm, enabling the specific interaction of SET with CD47-LU protein (Ma and Mayr, 2018).

The examples given illustrate the various possibilities of targeting mRNAs to the ER. Especially the observations made for *CD47* localisation highlight the complexity of the issue, as it involves also cytosolic RBPs. Further research will likely reveal more of the complex interplay of protein- or RNA-mediated signals that determine mRNA localisation to the ER.

1.3 Circular RNAs – a novel class of noncoding RNAs

1.3.1 Discovery and history

Circular RNAs are endogenous, covalently closed transcripts lacking free 5' or 3' ends. They were only recognised as an entire class of noncoding RNAs during the last decade, although the first circRNA was discovered 45 years ago. Electron microscopy images from Sanger *et al.* (1976) showed that plant viroids are single-stranded circular RNAs and validated this, inter alia, by the inability to enzymatically label the 3' or 5' ends. Circularity was later confirmed by sequencing of a viroid (Gross *et al.*, 1978). Furthermore, hepatitis delta virus (HDV) was shown to have a circular RNA genome, but in contrast to viroids, its genome is larger and codes for proteins involved in viral replication (Kos *et al.*, 1986; Weiner *et al.*, 1988). Adding up to the diversity of circRNAs, generation from self-splicing ribosomal RNA (rRNA) introns in a unicellular eukaryote as well as from rRNA introns in an archaebacterium was reported (Grabowski *et al.*, 1981; Kjems and Garrett, 1988).

In the 1990s, several discoveries of circRNAs in metazoa were reported. By examining spliced transcripts from a tumour suppressor gene in human and rat cells, Nigro *et al.* (1991) found transcripts with correctly spliced exons in an unexpected order, i.e. the end of a downstream exon joined to the beginning of an upstream exon, hence terming them “scrambled exons”. These transcripts were mainly cytoplasmic, did not possess a poly(A) tail, and were of lower abundance than transcripts containing exons in the conventional order (Nigro *et al.*, 1991). In

agreement, scrambled exons were also found for the human *ets-1* transcripts and were shortly thereafter identified as stable circular RNAs resulting from “mis-splicing” of nuclear pre-mRNA (Cocquerelle *et al.*, 1992; Cocquerelle *et al.*, 1993). Unlike the previous described examples, the mouse sex-determining region Y (*Sry*) gene expresses a circRNA consisting of a single exon (Capel *et al.*, 1993). Moreover, this circRNA was higher expressed than its linear counterpart in adult testis, and its generation was proposed to be facilitated by the long inverted repeats flanking the *Sry* exon (Capel *et al.*, 1993). During the next years, other circRNAs were reported from individual mammalian protein-coding genes, but e.g. also found in *Drosophila* or generated from noncoding RNAs (Burd *et al.*, 2010; Houseley *et al.*, 2006).

However, not much attention was paid to circRNAs, as they were mostly regarded as splicing by-products. High-throughput RNA-sequencing (RNA-seq) approaches finally led to their re-discovery, as it revealed hundreds of human circRNA isoforms expressed at comparable level to their linear counterpart (Salzman *et al.*, 2012). A different RNA-seq approach comparing exonuclease RNase R-digested samples to undigested samples showed that circRNAs are conserved and flanked by long introns containing inverted Alu repeat sequences (Jeck *et al.*, 2013). Both publications convincingly demonstrated that circRNAs are more than mis-spliced by-products, but instead a common feature of eukaryotic gene expression. Further properties of circRNAs were found in the following years, such as a developmental-stage- and cell-type-specific expression (Memczak *et al.*, 2013; Salzman *et al.*, 2013). Especially the nervous system is known to contain high numbers of circRNAs, as shown for human, mouse, and *Drosophila* (Rybak-Wolf *et al.*, 2015; Westholm *et al.*, 2014).

Up to now, thousands of circRNAs have been predicted in different eukaryotic species by RNA-seq. However, bioinformatic filtering for circRNAs also includes false-positives resulting from *trans*-spliced genes, tandem DNA duplications, or by template-switching of the reverse transcriptase during RT-PCR (Jeck and Sharpless, 2014). Experimental validation is therefore crucial despite its own drawbacks, as e.g. RNase R digestion, one of the gold standards for circRNA identification, is unable to degrade highly-structured linear RNAs (Panda *et al.*, 2017). Therefore, reliable circRNA prediction should combine different algorithms and experimental validation strategies, in particular Northern blot analysis (Hansen, 2018; Pfafenrot and Preußner, 2019; Szabo and Salzman, 2016).

1.3.2 Biogenesis and function

CircRNAs are generated through a specific form of alternative splicing, called backsplicing. In contrast to conventional linear splicing, a downstream splice donor is joined to an upstream splice acceptor. The splicing process itself is mediated by the canonical spliceosome machinery (Ashwal-Fluss *et al.*, 2014; Starke *et al.*, 2015). The resulting circRNA contains the backsplicing junction (BSJ), which is characteristic for circRNAs and thus often referred to as circ-junction. It is both bioinformatically and experimentally used to distinguish between a circRNA and its linear counterpart.

There are several options how backsplicing is facilitated. The common idea is that the corresponding splice sites are brought into proximity either by base-pairing of inverted repeats in the flanking introns (e.g. by Alu elements) and/or with the help of *trans*-acting factors, i.e. RNA-binding proteins (Fig. 1.10). The hypothesis of inverted repeats promoting the formation of circRNAs was first proposed for the *Sry* gene and later found to be valid for a variety of circRNAs (Capel *et al.*, 1993; Jeck *et al.*, 2013; Zhang *et al.*, 2014). Proximity of splice sites was also shown to be created by RBPs, with Quaking and FUS as prominent examples (Conn *et al.*, 2015; Errichelli *et al.*, 2017). Quaking binds to distinct motifs located in flanking introns and dimerises, thereby enhancing the formation of hundreds of circRNAs during human epithelial to mesenchymal transition (Conn *et al.*, 2015). Similarly, FUS enhances backsplicing of multiple transcripts in murine motor neurons (Errichelli *et al.*, 2017). Meanwhile, a report from circRNA biogenesis in *Drosophila* indicated that multiple hnRNP (heterogeneous nuclear ribonucleoprotein) and SR (serine/arginine-rich) proteins, combined with inverted repeat sequences, regulate circRNA expression (Kramer *et al.*, 2015). Either way, circRNAs comprised of one or several exons emerge, and in rare cases also with retained introns, named exon-intron circRNA (ElciRNA) (Fig. 1.10).

Conventional linear splicing is normally favoured over backsplicing (Zhang *et al.*, 2016). Moreover, linear splicing is preferred if base-pairing of inverted repeats is inhibited by RBPs. Both DHX9 (ATP-dependent RNA helicase A) and ADAR (double-stranded RNA-specific adenosine deaminase) were shown to repress circRNA formation by interacting with the flanking reverse-complementary sequences, maybe even in a collaborative manner (Aktaş *et al.*, 2017; Ivanov *et al.*, 2015; Rybak-Wolf *et al.*, 2015; Fig. 1.10). Yet, distinct circRNAs were shown to be generated from re-splicing of lariat intermediates, consisting either of one intron or introns plus a skipped exon (Barrett *et al.*, 2015; Zhang *et al.*, 2013).

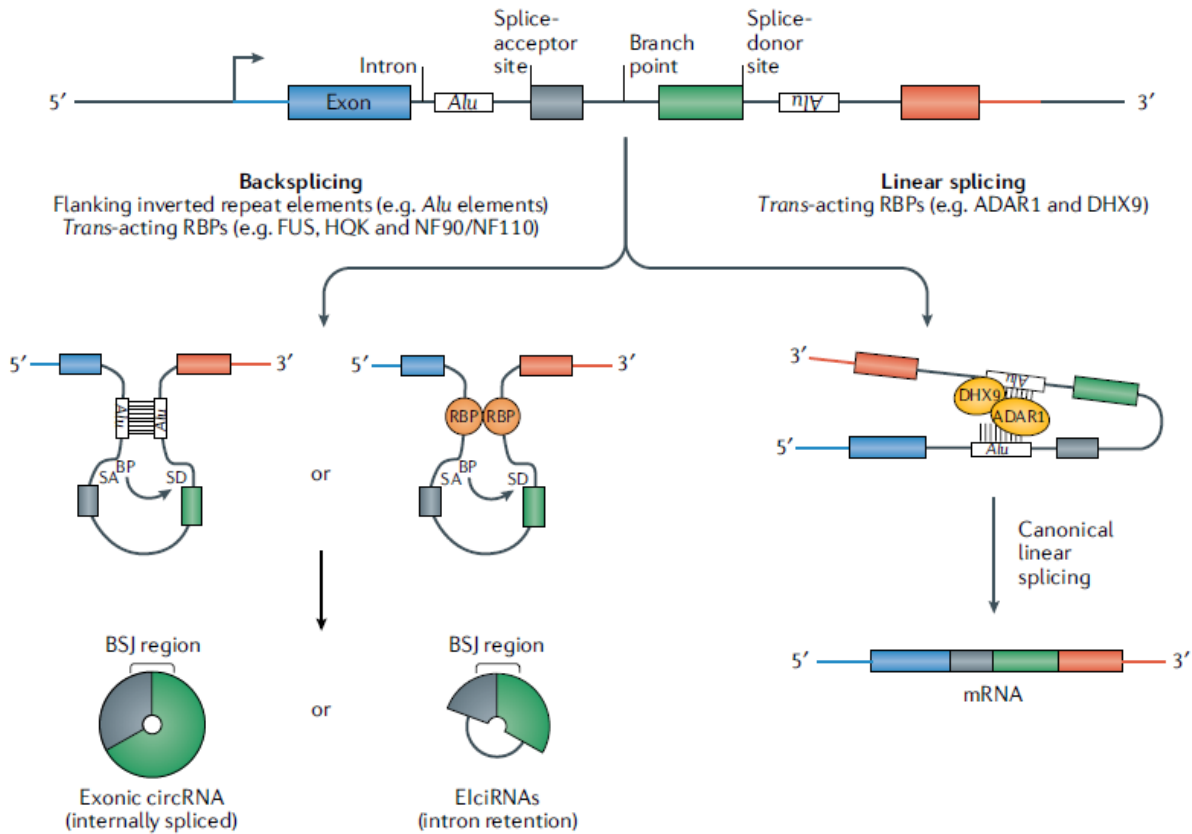


Figure 1.10: Biogenesis of circular RNAs.

Pre-mRNAs containing exons (coloured boxes), introns and inverted repeat elements such as Alu sequences can be backspliced resulting in circRNA formation (left) or canonical linear spliced to yield linear mRNAs (right). Backsplicing is promoted by bringing a downstream splice donor (SD) in proximity to an upstream splice acceptor (SA). This is facilitated by base-pairing of inverted repeat sequences (left) or dimerising RBPs (middle). The resulting circRNA contains an intron, which can either be retained (ElciRNA) or removed through internal splicing (exonic circRNA). Both circRNAs contain the characteristic backsplicing junction (BSJ) region. Conventional linear splicing is favoured if none of the backsplicing promoting elements are present or if they are blocked by *trans*-acting RBPs. Modified from Kristensen *et al.*, 2019.

For the majority of circRNAs, their function is still unknown. One hypothesis is that the circRNA generation itself might be their function, as backsplicing decreases linear splice products (Ashwal-Fluss *et al.*, 2014; Liang *et al.*, 2017). For distinct circRNAs, association with microRNAs or proteins was reported, in which circRNAs can e.g. function as a sponge for the interaction partner (see next section). Whether circRNAs might serve as a template for translation is highly debated (Schneider and Bindereif, 2017). CircRNA translation has been reported in some publications (Legnini *et al.*, 2017; Pamudurti *et al.*, 2017; Yang *et al.*, 2017), but the majority of circRNAs was reported not to be translated (Guo *et al.*, 2014; Jeck *et al.*, 2013; Schneider *et al.*, 2016; Stagsted *et al.*, 2019; You *et al.*, 2015). A recent study indicates that putative circRNA translation is only observed if the circRNA is artificially overexpressed from plasmids, but that translation does not rely on the formation of the circRNA itself, but

rather on *trans*-spliced linear by-products (Ho-Xuan *et al.*, 2020). In addition, no endogenous protein product could be detected, arguing further against translation (Ho-Xuan *et al.*, 2020).

Interestingly, circRNA expression is also reported in the context of aging and diseases. CircRNA levels increase in differentiated cells, a fact which has been also observed in the nervous system of aging animals (Gruner *et al.*, 2016; Kristensen *et al.*, 2018b; Westholm *et al.*, 2014). In addition, association with age-related diseases such as cancer, diabetes mellitus, Alzheimer disease, as well as cardiovascular diseases was also described (e.g. Dube *et al.*, 2019; Holdt *et al.*, 2016; Kristensen *et al.*, 2018a; Stoll *et al.*, 2020). Of note, circRNA characterisation was not always satisfactory, as e.g. only RNA-seq data were analysed but no stringent experimental validation performed. Hence, the role of circRNAs as biomarkers for diseases remains to be clarified by further research.

1.3.3 Interactions with proteins and microRNAs

The first reported function of circRNAs was their interaction with microRNAs. The circRNA *Sry* contains 16 binding sites for miRNA-138, and CDR1as/ciRS-7 (cerebellar degeneration-related protein 1 antisense / circular RNA sponge for miR-7) harbours more than 70 conserved binding sites for miR-7 (Hansen *et al.*, 2013a; Memczak *et al.*, 2013). Up to now, ciRS-7 remains to be the best-studied circRNA. It is highly expressed in human and mouse brain, whereas the linear transcript is hardly detectable (Hansen *et al.*, 2011; Hansen *et al.*, 2013a; Memczak *et al.*, 2013). In addition to containing multiple seed matches for miR-7, ciRS-7 possesses an almost perfect complementary binding site for miR-671, which leads to Argonaute 2 (Ago2)-mediated circRNA cleavage (Hansen *et al.*, 2011; Piwecka *et al.*, 2017). CiRS-7 knockout mice displayed reduced miR-7 levels in brain tissues, leading to enhanced expression of miR-7 target genes (Piwecka *et al.*, 2017). Thus, the hypothesis that ciRS-7 functions as a microRNA sponge that stores or transports miR-7 until miR-671/Ago2-mediated cleavage releases miR-7 was further supported (Fig. 1.11). More recent evidence suggest that the interplay between miR-7, miR-671 and ciRS-7 is complemented by a long noncoding RNA, forming a regulatory network in mammalian brains (Kleaveland *et al.*, 2018). Since miR-7 is a known tumour suppressor (Kalinowski *et al.*, 2014), reports about overexpression of ciRS-7 in cancer suggest an oncogenic role of the circRNA. However, a recent publication examined ciRS-7 levels in single cells and found no expression in cancer cells, but within tumour stromal cells, where it correlated negatively with cancer cell-enriched genes (Kristensen *et al.*, 2020). Besides the interaction with other RNAs, ciRS-7 was also proposed to interact with IMP3

protein (Hanniford *et al.*, 2020). Upon depletion of ciRS-7, IMP3-mediated melanoma invasion and formation of metastasis was enhanced, independently of miR-7 (Hanniford *et al.*, 2020). More research is needed to understand the precise mechanism of this interplay and the role of ciRS-7 in cancer.

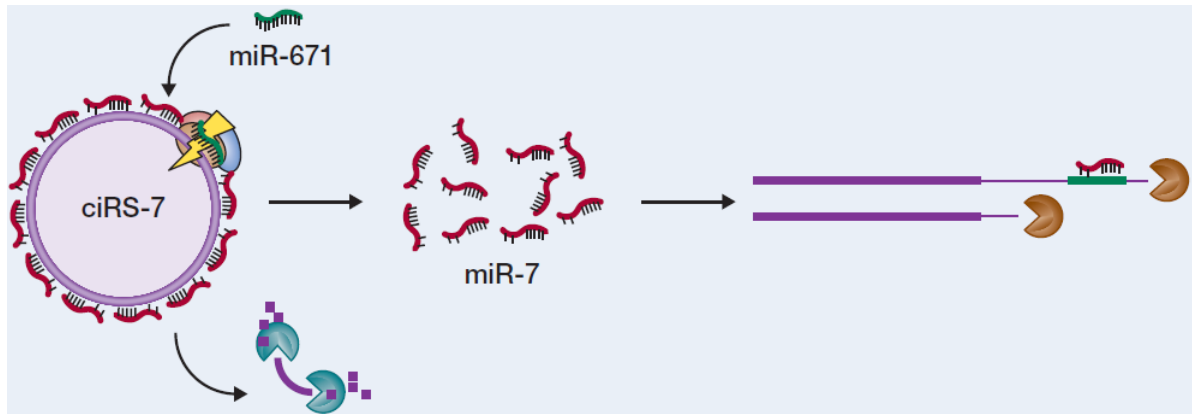


Figure 1.11: Regulatory network of ciRS-7, miR-7 and miR-671.

Multiple miR-7 molecules are bound to ciRS-7. Binding of miR-671 leads to cleavage of ciRS-7, thereby facilitating ciRS-7 degradation and release of miR-7. MiR-7 can then bind to its target mRNAs and enhance their repression. Adapted from Hansen *et al.*, 2013b.

MiRNA sponging was also reported for other circRNAs, but the possession of a high copy number of binding sites for the same miRNA is not a common feature of circRNAs (Enuka *et al.*, 2016; Guo *et al.*, 2014). Thus, circRNAs must have other (yet partially unknown) functions, one of it being their interaction with proteins. One of the first reported RBPs associated with circRNA regulation was the splicing factor muscleblind (MBL). In *Drosophila* and humans, exon 2 of the *muscleblind* mRNA (or *muscleblind-like protein 1* mRNA in humans) was shown to circularise, with the level of *circMbl* depending on the muscleblind protein itself (Ashwal-Fluss *et al.*, 2014). MBL enhances formation of its circRNA and thus downregulation of its corresponding mRNA, based on binding to the flanking introns and probably bringing them in proximity, as has been later reported for Quaking (Conn *et al.*, 2015). In sum, this provides evidence for an autoregulatory feedback loop, in which MBL represses expression of its own mRNA by enhancing *circMbl*.

Furthermore, the post-transcriptional gene regulator HuR was shown to bind *circPABPN1*, a circRNA derived from the HuR target mRNA *PABPN1* (nuclear poly(A)-binding protein 1; Abdelmohsen *et al.*, 2017). By interacting with *circPABPN1*, HuR binding to *PABPN1* mRNA or *ATG16L1* (autophagy-related gene 16 like 1) mRNA is repressed and consequently the HuR-mediated enhancement of the translation diminished (Abdelmohsen *et al.*, 2017; Li *et al.*, 2020).

This exemplifies how circRNAs can act as protein sponges and suppress the interaction of RBPs with their target mRNAs.

In addition, circRNAs were shown to be bound by protein kinase R (PKR), an enzyme known to recognise double-stranded (viral) RNA (Liu *et al.*, 2019). In this study, PKR was shown to interact preferentially with the circRNA rather than the linear isoform. This was due to the formation of short dsRNA regions within the circRNA. Functionally, circRNA binding led to inhibition of PKR, which could be reversed in virus-infected cells by activated RNase L, an endoribonuclease shown to degrade circRNAs under these conditions (Liu *et al.*, 2019). This is the only circRNA degradation pathway known so far.

Specific circRNA-protein interactions have also been described in other publications. However, most discovered circRNPs have no assigned functions. As an example, IMP3 was found to bind to a subset of 34 circRNAs, but a common function of this remains elusive (Schneider *et al.*, 2016). The limited insight into circRNA-protein interactions is also due to the special challenges in circRNA research, which in turn means that only a small repertoire of investigation methods has been used so far (Ulshöfer *et al.*, 2021).

1.3.4 Methods of circRNA synthesis and expression

The study of circRNA function often requires the presence of the desired circRNA in relatively high amounts. This can be either achieved by *in vitro* synthesis or by *in vivo* expression in cell systems. Several strategies are available for both ways, each with own benefits and drawbacks (Costello *et al.*, 2020; Petkovic and Müller, 2015).

In vitro circRNA synthesis requires first the production of a linear RNA molecule. This is normally mediated by T7 polymerase *in vitro* transcription from a DNA template. In a next step, a circular RNA molecule has to be formed. While this can also result from chemical conjugation, the standard method is the use of enzymatic ligation by T4 RNA ligase. In the ligation reaction, the intramolecular end joining needs to be favoured over the intermolecular ligation of linear RNA molecules. This can be achieved by bringing the 5' and 3' ends in proximity, e.g. with the help of a linear or hairpin (splint) oligonucleotide, or by including sequences at both ends of the RNA that base pair to form a stem (Müller and Appel, 2017). The latter technique is also suitable to efficiently produce circRNAs in large amounts (Breuer and Rossbach, 2020). However, the limitation with the described circularisation approaches is their inefficiency in the synthesis of large circRNAs, as a complex RNA secondary structure can

cause a significant distance between the 5' and 3' end. For this purpose, the use of ribozyme-mediated circRNA formation is beneficial. Recently, Wesselhoeft and colleagues optimised the long-known procedure to efficiently produce circRNAs of up to 5 kb length (Wesselhoeft *et al.*, 2018). In this strategy, permuted group I self-splicing introns flank two small exons, in which a gene of interest is cloned in between (Fig. 1.12A). Outer and inner homology regions base pair and help to bring the introns into proximity by creating a “splice bubble”. Complete splicing results in two separate introns and a circRNA comprised of all sequences present between the two small exons. The so-called permuted-exon intron (PIE) strategy can be also used for *in vivo* protein translation by inserting an IRES (internal ribosome entry site) in front of a protein-coding sequence (Wesselhoeft *et al.*, 2018).

Independently of the *in vitro* approach used, undesired RNA products will be present after circularisation. Enzymatic ligation results in a mixture of linear RNA, circular RNA and linear concatamers. Using the PIE strategy, precursor, introns, splicing intermediates, and nicked circular RNA molecules will be present. Hence, synthesised circRNAs need to be purified prior to usage. For small and mid-sized circRNAs, gel extraction can be performed from denaturing polyacrylamide gels. Purification of large circRNAs from the PIE strategy was achieved by first enriching circRNAs upon RNase R treatment and subsequently separating remaining RNA species using high-performance liquid chromatography (Wesselhoeft *et al.*, 2018). Both purification approaches are laborious, time-consuming and lead to decreased yields, which is why circRNA *in vivo* production might be preferred.

In vivo circRNA synthesis is mediated from artificial DNA constructs transiently transfected into cells or, less common, stably integrated in the cellular genome. Initial approaches were based on endogenous circRNA biogenesis, in which inverted repeats in flanking introns promote backsplicing of the RNA. Liang and Wilusz (2014) created an expression vector based on the *ZKSCAN1* (zinc finger protein with KRAB and SCAN domains 1) gene, which naturally forms a circRNA in humans. They took parts of the flanking introns containing inverted oriented Alu sequences and inserted a multiple-cloning site in between so that desired sequences can be included. After plasmid transfection, *in vivo* transcription was mediated by a cytomegalovirus (CMV) promoter and the polymerase II machinery. The ZKSCAN expression vector produced circular RNAs of different length and sequences, yet with different efficiencies, and the linear form was still the predominant outcome in this expression system (Liang and Wilusz, 2014).

Litke and Jaffrey (2019) introduced a more efficient *in vivo* circularisation approach, the so-called Tornado (Twister-optimised RNA for durable overexpression) system. Twister ribozyme sequences were encoded next to the desired circRNA sequence on a polymerase III expression plasmid (Fig. 1.12B). Consequently, circRNA sequences must not contain U stretches as this would lead to transcription termination (Richard and Manley, 2009). Upon transfection, circRNAs are generated *in vivo* by autocatalytic ribozymal cleavage of the transcribed RNA with subsequent enzymatic ligation by the endogenous RtcB tRNA ligase. This way, small circRNAs were efficiently produced in amounts comparable to the abundant 5S RNA with hardly detectable linear precursors. In addition, RNA aptamers can be introduced to enable the detection of the circRNA by fluorogen staining of gels or in fluorescent microscopy assays (Litke and Jaffrey, 2019).

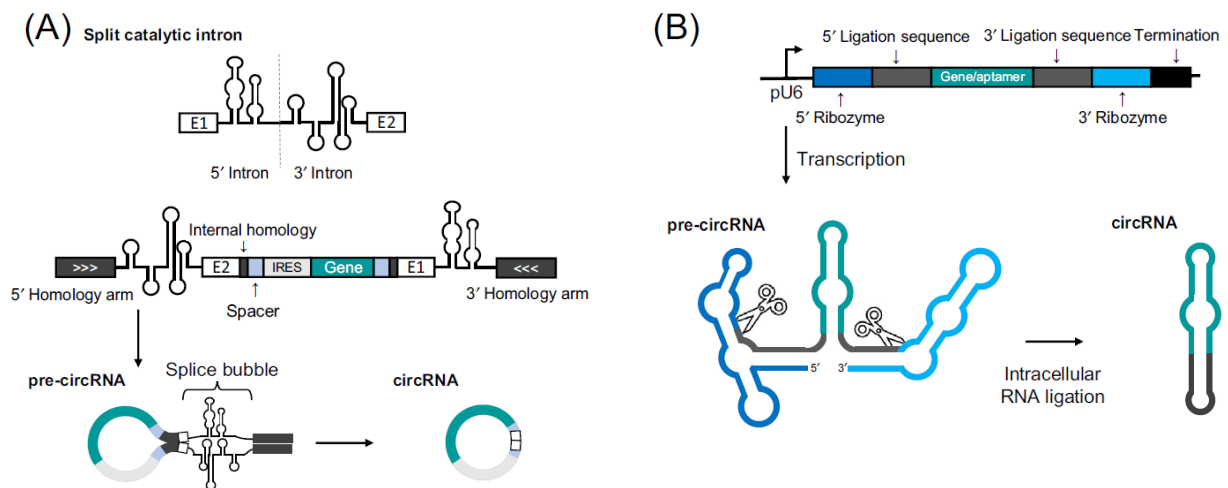


Figure 1.12: Exemplified methods for generation of synthetic circRNAs.

(A) Permuted exon-intron (PIE) strategy for *in vitro* synthesis of circRNAs. Group I autocatalytic introns are split and together with exon 1 or 2 (E1/E2) swapped in their order. Desired sequences can be inserted between E2 and E1, e.g. a gene of interest with a preceding IRES site for translation. Outer and inner homology regions facilitate base pairing and the creation of a splice bubble; spacer regions ensure the formation of correct secondary structures.

(B) Tornado expression system for *in vivo* circRNA expression. The gene of interest is flanked by ligation sequences as well as ribozyme-encoding sequences. Transcription is mediated by polymerase III from a U6 promoter and directly terminated after the 3'ribozyme. In the resulting pre-circRNA, ribozymes are formed and facilitate the cleavage after the ligation sequence. The ligation sequence base pairs and forms a stem, which is then ligated intracellularly to yield the final circRNA.

Modified from Costello *et al.*, 2020.

Despite the numerous recent advances in circRNA generation, there is, for example, no method available for producing circRNAs *in vivo* in near endogenous levels without their linear counterparts. Hence, developing further methods to generate circRNAs will be highly beneficial for circRNA research.

1.3.5 Design and application of circRNAs in molecular medicine

CircRNAs are highly stable molecules, with half-lives significantly exceeding those of their linear counterparts (Enuka *et al.*, 2016; Jeck *et al.*, 2013; Memczak *et al.*, 2013). This makes them highly attractive as a potential tool for molecular medicine. So far, synthetic circRNAs have been shown to efficiently function as miRNA sponges (Jost *et al.*, 2018; Lavenniah *et al.*, 2020; Liu *et al.*, 2018; Wang *et al.*, 2019). In the first study, circRNAs containing 8 miR-122 binding sites were designed (Jost *et al.*, 2018). MiR-122 is important for Hepatitis C viral replication and successful targeting of this miRNA by antogomiRs like the DNA/LNA-mixmer Miravirsen was shown (Baek *et al.*, 2014). *In vitro* produced circRNA miR-122 sponges showed comparable inhibitory effects on viral protein production as Miravirsen in cell culture, demonstrating the applicability of circRNAs in a medical context (Jost *et al.*, 2018). Other studies focused on circRNA-mediated miRNA sponging to inhibit cancer cell proliferation (Liu *et al.*, 2018; Wang *et al.*, 2019) or treat cardiac disease (Lavenniah *et al.*, 2020). In these approaches, circRNAs targeting one miRNA (Liu *et al.*, 2018) or two different miRNAs (Lavenniah *et al.*, 2020; Wang *et al.*, 2019) were used. Further studies will reveal the potential of miRNA sponging by circRNAs and clarify if they are an alternative to available antagomiRs.

Similar to microRNA sponging, circRNAs could be used to sequester RNA-binding proteins. Indeed, expression of an NF- κ B (nuclear factor κ B) aptamer with the Tornado system was shown to inhibit NF- κ B signalling (Litke and Jaffrey, 2019). Further, the Tornado-generated circRNA aptamer was more efficient than an expressed linear aptamer, likely due to a better folded secondary structure (Litke and Jaffrey, 2019). Moreover, in a recent publication from our lab, artificial circRNAs were employed to sponge the splicing factor hnRNP L (Schreiner *et al.*, 2020). The functionality of this principle was demonstrated by employing circRNAs of varying sequences (i.e. length and binding motif, as well as varying copy numbers of the latter) expressed by different strategies. Designed circRNA sponges were shown to bind hnRNP L and alter alternative splicing pattern of hnRNP L target transcripts similar to siRNA-mediated hnRNP L knockdown (Schreiner *et al.*, 2020). Thus, protein sponging by circRNAs could be an alternative to currently used protein knockdown techniques and would be also applicable to RBPs overexpressed in diseases, which applies to many tumour markers. The only prerequisite for this application is a known RNA-binding motif of the protein.

Besides the use of artificial circRNAs as sponges, they can also function as templates for *in vivo* translation of proteins. Translation initiation is facilitated by inclusion of an IRES element within the circRNA (Chen and Sarnow, 1995; Wang and Wang, 2015). Efficiency of circRNA

translation relies on the IRES element used, i.e. from which virus the IRES was derived (Meganck *et al.*, 2021; Wesselhoeft *et al.*, 2018). Protein generation from circRNAs was demonstrated in cell culture and mice, either by introducing *in vitro* generated circRNAs or circRNA-encoding plasmids (Meganck *et al.*, 2021; Wesselhoeft *et al.*, 2018; Wesselhoeft *et al.*, 2019). Translation from *in vitro* generated circRNAs does not require incorporation of modified nucleosides to evade immune response and leads to an enhanced and prolonged protein expression compared to synthetic linear mRNAs, although these effects are tissue-dependent (Wesselhoeft *et al.*, 2019). In sum, this outlines the potential of circRNAs as new vectors in gene therapy applications.

1.4 Aims of this work

This work focuses on the tumour marker and RNA-binding protein IMP3, which is upregulated in a variety of tumour types. In a first step, IMP3 was inhibited by synthetic designer circRNA sponges. Therefore, circRNAs were designed based on the RNA-binding motif previously revealed by our lab. They contained either part of an endogenous circRNA target or an artificial, SELEX-derived sequence. Binding characteristics of IMP3 to designer circRNA sponges were first tested *in vitro* by measuring the dissociation constants of recombinant IMP3 with radioactively labelled linear or circular RNAs with electrophoretic mobility shift assays. After the confirmation of a tight association *in vitro*, *in vivo* binding was examined. Two different strategies were pursued: (1) CircRNA sponges were stably integrated into the genome and inducibly expressed, or (2), transiently overexpressed from transfected plasmids using the Tornado system. Ectopic circRNA expression was controlled and binding to IMP3 examined by RNA-immunoprecipitation (RIP) assays.

Apart from IMP3 inhibition, we wanted to gain further insights on how IMP3 regulates gene expression. Generally, it is known that the IMP family functions in RNA localisation, stability and translation. Preliminary data from our lab suggested that IMP3 might also function in the secretory pathway, in which RNAs are guided to the endoplasmic reticulum and the resulting protein is translocated into the ER lumen. To obtain more insight on a global transcriptome level, we combined subcellular fractionation with next-generation RNA-sequencing and individual-nucleotide resolution crosslinking and immunoprecipitation (iCLIP) in human ES-2 cells. For RNA-seq, ES-2 cells depleted of IMP3 either by transient siRNA-mediated knockdown or by stable CRISPR/Cas9-mediated knockout were additionally analysed.

Combining the RNA-seq and iCLIP datasets, we found a subset of direct mRNA targets downregulated in the membrane organelle fraction upon IMP3 knockdown. Selected mRNA targets belonging to the secretory pathway were then biochemically validated, first, by IMP3 RIP experiments, and further, by RT-qPCR in cellular fractions to confirm changes in their gene expression levels. Moreover, we examined whether IMP3 has an effect on the stability of the target mRNAs. Finally, it was tested whether the presence of IMP3 circRNA sponges led to a comparable downregulation of mRNA targets in the membrane organelle fraction as shown upon IMP3 knockdown.

2 Material

2.1 Bacterial and eukaryotic cells

Cell line/ bacterial strain	Description	Source
ES-2	Human ovarian clear cell carcinoma cells	Kindly provided by Stefan Hüttelmaier (Martin-Luther-Universität, Halle-Wittenberg)
ES-2 IMP3 knockout	CRISPR/Cas9-mediated genomic deletion of IMP3 in ES-2 cells	Kindly provided by Stefan Hüttelmaier (Martin-Luther-Universität, Halle-Wittenberg)
HeLa	Human cervix carcinoma cells	Leibniz-Institute DSMZ
HeLa Flp-In T-REx	HeLa cells containing stably integrated pFRT/lacZeo and pcDNA TM 6/TR	Kindly provided by Lienhard Schmitz (Justus-Liebig-Universität Gießen), initially from Thermo Scientific
<i>E. coli</i> BL21 (DE3)	Chemically competent cells	Thermo Scientific
<i>E. coli</i> KRX	Single Step (KRX) competent cells	Promega
<i>E. coli</i> TOP10	One Shot TOP10 chemically competent <i>E. coli</i>	Invitrogen

2.2 Antibodies

Antibody	Supplier	Dilution (WB)
Anti-Mouse IgG peroxidase antibody	Sigma-Aldrich	1:10,000
Anti-Rabbit IgG peroxidase antibody	Sigma-Aldrich	1:10,000
Calnexin, monoclonal antibody (H-70)	Santa Cruz Biotechnology	1:2,000
C-Myc, monoclonal antibody (9E10)	Santa Cruz Biotechnology	/
FLAG monoclonal antibody (M2)	Sigma-Aldrich	1:1,000
GAPDH, monoclonal antibody (71.1)	Sigma-Aldrich	1:5,000
HnRNP A1, monoclonal antibody (4B10)	Santa Cruz Biotechnology	1:1,000
IGF2BP3 (IMP3), polyclonal (07-104)	Millipore	1:4,000
IMP1 monoclonal antibody (6A9)	BSBS AB facility	1:1,000
RIPAb+ IGF2BP2 (IMP2), monoclonal	Millipore	1:10,000
γ -tubulin, monoclonal antibody (GTU-88)	Sigma-Aldrich	1:5,000

2.3 Enzymes

All restriction enzymes were purchased from New England Biolabs and are not listed below.

Enzyme	Supplier
DNase I (1 mg/ml)	Sigma-Aldrich
Lysozyme (50 mg/ml)	Roth
Phusion DNA Polymerase (2 U/ μ l)	New England Biolabs
Phusion HF PCR MasterMix	New England Biolabs
Proteinase K (20 mg/ml)	Roth
RNase A (100 mg/ml)	QIAGEN
RNase I (100 U/ μ l)	Ambion
RNase R (20 U/ μ l)	Epicentre
RNaseOUT (40 U/ μ l)	Invitrogen
RQ1 DNase (1 U/ μ l)	Promega
SuperScript III RT (200 U/ μ l)	Invitrogen
T4 DNA Ligase (400 U/ μ l)	New England Biolabs
T4 Polynucleotide Kinase (10 U/ μ l)	New England Biolabs
T4 RNA Ligase 1 (10 U/ μ l)	New England Biolabs
T4 RNA Ligase 1, high concentration (30 U/ μ l)	New England Biolabs
T7 RNA Polymerase (20 U/ μ l)	Thermo Scientific
<i>Taq</i> DNA Polymerase	Purified by Silke Schreiner
TURBO DNase (2 U/ μ l)	Invitrogen

2.4 Plasmids

Plasmid	Source
pAV-U6+27-Tornado-101-mer	generated within this thesis
pAV-U6+27-Tornado-allUG	generated within this thesis
pAV-U6+27-Tornado-ANKRD17	generated within this thesis
pAV-U6+27-Tornado-Broccoli	gift from Samie Jaffrey (Addgene plasmid #124360)
pcDNA3.1(+)-ZKSCAN1-1xallUG	generated within this thesis
pcDNA3.1(+)-ZKSCAN1-1xANKRD17	generated within this thesis
pcDNA3.1(+)-ZKSCAN1-2xallUG	generated within this thesis
pcDNA3.1(+)-ZKSCAN1-2xANKRD17	generated within this thesis
pcDNA3.1(+)-ZKSCAN1-MCS exon vector	gift from Jeremy Wilusz (Addgene plasmid #69901)
pcDNA5/FRT/TO-BGH	kindly provided by Silke Schreiner
pcDNA5/FRT/TO-BGH-WV-1xallUG	generated within this thesis
pcDNA5/FRT/TO-BGH-WV-1xANKRD17	generated within this thesis
pcDNA5/FRT/TO-BGH-WV-2xallUG	generated within this thesis
pcDNA5/FRT/TO-BGH-WV-2xANKRD17	generated within this thesis
pDEST-3xFLAG-IMP3	generated within this thesis

pDEST-mycIGF2BP3	gift from Thomas Tuschl (Addgene plasmid #19879)
pGEX-6P2-GST_IMP3-FL_TEV_His	kindly provided by Tim Schneider (Schneider <i>et al.</i> , 2019)

2.5 Oligonucleotides

Small interfering RNAs (siRNAs)

Name	Sequence/Information	Supplier
Luciferase GL2	CGUACGCGGAAUACUUCGATT	Sigma-Aldrich
Silencer Select siRNA targeting IGF2BP3 (IMP3)	siRNA ID #: s20920	Ambion

CircRNA sponge detection primers

Stable sponges

<i>1xANKRD total fwd</i>	CCGAGTAGACAAGACAAGTAGC
<i>ANKRD, allUG total rev</i>	CGGATCAGACTCGACGCTAG
<i>1xANKRD circ fwd</i>	AACAACAGTCACAACCACGG
<i>1xANKRD, allUG circ rev</i>	GCTACTTGTCTTGTCTACTCGG
<i>2xANKRD fwd</i>	TCGTCAGCACTCAGTCTGTC
<i>2xANKRD circ rev</i>	GCCTTCGGACAGAGCTACTT
<i>ANKRD prec rev</i>	GCCTTCGGACAGAGCTACTT
<i>1xallUG total fwd</i>	CAAGACAAGTAGCAGGGAGGA
<i>1xallUG circ fwd</i>	TGTGTATCGCAGCTAAAATGTG
<i>2xallUG fwd</i>	GTCGTCAGCACTCAGAGGG
<i>allUG prec rev</i>	TCCTCCCTGCTACTTGTCTTG

Tornado circRNAs

<i>101mer Torn circ fwd</i>	CAGAATGCGGCTATCCACAC
<i>101mer Torn rev</i>	AAATTGCCTTCCTCCCTCCC
<i>allUG Torn circ fwd</i>	CAGAATGTGTATCGCAGCTAAAA
<i>allUG Torn circ rev</i>	ACTCGGCATGGTTCTACAGT
<i>allUG Torn prec rev</i>	AATCACATTCCTCCCTCCCG
<i>ANKRD circ fwd</i>	AACAACAGTCACAACCACGG
<i>ANKRD circ rev</i>	GCTACTTGTCTTGTCTACTCGG
<i>ANKRD prec rev</i>	GCCTTCGGACAGAGCTACTT
<i>Tornado prec fwd</i>	CTTCGGCAGCACATATACTAGTC

Transfected circRNAs

<i>101mer tag circ fwd</i>	TCCACACACAAACGGGCTAG
<i>101mer tag circ rev</i>	GCCTTCCTCCCTGCTACTTG
<i>allUG tag circ fwd</i>	GATCTGTGTGTGAACGGGCT
<i>allUG tag circ rev</i>	CACATTCCTCCCTGCTACTTGT

<i>ANKRD tag circ fwd</i>	CGGCAAGCAACAACAACACT
<i>ANKRD tag circ rev</i>	TTGTCTACTCGGCTTACTCCCT

Reference and control genes

<i>ANKRD17_E29-30 circ fwd</i>	CAGGAGGTCAGATGTACGGA
<i>ANKRD17_E29-30 circ rev</i>	TCTTGTTGATTTCAGTGCCACC
<i>CAMSAP1 circ fwd</i>	CCCTGATGATGGCCTACACT
<i>CAMSAP1 circ rev</i>	TGTGCTCCTGCTCATACTGG
<i>FTL linE3-4 fwd</i>	ATCTTCATGCCCTGGGTTCT
<i>FTL linE3-4 rev</i>	GAGGTGGTTCAGGTGGTCA
<i>GAPDH fwd</i>	TGCACCACCAACTGCTTAGC
<i>GAPDH rev</i>	GGCATGGACTGTGGTCATGAG
<i>snoRD U78 fwd</i>	GTGTAATGATGTTGATCAAATGT
<i>snoRD U78 rev</i>	TTCTTCAGTGTTACCTTTGTCTA
<i>U6 fwd</i>	CTCGCTTCGGCAGCACATA
<i>U6 rev</i>	GCTTCACGAATTTGCGTGTC

Endogenous IMP3 target validation primers

IMP3 targets

<i>CXCL5 E3-4 fwd</i>	TGTCTTGATCCAGAAGCCCCT
<i>CXCL5 E3-4 rev</i>	TCCATGCGTGCTCATTTCTCT
<i>LAMA4 E37-38 fwd</i>	GGGAGCCTGTGTTTGTGGGA
<i>LAMA4 E37-38 rev</i>	GCTGACCAGGGCTGCTTTA
<i>MFSD1 E14-16 fwd</i>	TTTGGTGAATCGTGCCCAGG
<i>MFSD1 E14-16 rev</i>	ACGATGTGTTAAGCCCATTTCTCA
<i>MMP1 E9-10 fwd</i>	CACATGACTTTTCTGGAATTGGC
<i>MMP1 E9-10 rev</i>	TTTCTGTCAGTTGAACCAGCT
<i>SERPINB7 E7-8 fwd</i>	TGTACGTTCTGCTGCCTGAG
<i>SERPINB7 E7-8 rev</i>	GGTCATTCGCCTTGGATTGGT
<i>SRGN E2-3 fwd</i>	CGGAGAGCCAGGTACCAATG
<i>SRGN E2-3 rev</i>	CGATTCAAGTCCTGGATTCTCGT
<i>TNC E22-23 fwd</i>	ACTGTCACCCTGTCAACCTG
<i>TNC E22-23 rev</i>	GATTGAGTGTTTCGTGGCCCT
<i>ELTD1 E10-11 fwd</i>	AGCACCAGGACAACAATTCA
<i>ELTD1 E10-11 rev</i>	CACATCCATGCAAAAGCAGCT
<i>MCOLN2 E12-13 fwd</i>	GTGTGGCTGTTTCAGTCGTCT
<i>MCOLN2 E12-13 rev</i>	GGAATTCCTGCAAAATCCGTTTCA

Reference and control genes

<i>GAPDH fwd</i>	TGCACCACCAACTGCTTAGC
<i>GAPDH rev</i>	GGCATGGACTGTGGTCATGAG
<i>FKBP10 E3-4 fwd</i>	CGACTTTGTCCGCTACCACT
<i>FKBP10 E3-4 rev</i>	TTGATCAGCCAACCAGAGCC
<i>GANAB E23-24 fwd</i>	TGATGGGCACACGTTCAACT

<i>GANAB E23-24 rev</i>	CCACCCGCTCAATCCAGATT
<i>snoRD U78 fwd</i>	GTGTAATGATGTTGATCAAATGT
<i>snoRD U78 rev</i>	TTCTTCAGTGTTACCTTTGTCTA
<i>FTL linE3-4 fwd</i>	ATCTTCATGCCCTGGGTTCT
<i>FTL linE3-4 rev</i>	GAGGTTGGTCAGGTGGTCA
<i>18S rRNA fwd</i>	GTAACCCGTTGAACCCCAT
<i>18S rRNA rev</i>	CCATCCAATCGGTAGTAGCG
<i>MYC E2 fwd</i>	CGTCCCTCGGATTCTCTGCTC
<i>MYC E3 rev</i>	CCCTCTTGGCAGCAGGATAG

NEBNext index primers for RNA-seq libraries

All index primers contain a phosphorothioate bond between the last two nucleotides at the 3' end (-s-).

<i>Index 36 primer</i>	CAAGCAGAAGACGGCATAACGAGAT TGTTGG GTGACTGGAGTTCAGACG TGTGCTCTTCCGATC-s-T
<i>Index 37 primer</i>	CAAGCAGAAGACGGCATAACGAGAT ATTCCG GTGACTGGAGTTCAGACG TGTGCTCTTCCGATC-s-T
<i>Index 38 primer</i>	CAAGCAGAAGACGGCATAACGAGAT AGCTAG GTGACTGGAGTTCAGACG TGTGCTCTTCCGATC-s-T
<i>Index 39 primer</i>	CAAGCAGAAGACGGCATAACGAGAT GTATAG GTGACTGGAGTTCAGACG TGTGCTCTTCCGATC-s-T
<i>Index 40 primer</i>	CAAGCAGAAGACGGCATAACGAGATT GATCAC GTGACTGGAGTTCAGA CGTGTGCTCTTCCGATC-s-T
<i>Index 41 primer</i>	CAAGCAGAAGACGGCATAACGAGAT GTCGTC GTGACTGGAGTTCAGACG TGTGCTCTTCCGATC-s-T
<i>Index 43 primer</i>	CAAGCAGAAGACGGCATAACGAGAT GCTGTA GTGACTGGAGTTCAGACG TGTGCTCTTCCGATC-s-T
<i>Index 44 primer</i>	CAAGCAGAAGACGGCATAACGAGAT ATTATA GTGACTGGAGTTCAGACG TGTGCTCTTCCGATC-s-T
<i>Index 45 primer</i>	CAAGCAGAAGACGGCATAACGAGAT GAATGA GTGACTGGAGTTCAGACG TGTGCTCTTCCGATC-s-T
<i>Index 46 primer</i>	CAAGCAGAAGACGGCATAACGAGAT TCGGGA GTGACTGGAGTTCAGACG TGTGCTCTTCCGATC-s-T
<i>Index 47 primer</i>	CAAGCAGAAGACGGCATAACGAGAT CTTCGA GTGACTGGAGTTCAGACG TGTGCTCTTCCGATC-s-T
<i>Index 48 primer</i>	CAAGCAGAAGACGGCATAACGAGAT TGCCGA GTGACTGGAGTTCAGACG TGTGCTCTTCCGATC-s-T

iCLIP oligonucleotides

All iCLIP linkers contain a dideoxycytosin modification at their 3' end (3ddC). The 5' end is either pre-adenylated (5rApp) or phosphorylated (5Phos).

<i>Pre-adenylated L3-App</i>	/5rApp/AGATCGGAAGAGCGGTTTCAG/3ddC/
<i>RT1 oligo</i>	GGATCCTGAACCGCT
<i>P5Solexa_s</i>	ACACGACGCTCTTCCGATCT
<i>P3Solexa_s</i>	CTGAACCGCTCTTCCGATCT
<i>P5Solexa</i>	AATGATACGGCGACCACCGAGATCTACACTCTTTCCCTACACGACGCT CTTCCGATCT

<i>P3Solexa</i>	CAAGCAGAAGACGGCATAACGAGATCGGTCTCGGCATTCTGCTGAACC GCTCTTCCGATCT
<i>L01clip2.0</i>	/5Phos/NNNN ATCACG NNNNNAGATCGGAAGAGCGTCGTG/3ddC/
<i>L02clip2.0</i>	/5Phos/NNNN CGATGT NNNNNAGATCGGAAGAGCGTCGTG/3ddC/
<i>L03clip2.0</i>	/5Phos/NNNN TTAGGC NNNNNAGATCGGAAGAGCGTCGTG/3ddC/
<i>L04clip2.0</i>	/5Phos/NNNN TGACC NNNNNAGATCGGAAGAGCGTCGTG/3ddC/
<i>L08clip2.0</i>	/5Phos/NNNN ACTTG NNNNNAGATCGGAAGAGCGTCGTG/3ddC/
<i>L10clip2.0</i>	/5Phos/NNNN TAGCTT NNNNNAGATCGGAAGAGCGTCGTG/3ddC/
<i>L16clip2.0</i>	/5Phos/NNNN CCGTCC NNNNNAGATCGGAAGAGCGTCGTG/3ddC/
<i>L21clip2.0</i>	/5Phos/NNNN GTTTCG NNNNNAGATCGGAAGAGCGTCGTG/3ddC/

T7 template preparation oligonucleotides

<i>ANKRD17 s</i>	TCTGTCCGAAGGCAGCTTTTTGTGCACAGTTGTGAAGACATCCAATCGC CACACAACAACAGTCACAACCACGGCAAGCAACAACAACACTGCACCC ACAAATGCCACATATCCTATGC
<i>ANKRD17 as</i>	GCATAGGATATGTGGCATTGTGGGTGCAGTGTGTTGTTGCTTGCCG TGGTTGTGACTGTTGTTGTGTGGCGATTGGATGTCTTCACAACACTGTGA CAAAAAGCTGCCTTCGGACAGA
<i>101-mer s</i>	TAATACGACTCACTATAGGGAGGGAGGAAGGCAATTTTGGAGGAACTA CAGAACACATATCGCAGCTAAAACACAATTTTGGAGGAACTACAGAAT GCGGCTATCCACACACAAAGG
<i>101-mer as</i>	CCTTTTGTGTGTGGATAGCCGATTCTGTAGTTCCTCCAAAATTGTGT TTTAGCTGCGATATGTGTTCTGTAGTTCCTCCAAAATTGCCTTCCTCC CTCCCTATAGTGAGTCGTATTA
<i>allUG s</i>	TAATACGACTCACTATAGGGAGGGAGGAATGTGATTTTGGAGGAACTA CAGAATGTGTATCGCAGCTAAAATGTGATTTTGGAGGAACTACAGAAT GTGTGTATCTGTGTGTGAAGGG
<i>allUG as</i>	CCTTCACACACAGATACACACATTCTGTAGTTCCTCCAAAATCACAT TTTAGCTGCGATACACATTCTGTAGTTCCTCCAAAATCACATTTCCTCC CTCCCTATAGTGAGTCGTATTA
<i>ANKRD17_stem fwd</i>	TAATACGACTCACTATAGGGAGTAAGCTCTGTCCGAAGGCAGCTTTTT GTCA
<i>ANKRD17_stem rev</i>	TACTGTAAGCGCATAGGATATGTGGCATTGTGGGTGC
<i>101-mer_stem fwd</i>	TAATACGACTCACTATAGGGAGTAAGCAGGGAGGAAGGCAATTTTGG GGA
<i>101-mer_stem rev</i>	TACTGTAAGCCCCTTTGTGTGTGGATAGCCG
<i>allUG_stem fwd</i>	TAATACGACTCACTATAGGGAGTAAGCAGGGAGGAATGTGATTTTGG GGA
<i>allUG_stem rev</i>	TACTGTAAGCCCCTTCACACACAGATACACACATTCTGTAGTTC
<i>T7, stem, tag fwd</i>	TAATACGACTCACTATAGGGAGTAAGCCGAGTAGACAAGACAAGTAGC
<i>Stem tag rev</i>	TACTGTAAGCCC GCGGATCAGACTCGA

Cloning oligonucleotides

Stable sponges

<i>1x/2xANKRD17 1</i>	TGACATGATATCCGAGTAGACAAGACAAGTAGCTCTGTCCGAAGGCAG CTTTTTGTGCAGTTGTGAAGACATCCAATCGCCACACAACAACAGTC ACAACCACGGCAAGCAACAAC
<i>1xANKRD17 2</i>	CATACTCCGCGGATCAGACTCGACGCTAGCGCATAGGATATGTGGCAT TTGTGGGTGCAGTGTGTTGTTGCTTGCCGTGGTTG

<i>2xANKRD17 2</i>	GTGGCGATTGGATGTCTTCACAACCTGTGACAAAAAGCTGCCTTCGGAC AGACTGAGTGCTGACGACGCATAGGATATGTGGCATTGTGGGTGCAG TGTTGTTGTTGCTTGCCGTGGTTG
<i>2xANKRD17 3</i>	TGAAGACATCCAATCGCCACACAACAACAGTCACAACCACGGCAAGCA ACAACAACACTGCACCCACAAATGCCACATATCCTATGCGCTAGCGTC GAGTCTGATCCGCGGAGTATG
<i>1x/2xallUG 1</i>	TGACATGATATCCGAGTAGACAAGACAAGTAGCAGGGAGGAATGTGAT TTTGGAGGAACTACAGAATGTGTATCGCAGCTAAAATGTGATTTTGA GGAACTACAGAATGTGTG
<i>1xallUG 2</i>	CATACTCCGCGGATCAGACTCGACGCTAGCCCGTTCACACACAGATAC ACACATTCTGTAGTTCCTC
<i>2xallUG 2</i>	CCTCCAAAATCACATTTTAGCTGCGATACACATTCTGTAGTTCCTCCA AAATCACATTCTCCCTCTGAGTGCTGACGACCCGTTACACACAGAT ACACACATTCTGTAGTTCCTC
<i>2xallUG 3</i>	CTAAAATGTGATTTTGGAGGAACTACAGAATGTGTGTATCTGTGTGTG AACGGGCTAGCGTCGAGTCTGATCCGCGGAGTATG
<i>ANKRD allUG fwd</i>	TGACATGATATCCGAGTAGACAAGA
<i>ANKRD allUG rev</i>	CATACTCCGCGGATCAGAC

Tornado circRNAs

<i>Torn-ANKRD17 1</i>	TGATATGGGTCCCCGAGTAGACAAGACAAGTAGCTCTGTCCGAAGGCA GCTTAATGTCACAGTTGTGAAGACATCCAATCGCCACACAACAACAGT CA
<i>Torn-ANKRD17 2</i>	CATATTGGGACCCGCGGATCAGACTCGACGCTAGCGCATAGGATATGT GGCATTGTGGGTGCAGTGTGTTGTTGCTTGCCGTGGTTGTGACTGT TGTTGTGTGGCG
<i>Torn-101-mer s</i>	GGCCGCGGGAGGGAGGAAGGCAATTTAGGAGGAACTACAGAACACATA TCGCAGCTAAAACACAATTTAGGAGGAACTACAGAATGCGGCTATCCA CACACAAAGGGCCGC
<i>Torn-101-mer as</i>	GGCCCTTTGTGTGTGGATAGCCGATTCTGTAGTTCCTCCTAAATTGT GTTTTAGCTGCGATATGTGTTCTGTAGTTCCTCCTAAATTGCCTTCCT CCTCCCGC
<i>Torn-allUG s</i>	GGCCGCGGGAGGGAGGAATGTGATTTAGGAGGAACTACAGAATGTGTA TCGCAGCTAAAATGTGATTTAGGAGGAACTACAGAATGTGTGTATCTG TGTGTGAAGGGCCGC
<i>Torn-allUG as</i>	GGCCCTTCACACACAGATACACACATTCTGTAGTTCCTCCTAAATCAC ATTTTAGCTGCGATACACATCTGTAGTTCCTCCTAAATCACATTCTC CCTCCCGC
<i>ANKRD NotI fwd</i>	TGATATGCGGCCCGCCGAGTAGACAAGACAAGTAGCTC
<i>ANKRD SacII rev</i>	GACCCGCGGATCAGACTC

FLAG-tagged IMP3

<i>3xFLAG pDEST s</i>	GGTACCACCATGGACTACAAAGACCATGACGGTGATTATAAAGATCAT GACATCGATTACAAGGATGACGATGACAAGGGAGGCTCAGGAGGCG
<i>3xFLAG pDEST as</i>	TCGACGCCTCCTGAGCCTCCCTTGTTCATCGTCATCCTTGTAATCGATG TCATGATCTTTATAATCACCGTCATGGTCTTTGTAGTCCATGGTGGTA CCGC
<i>3xFLAG pDEST KPCR fwd</i>	ATGACGATGACAAGGGAGGC
<i>3xFLAG pDEST KPCR rev</i>	GTAGCCAGTCTTCACCAGGA

2.6 Markers

Marker	Supplier
GeneRuler 1 kb DNA Ladder	Thermo Scientific
GeneRuler DNA Ladder Mix	Thermo Scientific
GeneRuler Low Range DNA Ladder	Thermo Scientific
GeneRuler Ultra Low Range DNA Ladder	Thermo Scientific
peqGOLD Protein Marker IV	VWR Peqlab
Riboruler Low Range RNA Ladder	Thermo Scientific

2.7 Commercial kits

Kit	Supplier
Bioanalyzer DNA 1000 kit	Agilent
Bioanalyzer High Sensitivity DNA kit	Agilent
Bioanalyzer RNA 6000 Nano/Pico kit	Agilent
HiScribe T7 High Yield RNA synthesis kit	New England Biolabs
Luna Universal qPCR reaction mix	New England Biolabs
MiSeq Reagent Kit v3	Illumina
NEBNext rRNA Depletion Kit	New England Biolabs
NEBNext UltraTM II Directional RNA Library Prep Kit for Illumina	New England Biolabs
NE-PER nuclear and cytoplasmic extraction reagents	Thermo Scientific
Plasmid Plus Maxi kit	QIAGEN
ProNex Size-Selective Chemistry	Promega
QIAGEN Plasmid Plus Maxi Kit	QIAGEN
QIAprep Spin Miniprep kit	QIAGEN
QIAquick Gel Extraction kit	QIAGEN
qScript cDNA synthesis kit	Quantabio
Qubit dsDNA HS Assay kit	Invitrogen
Qubit RNA BR Assay kit	Invitrogen
RNeasy Mini kit	QIAGEN

2.8 Chemicals and reagents

Reagent	Supplier
[α - ³² P]-UTP (5000 Ci/mmol, SCP-310)	Hartmann Analytic
[γ - ³² P]-ATP (800 Ci/mmol, SCP-801)	Hartmann Analytic
Actinomycin D	Sigma-Aldrich
Agarose	Roth
Ammonium persulfate (APS)	BioRad
Ampicillin	Roth
AMPure XP (beads)	Beckman Coulter
Bicine	Roth

Blasticidin	Thermo Scientific
Boric acid	Roth
Bovine serum albumin (BSA)	Roche
Bromphenol blue	Merck
Calcium chloride dihydrate	Roth
Chloroform	Roth
cOmplete ULTRA tablets (protease inhibitor)	Roche
Deoxynucleotide triphosphates (dNTPs)	Peqlab
Digitonin	Sigma-Aldrich
Dimethyl pyrocarbonate (DMPC)	Sigma-Aldrich
Dimethylsulfoxide (DMSO)	Roth
Dithiothreitol (DTT)	Roth
Dulbecco's Modified Eagle's medium (DMEM)	Gibco
ERCC RNA Spike-In Mix 1	Invitrogen
Ethanol (EtOH)	Roth
Ethidium bromide	Roth
Ethylenediaminetetraacetic acid (EDTA)	Roth
Fetal bovine serum (FBS)	Gibco
Formaldehyde	Roth
Glycerol	Roth
Glycine	Roth
Glycoblue	Thermo Scientific
Glycogen	VWR Peqlab
Halt protease inhibitor cocktail	Thermo Scientific
HEPES	Roth
Hygromycin	Thermo Scientific
Igepal CA-630 (NP-40)	Sigma-Aldrich
Imidazole	Roth
InstantBlue Protein Stain	Expedeon
Isopropanol	Roth
Isopropyl- β -D-thiogalactopyranosid (IPTG)	Roth
LB-Agar	Roth
Lipofectamine 2000 transfection reagent	Invitrogen
Lipofectamine RNAiMAX transfection reagent	Invitrogen
Lumi-Light (PLUS) Western blotting substrate	Roche
Magnesium chloride (MgCl ₂)	Merck
Magnesium sulphate	Roth
Methanol	Roth
Milk powder (fat-free)	Roth
MOPS	Roth
MyONE Silane beads	Invitrogen
Ni-NTA agarose	QIAGEN
Nukleotides (dNTP mix, single NTPs, GMP)	VWR, Roche, Sigma-Aldrich
NuPAGE LDS sample buffer	Invitrogen

NuPAGE sample reducing agent	Invitrogen
OptiMEM	Gibco
Orange G	Roth
PEG400	Roth
Phenol/chloroform/isoamylalcohol (25:24:1)	Roth
PhiX Control v3	Illumina
Phosphate-buffered saline (PBS), X10	Gibco
Potassium chloride (KCl)	Roth
Protein-A/G dynabeads	Thermo Scientific
RLT buffer	QIAGEN
Rotiphorese gel 30% (37.5:1)	Roth
Rotiphorese gel 40% (19:1)	Roth
Sodium acetate	Merck
Sodium chloride (NaCl)	Roth
Sodium di-hydrogen phosphate monohydrate	Roth
Sodium dodecyl sulfate (SDS)	Roth
Sodium hydroxide (NaOH)	Roth
Super Optimal Broth (SOC) medium	Invitrogen
SYBR Gold solution	Roche
Tetracycline	Sigma-Aldrich
Tetramethylethylenediamine (TEMED)	Biorad
Tris(hydroxymethyl)aminomethane (Tris)	Roth
TRIzol LS	Invitrogen
TRIzol reagent	Invitrogen
Trypsin-EDTA solution	Gibco
Tryptone	Roth
TurboFect transfection reagent	Thermo Scientific
Tween 20	Sigma-Aldrich
Urea	Roth
Yeast extract	Roth
Yeast tRNA	Roche
β -mercaptoethanol	Sigma-Aldrich

2.9 Laboratory equipment

Equipment	Company
Agfa Curix 60 processing machine (developing machine)	AGFA
Bioanalyzer 2100	Agilent
BLX 254 UV-crosslinker	Biobink
C25 incubator shaker	New Brunswick Scientific
Centrifuge Heraeus Fresco 21	Thermo Scientific
Criterion cell (midi electrophoresis system)	Bio-Rad
Excella Eco-170 CO ₂ incubator	New Brunswick Scientific
G:Box gel documentation	Syngene

Heraeus Multifuge X1R centrifuge	Thermo Scientific
InLab Expert Pro-ISM pH meter	Mettler Toledo
Micropipettors (0.5 µl to 1000 µl)	Eppendorf, Gilson
Mini PROTEAN electrophoresis system	Bio-Rad
Moxi Z Mini automated cell counter	ORFLO Technologies
NanoDrop 1000 spectrophotometer	Thermo Scientific
NuPAGE electrophoresis and blotting system	Invitrogen
Pipetus pipet filler	Hirschmann
QuantStudio 3 Real-Time PCR system	Thermo Scientific
Qubit 2.0 fluorometer	Invitrogen
Realplex Mastercycler (thermocycler)	Eppendorf
StepOnePlus Real-Time PCR system	Thermo Scientific
Subcell GT agarose gel system	Bio-Rad
SureBeads magnetic rack	Bio-Rad
Systec DB-23 autoclave	Systec
Thermo Scientific Safe 2020 (laminar flow)	Thermo Scientific
ThermoMixer C	Eppendorf
TMS inverted phase contrast microscope	Nikon
Trans-Blot semi-dry transfer cell	Bio-Rad
Trans-Blot Turbo transfer system	Bio-Rad
Tri-Carb 1600TR liquid scintillation counter	Packard Instrument
Typhoon FLA 9500 Phosphorimager system	GE Healthcare
Veriti thermal cycler	Applied Biosystems

2.10 Consumables

Consumables	Supplier
Cell culture dishes (10, 15 cm)	Greiner
Cell culture plates (6, 12 wells)	Greiner
Costar Spin-X centrifuge tube filters	Corning Incorporate
Eppendorf tubes (1.5 ml, 2 ml; Safe Lock)	Sarstedt
Falcon tubes (15 ml, 50 ml)	Sarstedt
High performance autoradiography films	GE Healthcare
High performance chemiluminescence films	GE Healthcare
MicroAmp fast optical 96-well reaction plate	Thermo Scientific
MicroAmp optical adhesive film	Thermo Scientific
Mini Quick Spin RNA columns	Roche
Multiply PCR strips and lids	Sarstedt
Needles	Braun
Phase lock gel tubes	5Prime
Pipette tips (10, 20, 2000, 1250 µl)	Sarstedt
qPCR seal optical clear films	VWR
qPCR semi-skirted plates	VWR
Rotilabo syringe filters (0.45 µm)	Roth

Sterile serological pipettes (5, 10, 25, 50 ml)
Syringes

Greiner
Braun

3 Methods

3.1 Cloning of DNA fragments into *E. coli*

3.1.1 Preparation of plasmid DNA

Plasmid DNA was isolated using the QIAGEN Plasmid Plus Maxi Kit from 50 ml of *E. coli* cell culture, grown overnight in LB medium containing 100 µg/ml ampicillin at 37°C, 200 rpm. DNA concentration and purity of plasmid DNA was determined by UV spectrometry at 260 nm and 280 nm. Correct sequence of purified plasmids was ensured by sequencing (Microsynth Seqlab) and alignment to generated plasmid maps.

3.1.2 Enzymatic restriction digest

DNA samples were digested with respective restriction enzymes (New England Biolabs) using 3 to 4 units of enzyme per µg DNA. The digestion mix was incubated at 37°C for 1 h and DNA purified via agarose gel extraction.

3.1.3 Agarose gel extraction

Agarose and samples were prepared as described in 3.4.6. Agarose concentration was adjusted to DNA fragment size, i.e. 0.8% were used for plasmid and 2% for inserts. For DNA markers, the GeneRuler DNA Ladder Mix or GeneRuler 1 kb DNA Ladder were used. Gels were run at 120V in 0.5x TBE and visualised with a gel documentation system (SynGene). Appropriate DNA bands were cut with a scalpel and DNA purified using the QIAquick Gel Extraction kit. Concentration of DNA was determined by UV spectrometry at 260 nm.

3.1.4 Ligation

Ligations of the insert with the vector were performed in a molar ratio of 3:1 or 5:1. 50 ng of vector DNA were used for a 20 µl reaction using 1 µl T4 DNA ligase. The ligation reactions were incubated overnight at 16°C.

3.1.5 Transformation

10 µl of ligation reaction or 50 ng of intact plasmid were added to 50 µl chemically competent *E. coli* KRX or TOP10 cells. Transformation was performed according to the manufacturer's instructions. Appropriate volumes of bacteria suspension were spread on LB plates containing 100 µg/ml ampicillin and incubated overnight at 37°C or for 2 – 3 days at room temperature.

3.1.6 Screening and analysis of bacterial clones

Multiple bacterial clones were picked and analysed for plasmid content. This was done by colony-PCR or enzymatic restriction digest. For colony PCR, a standard *Taq* polymerase-

mediated PCR with 30 cycles was applied with a few bacterial cells as DNA template and primers amplifying the region of interest. The results were then analysed by agarose gel electrophoresis. Selected positive clones were transferred into 5 ml LB-Amp medium and grown overnight at 37°C, 200 rpm. Plasmids were isolated using the QIAprep Spin Miniprep kit. If analysis occurred via enzymatic restriction digest, single colonies were picked and directly transferred into 5 ml LB-Amp medium, grown overnight, and plasmid-DNA isolated as described. Obtained RNA was then analysed by test enzymatic digestion with subsequent agarose gel electrophoresis. Either way, isolated plasmid DNA of one positive clone was sent for sequencing (Microsynth Seqlab) and DNA sequence compared to expected sequence.

3.2 Design and generation of constructs

3.2.1 *In vitro* circRNA sponge T7 templates

Previous work from our lab revealed an IMP3 RNA-binding motif based on SELEX analysis (Schneider *et al.*, 2019). The natural target ANKRD17 comprising the RNA-recognition sequence was taken as a comparison to synthetic 101-mer RNAs (Schneider *et al.*, 2019). In this thesis, the sequence extracted of ANKRD17 (121 nt) was compared to two synthetic 101-mer sequences harbouring either the same RNA-recognition elements (called 101-mer) or mutated elements (allUG). Sequences needed as templates for *in vitro* transcription were ordered as oligonucleotides (Sigma-Aldrich). Oligonucleotides were annealed by diluting equal amounts of respective sense and antisense strand in oligo annealing buffer (10 mM Tris pH 7.5, 50 mM NaCl) and denaturing them at 95°C for 3 min with subsequent slow cool down to 25°C within 39 min (annealed oligonucleotides were provided by Tim Schneider). Stem sequence and a T7 promoter were attached by PCR using 1 ng of DNA (annealed oligonucleotides or plasmid) as template. Quality of PCR products were controlled by agarose gel electrophoresis and DNA purified either by gel extraction (as described in 3.1.3) or directly by addition of 5 volumes of PB buffer (QIAprep Spin Miniprep Kit) and subsequent column purification (QIAquick Gel Extraction kit). Templates were quantified using UV spectrometry at 260 nm.

3.2.2 Design of IMP3 sponges for stable *in vivo* expression

Genomic integration of IMP3 sponge sequences was performed to achieve stable, inducible expression of circRNAs. Since endogenous circRNAs consist on average of two to three exons and are therefore rather large (Wilusz, 2018), constructs harbouring one or two repeats of the respective sponge sequence were generated. The sequence extracted of the endogenous

ANKRD17 RNA was chosen as an IMP3 sponge and the allUG construct as a control sponge (as in 3.2.1). A short spacer of 15 nt was included between the two repeats of the sponge sequence. In addition, flanking sequences were attached to mediate cloning and detection by PCR. Constructs were ordered as two (1xANKRD17/allUG) or three (2xANKRD17/allUG) oligonucleotides (Sigma-Aldrich) with overlapping regions. Equimolar amounts of corresponding oligonucleotides were mixed and amplified using Phusion DNA polymerase. PCR products were gel-extracted from agarose gels (3.1.3) and used as inserts for cloning. The vector pcDNA3.1(+)-ZKSCAN1-MCS (Addgene; Kramer *et al.*, 2015) containing inverted repeats necessary for circRNA generation was used for the first cloning step. Vector and plasmid were cleaved with *EcoRV*-HF and *SacII* and cloning procedure performed as described (3.1). Constructs plus the flanking inverted repeats were then cut out by *HindIII* and *XhoI* and re-cloned into a pcDNA5/FRT/TO genomic integration vector (Invitrogen) without the BGH polyadenylation site (deletion performed by Silke Schreiner). Stable cell lines were generated using these plasmids (see 3.3.4).

3.2.3 Cloning of Tornado sponge constructs

Transient overexpression of circRNAs was mediated by the Tornado system (Litke and Jaffrey, 2019). In principle, the same sequences were used as in 3.2.1, but U stretches containing more than three uridines were partially altered to adenine residues to prevent premature stop of transcription by DNA polymerase III *in vivo*. In addition, the ANKRD17 construct contained flanking tag sequences as in 3.2.2 to prevent mispriming during PCR to the endogenous RNA. All constructs were ordered as oligonucleotides (Sigma-Aldrich) and annealed as described in 3.2.1 (101-mer, allUG) or amplified by PCR as in 3.2.2 (ANKRD17). Generation of Tornado constructs was achieved by cloning between the *NotI* and *SacII* sites of the pAV-U6+27-Tornado-Broccoli (Addgene; Litke and Jaffrey, 2019) vector, replacing the Broccoli aptamer sequence.

3.2.4 Cloning of FLAG-IMP3 for transient expression in ES-2 cells

For iCLIP experiments, a FLAG-tagged IMP3 was used since attempts to target the endogenous protein did not work (data not shown). The available pDEST-mycIGF2BP3 vector (Addgene; Landthaler *et al.*, 2008) was used as the initial plasmid. The N-terminal myc-tag was removed and replaced by a triple FLAG-tag, thereby also eliminating regions necessary for the gateway cloning technique and instead introducing nucleotides coding for four glycines and one serine to gain a short flexible linker region (resulting in 7 amino acids in total between the FLAG sequence and the IMP3 start codon). The FLAG-tag sequence was ordered as oligonucleotides

(Sigma-Aldrich) with overlapping ends after annealing (procedure as described in 3.2.1), making it suitable for ligation. Cutting of the vector pDEST-mycIGF2BP3 was performed with *SacII* and *SalI*-HF and cloning performed as described (3.1).

3.3 Eukaryotic cell culture methods

3.3.1 Cultivation

All cells were cultivated at 37°C in a humidified atmosphere containing 5% CO₂. Dulbecco's Modified Eagle's Medium (DMEM) was supplied with 10% (v/v) heat-inactivated fetal bovine serum (FBS) and used as media for all cell lines. For cultivation of HeLa Flp-In T-REx cell lines, medium was additionally supplemented with 500 µg/ml hygromycin and 5 µg/ml blasticidin. Cells were split twice a week to prevent overgrowing. For this, cells were washed once with PBS and incubated with trypsin-EDTA solution at 37°C until detachment. Detached cells were resuspended into medium and appropriate volumes of cell suspension seeded into new dishes containing fresh medium.

3.3.2 Transfection of cells with plasmid DNA

Cells were harvested, counted with a cell counter, and desired number seeded one day prior transfection ("forward" transfection) or directly transfected ("reverse" transfection). 10 or 20 µg plasmid DNA were used for transfection of cells in 10 or 20 cm dishes, respectively. Transfection was mediated by the lipid-based transfection reagents TurboFect (for Tornado constructs) or Lipofectamine2000 (for FLAG-IMP3 and generation of stable cell lines) according to the manufacturer's protocol. Mock transfection was performed only with OptiMEM. Medium was exchanged 4 – 6 h after transfection to remove non-absorbed lipid-DNA-complexes. After a specific time period, cells were harvested as described in 3.3.1 and counted if desired. Cells were pelleted by centrifugation (300×g, 5 min, 4°C) and medium discarded. Cell pellets were either resuspended directly in TRIzol for isolation of total RNA or washed with PBS if used for RIP assays or subcellular fractionation. If not processed directly, cell pellets were snap-frozen with dry ice or liquid nitrogen and stored at -80°C.

3.3.3 Transfection of cells with RNA

Transient IMP3 knockdown was mediated by transfection of ES-2 cells with siRNA duplexes. One day prior transfection, 5x10⁵ (10 cm dish) or 8x10⁴ (6-well) ES-2 cells were seeded. Lipid-based transfection was performed using RNAiMAX and 300 pmol (10 cm dish) or 50 pmol (6-well) IMP3 or luciferase (control) targeting siRNAs according to the manufacturer's

instructions. Cells were harvested 72 h after transfection and a defined number subjected to subcellular fractionation (3.7.2). Alternatively, cells were treated with actinomycin D (5 µg/ml) for different time periods and RNA isolated using TRIzol (3.4.2). In addition, knockdown was analysed by SDS-PAGE and Western blotting (3.6.3) of cell lysate. The data presentation and curve fitting of *MYC* mRNA decay with a first-order decay function was performed with OriginPro (OriginLab).

For transfection of *in vitro* produced circRNAs, 3×10^5 (6-well) ES-2 cells were seeded one day prior transfection. Transfection was performed using Lipofectamine2000 or only OptiMEM (mock). Medium was exchanged 4 – 6 h after transfection to remove non-absorbed lipid-DNA-complexes. Cells were harvested 24 h after transfection and subcellular fractionated (3.7.2).

3.3.4 Generation of HeLa Flp-In T-REx stable cell lines

For stable expression of circular IMP3 sponges, the Flp-In T-REx system (Invitrogen) was used. HeLa Flp-In T-REx cells as well as needed materials were a kind gift of Lienhard Schmitz, JLU Gießen. In this system, HeLa cells are genetically modified to stably express a tetracycline repressor and contain a Flp recombination target (FRT) site. The first step of generating stable cell lines expressing the gene of interest (GOI) is a cotransfection of a Flp recombinase expression plasmid (pOG44) and the vector pcDNA5/FRT/TO containing the GOI expressed by a tetracycline inducible CMV promoter, a FRT site, as well as a hygromycin resistance. When both plasmids are taken up by a cell, homologous recombination is catalysed by the Flp recombinase between the FRT sites of the pcDNA5/FRT/TO plasmid and the genome. Cells containing the gene of interest are then selected based on the newly gained hygromycin resistance.

In this thesis, two sponge constructs (1xANKRD17, 2xANKRD17) as well as two control constructs (1xallUG, 2xallUG) were cloned in pcDNA5/FRT/TO plasmids containing inverted repeats for circRNA formation (see 3.2.2). 3×10^5 HeLa Flp-In T-REx cells were seeded in a 6 cm dish one day before transfection. The transfection was performed with a mix of Lipofectamine2000, 7.2 µg pOG44 and 0.8 µg of the respective pcDNA5/FRT/TO–BGH plasmid diluted in Opti-MEM. Medium was exchanged 6 h after transfection to remove unabsorbed material. Two days after transfection, cells were expanded to a 10 cm dish and medium changed to selection medium containing 100 µg/ml hygromycin. The selection process was intensified after several days by increasing the hygromycin concentration to 500 µg/ml and adding 5 µg/ml blasticidin, the latter is needed for maintenance of the tetracycline repressor. When cell clusters were recognisable, several were picked and cultured separately in high

hygromycin containing medium until a decent number of cells were grown. Four of these clones were tested for each cell line: First, expression of circRNA was induced with 1 µg/ml tetracycline for 24 h and RNA isolated. Then, RT-PCR with primers targeting precursor, circular, or 'total' (i.e. both linear and circular) RNA was performed. Cell clones with best circRNA expression were chosen for each cell line (data not shown). A time course was performed to determine the optimal time span for tetracycline induction.

3.4 General RNA-related methods

3.4.1 Analysis by denaturing polyacrylamide gel electrophoresis

In vitro produced transcripts or total RNA of Tornado transfected cells were visualised with denaturing urea polyacrylamide gel electrophoresis (PAGE). Samples for testing were mixed with one volume of 2x formamide RNA loading buffer (80% formamide, 10 mM EDTA pH 8.0, 0.025% (w/v) bromphenol blue) and denatured for 3 min at 95°C. Denaturing polyacrylamide (PAA) gels were cast using the Mini-PROTEAN electrophoresis system (Bio-Rad). Gels were prepared by mixing of a urea PAA solution (20% acrylamide (19:1 acrylamide/bisacrylamide) and 50% (w/v) urea in 1x TBE buffer) with a urea buffer solution (50% (w/v) urea in 1x TBE) in the desired ratio. Polymerisation was induced by adding 100 µl of 10% (w/v) ammonium persulfate (APS) and 10 µl of tetramethylethylenediamine (TEMED) per 10 ml of the PAA gel solution. The gels were pre-run for 10 minutes at 300 V in Mini-PROTEAN electrophoresis chambers (Bio-Rad) in 1x TBE running buffer (89 mM Tris, 89 mM boric acid, 2 mM EDTA) prior to sample loading. RNA was then electrophoresed for 30 – 45 minutes at 300 V. For size comparison, the reference marker Riboruler Low Range RNA Ladder or GeneRuler Ultra Low Range DNA Ladder was used. If radioactively labelled RNA was visualised, autoradiography was performed. For detection of non-labelled RNAs, gels were stained with ethidium bromide or SYBR Gold and documented with the SynGene Genetools program on a G:Box gel documentation system.

3.4.2 Isolation of cellular RNA

Cellular RNA was extracted with TRIzol and subsequently precipitated with isopropanol or (if desired RNA fragments were larger than 200 nt) purified with the RNeasy Mini kit according to the manufacturer's instructions. If the RNeasy Mini kit was not used and/or cells were transfected with plasmid DNA, samples were treated with RQ1 DNase at 37°C for 30 min to remove remaining DNA. After that, RNA was phenolised by adding one volume of

phenol/chloroform, mixed by vortexing, and centrifuged for 5 min at 20,000×g. The upper aqueous phase was transferred to a new reaction tube and mixed with 0.1 volumes of 3 M sodium acetate (pH 5.2), 3 volumes of ethanol, and 1 µl glycogen. Samples were precipitated at -20°C for at least 20 min and centrifuged (21,000×g, ≥ 30 min, 4°C). Pellets were washed with 70% ethanol and centrifuged ≥ 5 min as before. Dried pellets were dissolved in DMPC-treated milliQ water.

3.4.3 Quantification

RNA concentration was measured on a NanoDrop1000 spectrophotometer by absorption at 260 nm (total RNA) or with a Qubit 2.0 Fluorometer using the Qubit RNA BR (Broad-Range) assay kit (total RNA/ transcripts). For radioactive RNAs, the relative incorporation of [α -³²P]-UTP was determined by scintillation counting of the transcripts and comparison to the input. Transcription yield was then calculated employing the following equation:

$$mass_{RNA}[ng] = concentration_{unlabelled\ UTP} [\mu M] \times reaction\ volume [\mu l] \times incorporation [\%] \times 0.0132$$

3.4.4 Reverse transcription (RT)

For analysis of total RNA by (quantitative) PCR, RNA was first reverse-transcribed using random hexamer and oligo(dT) priming. For this, the qScript cDNA synthesis kit was used according to the manufacturer's protocol. Typically, 50 ng – 1 µg total RNA or 10% of RNA from RIP assays were taken per reaction. For cytoplasmic/nuclear fractionation of Tornado-transfected HeLa cells, equivalents were used for reverse transcription.

3.4.5 PCR

Semi-quantitative polymerase chain reaction (PCR) was performed with cDNA from the RT reaction. Primers were designed by employing the program primer 3. For detection of linear mRNAs, primers were set in two different exons to ensure the detection of spliced mRNAs. If circRNAs should be detected, divergent pairs of primers were designed. The PCR was performed in 25 µl reactions with 10% of RT reaction in *Taq* PCR buffer (10 mM Tris/HCl pH 9, 50 mM NaCl, 1.5 mM MgCl₂, 0.1% Triton X-100), 400 µM dNTPs (each), 0.5 mM MgCl₂, 0.8 µM primers (each), and 0.5 µl of *Taq* DNA polymerase (expressed and purified by Silke Schreiner). The following amplification profile was applied: denaturation at 95°C (2 min), 25 to 35 amplification cycles (20 sec at 95°C, 30 sec at 58°C, and 20-30 sec at 72°C), and a final elongation step (7 min at 72°C). The number of PCR cycles was set to 30 – 35 for RIP assays and reduced to 25 for the detection of expressed circRNAs.

3.4.6 Agarose gel electrophoresis

Agarose was melted in 0.5x TBE buffer (44.5 mM Tris, 44.5 mM boric acid, 1 mM EDTA), cooled down, and mixed with ethidium bromide (1:20,000 dilution, final concentration: 0.5 µg/ml). Samples were mixed with 6x DNA loading buffer (30 % glycerol, 3x TBE, 0.025% (w/v) bromophenol blue or orange G) prior to loading. The GeneRuler DNA Ladder Mix was used as a marker. Agarose gels (containing 2% agarose for PCR products) were run at 120V in 0.5x TBE and visualised with a gel documentation system (SynGene). For quantification of stably expressed IMP3 sponges in RIP assays, the Fiji software (Schindelin *et al.*, 2012) was used.

3.4.7 Quantitative PCR

Real-time PCR was performed using the Luna Universal qPCR Reaction Mix and the Realplex Mastercycler, QuantStudio 3 or StepOnePlus real time PCR systems. Primers were designed as described for semi-quantitative PCR (see 3.4.5) and suitability was tested by amplification efficiency determination and melting curve analysis. Measurements were performed with 10% cDNA from the RT reaction and conducted in triplicates, employing a two-step protocol. Average cycle threshold (Ct) values were used for calculations with the $\Delta\Delta C_t$ method. For normalisation, the Ct values of the reference genes GAPDH (total RNA and cytoplasmic fractions) or GANAB and FKBP10 (membrane organelle fractions) were used. In the mRNA stability experiment (actinomycin D treatment), 18S rRNA was used as a reference. In RIP assays, the fraction of bound target RNA was calculated by normalisation to the corresponding input fraction. To calculate the ratio of Tornado circRNAs in subcellular fractions, each fraction was also normalised to input fraction prior to calculation of the relative expression of RNAs in the extracts.

3.4.8 RNase R digestion

Circularity of synthetic circRNAs was examined by treatment with the exoribonuclease RNase R. 2.5 units RNase R per 1 µg RNA were used for the digestion, and the reaction mix was incubated for 30 min at 37°C. RNase R digested RNA was either purified or directly subjected to denaturing polyacrylamide electrophoresis (3.4.1).

3.5 RNA *in vitro* transcription and circularisation

3.5.1 Transcription of unlabelled RNA

IMP3 sponge templates for RNA transcription were generated as described above (3.2.1). *In vitro* transcription was performed with the HiScribe T7 High Yield RNA synthesis kit with the addition of GMP (40 mM). This 4-fold excess was employed to obtain mainly 5'-monophosphorylated transcripts, which are required for efficient RNA ligation.

3.5.2 Transcription of ³²P-labelled RNA

Radioactive *in vitro* transcription was performed using the same templates as for unlabelled RNA generation. RNA was synthesised with equal amounts of ATP, GTP and CTP (0.5 mM each), 0.04 mM UTP and 0.37 MBq (10 µCi) [α -³²P]-UTP. In addition, 10 mM DTT and a 4-fold excess of GMP (2 mM) was employed. Transcription was performed by T7 RNA polymerase with 1 µg of template DNA for 1 h at 37°C.

3.5.3 Purification of transcripts

Template DNA was removed by enzymatic digestion with RQ1 DNase for 30 min at 37°C. Transcribed RNA was purified with the Mini Quick Spin RNA columns and quantified as described (3.4.3).

3.5.4 CircRNA generation by ligation

Transcripts were ligated with T4 RNA ligase 1 at 16°C overnight. For this, max. 5 µg or 10 µl RNA was used in a 50 µl reaction. The reaction was supplemented with 15% DMSO, 1 mM ATP and RNase inhibitor. After ligation, RNA was extracted with phenol/chloroform and subsequently precipitated with ethanol.

3.5.5 CircRNA purification by gel extraction

To obtain pure circRNA for EMSA assays or transfection, RNA from the ligation reaction was subjected to denaturing urea PAGE (see 3.4.1). The exact position of RNA was determined by UV-shadowing (unlabelled RNA) or wrapping the gel in a plastic bag and exposing it to an autoradiography film in a film cassette with intensifying screen (³²P-labelled RNA). The film was then used as a template to cut the respective circRNA band from the gel. Gel pieces were transferred into 0.5 ml pierced tubes and crushed by centrifugation into 1.5 ml tubes. Elution of RNA was facilitated by addition of 400 µl PK buffer (100 mM Tris/HCl pH 7.5, 150 mM NaCl, 12.5 mM EDTA, 1% SDS) and shaking for 1 h at 50°C. Gel pieces were removed by centrifuging through Costar Spin-X centrifuge tube filters and phenol/chloroform extraction. To lower the volume, RNA was precipitated with ethanol.

3.6 General protein-related methods

3.6.1 SDS-PAGE

Proteins were gel electrophoresed using the discontinuous Laemmli system. An 8-10% acrylamide/bisacrylamide (37.5:1) solution was prepared in separating gel buffer (375 mM Tris/HCl pH 8.8, 0.1% SDS). Polymerisation was initiated by 0.01% APS and 0.005% TEMED. Stacking gels contained 5% acrylamide/bisacrylamide (37.5:1) solution in stacking gel buffer (125 mM Tris/HCl pH 6.8, 0.1% SDS) and polymerised as separating gels. Protein samples were diluted in 2x SDS loading buffer (100 mM Tris/HCl pH 6.8, 20% glycerol, 4% SDS, 5% β -mercaptoethanol, 0.025% (w/v) bromphenol blue) and boiled for 10 min prior to loading. Gel electrophoresis was performed using the Mini-PROTEAN (mini gels) or Criterion (midi gels) electrophoresis system. Gels were run in SDS running buffer (25 mM Tris/HCl pH 8.8, 192 mM glycine, 0.1% SDS) at 170 V (mini) or 200 V (midi) for 55 - 60 min. For size comparison, the peqGOLD Protein Marker IV was used.

3.6.2 Coomassie staining

For general detection of proteins, gels from 3.6.1 were stained with the InstantBlue Protein Stain (Coomassie solution). For this, gels were first washed three times with distilled water and heated briefly to remove excessive SDS. Afterwards, gels were covered in Coomassie staining solution and briefly heated in a microwave before shaking for 10 min at room temperature. Background staining was removed by repeated washing and heating in distilled water. Destained gels were transferred into transparent covers and scanned for documentation.

3.6.3 Western blot

For specific detection of proteins, Western blotting was performed. After SDS-PAGE, gels as well as nitrocellulose membrane and blotting paper was equilibrated in transfer buffer (25 mM Tris, 190 mM glycine, 0.023% SDS, 20% methanol). Equilibrated components were layered and transfer performed using the standard settings (25 V, 1.3 A, 30 min) of the Trans-Blot Turbo transfer system. Membranes were blocked for 1 h in milk solution (5% (w/v) milk powder in PBS-T (0.1% Tween 20 in PBS)) at room temperature. Incubation with primary antibodies diluted in milk solution (see 2.2) occurred overnight at 4°C. Excessive antibody was removed by washing three times for 10 min with PBS-T. Secondary antibodies were diluted 1:10,000 in milk solution and added to membranes for 1 h at room temperature. Membranes were washed as before and incubated with Lumi-Light or Lumi-Light^{PLUS} Western blotting substrate for 5 min. Excessive solution was removed and membranes exposed to Amersham Hyperfilm ECL for visualisation.

3.6.4 Purification of recombinant IMP3

E. coli BL21 cells were used to generate GST-His-tagged IMP3. First, cells were transformed with the IMP3-expression plasmid pGEX-6P2-GST-IMP3-FL-TEV-His (Schneider *et al.*, 2019) and cultured in 5 ml LB-Amp medium at 37°C, 225 rpm overnight. The next day, LB-Amp medium was supplemented with 1% of the overnight grown culture and grown at 37°C, 225 rpm until an OD_{600nm} of 0.4 – 0.6 was reached. Protein expression was induced with IPTG (1 mM final concentration) and cultured overnight at 16 – 20°C. OD_{600nm} was controlled and cells pelleted by centrifugation at 4°C. Pellets were then either processed directly or snap-frozen with liquid nitrogen and stored at -80°C.

Purification of recombinant IMP3 was performed with *E. coli* cell pellets from a 50 ml culture provided by Tim Schneider. First, cells were lysed in 10 ml lysis buffer (50 mM NaH₂PO₄, 2 M NaCl, 50 mM imidazole, 10 mM β-mercaptoethanol, 10% glycerin, 0.05% Tween 20) supplemented with protease inhibitor and lysozyme (1 mg/ml). Cell lysis occurred by incubation on ice for 30 min with occasionally vortexing and subsequent sonification. RNase A (10 µg/ml) and DNase I (5 µg/ml) plus MgCl₂ (25 mM) was added to cell lysate, mixed, and incubated for 15 min on ice. Then, lysate was centrifuged (21,000×g, 20 min, 4°C) and the supernatant filtered (0.45 µM filter). Purification of GST-His-tagged IMP3 was mediated by Ni-NTA agarose. Filtered lysate was added to equilibrated agarose beads and binding allowed for 60 min at 4°C with end-over-end incubation. Agarose beads were pelleted (400×g, 3 min, 4°C) and washed six times with 10 ml lysis buffer to remove unspecifically bound proteins. After washing, beads were resuspended in 1 ml lysis buffer and transferred to a chromatographic column. The flow-through was discarded and the column sealed before the beads were resuspended in 1 ml elution buffer (50 mM NaH₂PO₄, 300 mM NaCl, 250 mM imidazole, pH 8.0). Protein was eluted for 30 min at 4°C and eluate 1 collected. The elution was repeated for a second time. To remove imidazole, both eluates were combined and transferred into a dialysis tube. Dialysis was performed by stirring overnight at 4°C in 2 l dialysis buffer (20 mM Tris-HCl pH 7.8, 100 mM KCl, 0.2 mM EDTA, 20 % (v/v) glycerol, 1 mM DTT). Dialysed protein was aliquoted, snap-frozen in liquid nitrogen and stored at -80°C. Purification of IMP3 was controlled by SDS-PAGE and Coomassie staining (see 3.6.1 and 3.6.2). Quantification of purified IMP3 was mediated by comparing a BSA standard to different volumes of protein eluate via SDS-PAGE and Coomassie staining.

3.7 Subcellular fractionation of eukaryotic cells

3.7.1 Cytoplasm/nucleus fractionation of Tornado-transfected HeLa cells

HeLa cells were harvested 72 h after transfection with Tornado constructs. Prior to fractionation, 10 % of cells were taken for RNA extraction and 5 % for Western blot analysis as input samples. Remaining cells were pelleted (300×g, 5 min, 4°C) and the volume of the pellet estimated to be able to scale the buffer volumes of the employed NE-PER Nuclear and Cytoplasmic Extraction Kit. Together with the Halt protease inhibitor cocktail, the kit was used according to the manufacturer's instructions to prepare cytoplasmic and nuclear extracts. From both extracts, samples were taken for Western blot analysis and RNA extraction. Protein levels in input, cytoplasmic and nuclear fraction were analysed by Western blotting by loading 1 % of each fraction. RNA extraction was performed with TRIzol LS and subsequent isopropanol precipitation. RT-qPCR was used to analyse the distribution of Tornado-circRNAs with circ-specific primers and of the marker genes GAPDH (cytosol) and snoRD U78 (nucleus).

3.7.2 Cytoplasm/membrane organelle fractionation of ES-2 cells

ES-2 cells were harvested 72 h after siRNA treatment (control k.d. and IMP3 k.d., see 3.3.3) or seeding (wt and IMP3 k.o. cells). Cells were counted and the following number of cells used: 3×10^6 cells for extraction of total RNA ("input") and 6×10^6 cells for subcellular fractionation. In addition, cells of control and IMP3 k.d. were taken for Western blot analysis of knockdown efficiency. In the IMP3 sponge fractionation experiment, cells were transfected with Tornado plasmids or *in vitro* produced circRNA and harvested after 24 h. 1×10^5 cells were used for extraction of total RNA ("input") and 5×10^5 cells for subcellular fractionation. All cells were pelleted (100×g, 8 min, 4°C), washed with ice-cold PBS, pelleted again, and washed with 1 ml ice-cold PBS to transfer cells into 1.5 ml tubes. Here, cells were centrifuged as before and supernatant discarded. Pelleted cells for input samples were resuspended in TRIzol and stored at -20°C.

Subcellular fractionation of cells was performed according to Holden and Horton, 2009. Therefore, cell pellets were gently resuspended in digitonin buffer (50 mM HEPES pH 7.4, 150 mM NaCl, 25 µg/ml digitonin) and incubated end-over-end at 4°C for 10 minutes. Centrifugation of the cell suspension (2,000×g, 5 min, 4°C) was performed and supernatant transferred to a new tube. The supernatant corresponded to the cytosolic fraction. Parts of it were mixed with 2xSDS-LD (Western blot analysis) or TRIzol (RNA extraction) and stored at -20°C; the remaining supernatant was snap frozen with liquid nitrogen.

The cell pellet was washed twice with 1 ml PBS to be sure of removal of any remaining digitonin extract. The pellet was then resuspended into NP40 buffer (50 mM HEPES pH 7.4, 150 mM NaCl, 1% NP40) by vortexing and incubated for 30 min on ice. The cell suspension was centrifuged (7,000×g, 10 min, 4°C) to pellet nuclei and cell debris. The supernatant comprised membrane organelles such as endoplasmic reticulum, Golgi complex and mitochondria, and was transferred to a new tube. Again, samples for Western blotting and RNA extraction were taken and the remaining extract snap frozen. The nuclear/cell debris pellet was washed once with PBS and then either resuspended in TRIzol for RNA extraction or SDS-LD for protein analysis.

RNA purification of all samples was performed simultaneously with TRIzol and RNeasy Mini columns or, in the case of IMP3 sponges, with TRIzol, isopropanol precipitation and DNA digestion. Protein analysis by Western blotting was performed by loading equivalents of fractions. Digitonin concentration was optimised beforehand by fractionation of equal numbers of ES-2 wt and IMP3 k.o. cells with 0 – 200 µg/ml digitonin in the first buffer.

3.8 Electrophoretic mobility shift assay (EMSA)

EMSAs were performed with purified, recombinant IMP3 (see 3.6.4) and radioactively labelled linear or circular RNA (see 3.5), which was quantified by a scintillation counter (see 3.4.3). Binding reactions were conducted in binding buffer (10 mM Tris-HCl, pH 7.5, 150 mM NaCl, 0.5 mM EDTA, 0.5 mM DTT, 0.1% NP-40, 5% glycerol, supplemented with RNaseOUT, as well as 1 µg tRNA and 1 µg BSA as nonspecific competitors) containing 5 nM of labelled RNA and varying IMP3 concentrations ranging from 0 – 40 nM (ANKRD17, 101-mer) or 0 – 160 nM (allUG). The reactions were first incubated for 30 min at 25°C and then placed on ice for 5 min. Loading buffer (1x TBE, 0.025% bromophenol blue) was added to each sample prior to loading on a cold, native 5% TBE gel (containing 5% glycerol), which was pre-run for 20 min. Gel electrophoresis was performed for 45 min with 45 mA at 4°C. Visualisation of radioactive signals was conducted by the Typhoon FLA 9500 Phosphorimager system and intensities quantified. Curve fitting of raw data using the quadratic binding equation (Altschuler *et al.*, 2013) and K_D calculations from experimental triplicates were performed with OriginPro (OriginLab).

3.9 RNA immunoprecipitation (RIP)

In vivo binding of IMP3 to RNAs was examined by RNA-immunoprecipitation experiments. For circular RNA sponges, either HeLa Flp-In T-REx cells stably expressing ANKRD17 sponge constructs or HeLa cells transiently expressing Tornado sponge constructs were examined. The expression of circular RNAs in stable cell lines was induced with 1 µg/ml tetracycline for 3 days prior to harvesting. Transfection of Tornado sponge constructs was performed 8, 24 or 72 h before cells were collected. Validation of iCLIP experiments were performed with ES-2 cells transfected with FLAG-IMP3 or mock for 24 h to examine binding to RNA candidates to transiently expressed FLAG-IMP3 or endogenous IMP3, respectively.

For all RIP experiments, cells were harvested using trypsin-EDTA (see 3.3.1) and counted. Equal numbers of cells were collected, pelleted, and washed once with PBS. Cell pellets were either processed directly or snap frozen in liquid nitrogen and stored at -80°C. Cell lysis was achieved by resuspending pellets in RIPA buffer (50 mM Tris-HCl pH 7.4, 150 mM NaCl, 5 mM EDTA, 1% NP-40, 0.1% SDS, protease inhibitor) and incubation on ice for 15 min with vortexing in between. Insoluble material was removed by centrifugation (21,000×g, 20 min, 4°C) and supernatant was filtered through a 0.45 µm membrane-filter. Lysate was pre-cleared by end-over-end incubation with protein G dynabeads for 15 min at 4°C. Beads were removed by putting samples on the magnetic stand and transferring the supernatant to new tubes. Here, input samples were taken for Western blot analysis (2%) and RNA extraction (5%). Pre-cleared lysates were then split for immunoprecipitation of target proteins (i.e. IMP3, FLAG-IMP3, or IMP1) or mock controls (anti-FLAG antibody except for FLAG-IMP3 experiments, here anti-c-Myc antibody). After the addition of equal amounts of antibodies to equal volumes of cell lysates, all samples were supplemented with RNaseOUT and incubated end-over-end at 4°C overnight. The next day, precipitated complexes were removed by centrifugation (21,000×g, 10 min, 4°C) and protein G (IMP3, IMP1, FLAG as negative control) or protein A (FLAG-IMP3, c-Myc control) dynabeads added. Samples were incubated on a wheel for 2 h at 4°C. Protein-RNA complexes were washed multiple times with TBS-T (50 mM Tris-HCl pH 7.4, 150 - 600 mM NaCl, 0.05% Tween 20) by increasing the stringency up to 600 mM NaCl. To examine protein pulldown, Western blot IP samples were taken from the last wash. Remaining beads were subjected to RNA extraction with TRIzol. To examine binding to circRNA sponges, TRIzol extracted RNA was precipitated with isopropanol. For iCLIP validation, purification by RNeasy Mini columns (see 3.4.2) was performed after TRIzol extraction. Either way, RNA was

further purified by DNase digestion (3.4.2) and precipitated again with ethanol. RNA pellets were dissolved in 20 μ l DMPC-H₂O and equivalents used for RT-(q)PCR analysis.

3.10 Library preparation for RNA-seq

Subcellular fractionated ES-2 cells were analysed by high-throughput sequencing. For each cell type (i.e. ES-2 wt, ES-2 IMP3 k.o., ES-2 control k.d., and ES-2 IMP3 k.d., see 3.7.2), the cytosol and membrane organelle fraction as well as unfractionated (“input”) cells were used for RNA library preparation. RNA quality was first controlled by Bioanalyzer measurements using the RNA 6000 Nano kit and concentrations determined using a Qubit fluorometer (3.4.3). Then, the ERCC RNA Spike-In Mix 1 was added to 1 μ g of each sample according to the manufacturer’s instructions. Samples were first depleted of ribosomal RNA using the NEBNext rRNA Depletion Kit as described in the manual and depletion controlled by Bioanalyzer measurements with the RNA 6000 Pico kit. Libraries were prepared using the NEBNext UltraTM II Directional RNA Library Prep Kit for Illumina according to the manufacturer’s instructions. Within the protocol, the only modification was the usage of AMPure XP beads instead of NEBNext Sample Purification beads for cDNA/PCR product purification. The following NEBNext index primers were used:

	Input	Cytosol	MO
ES-2 wt	#37	#38	#39
ES-2 IMP3 k.o.	#40	#41	#36
ES-2 ctr k.d.	#43	#44	#45
ES-2 IMP3 k.d.	#46	#47	#48

Libraries were quality controlled with the DNA 1000 kit run on a Bioanalyzer and concentrations measured using the Qubit dsDNA HS Assay kit. Sequencing was performed on an Illumina NextSeq 500 (single-end read, 150 bp) in the Max Planck Institute in Bad Nauheim.

3.11 Individual-nucleotide resolution crosslinking and immunoprecipitation (iCLIP)

RNAs bound by IMP3 in subcellular fractionated ES-2 cells were determined by iCLIP experiments according to the iCLIP2 protocol (Buchbender *et al.*, 2020) with minor modifications.

Step 1: UV-crosslinking and cell lysis

First, several 10 cm dishes of ES-2 cells were transfected with FLAG-IMP3 (3.3.2). 24 h after transfection, cells were washed twice with PBS. Liquid was removed and cells were irradiated with 300 mJ/cm² UV light at 254 nm for crosslinking of proteins to nucleic acids. Cells were harvested in PBS using a cells scraper and washed again twice with PBS. Pelleted cells were either subjected to cell lysis with RIPA buffer (as in RIP assays, see 3.9) or subcellular fractionated (3.7.2).

Step 2: DNA and partial RNA digestion

Cell extracts were diluted 1:2 with RQ1 buffer (40 mM Tris/HCl pH 8, 10 mM MgSO₄, 1 mM CaCl₂), and supplied with TURBO DNase (1:500) and RNaseOUT (1:1000). Partial RNA digestion was mediated by preparing different dilutions of RNase I (1:10, 1:100, 1:500, and 1:1000) and adding 1:1000 of these dilutions to the corresponding extracts. Samples were incubated for 3 min at 37°C, 800 rpm and subsequently put on ice for 5 min. Then, 1:50 of a 5 M NaCl solution was added to achieve a final concentration of ~150 mM NaCl and samples were centrifuged (21,000×g, 5 min, 4°C) to precipitate large complexes.

Step 3: Immunoprecipitation

In the meanwhile, protein A dynabeads pre-bound to 3 µg anti-FLAG or anti-c-Myc antibody in TBS-T 150 (50 mM Tris-HCl pH 7.4, 150 mM NaCl, 0.05% Tween 20) for 2 h at 4°C, were washed twice with TBS-T 150. Supernatant of centrifuged extracts was then added to the beads and incubated rotating for 2 h at 4°C. Immunoprecipitated complexes were stringently washed four times with TBS-T 1000 (50 mM Tris-HCl pH 7.4, 1000 mM NaCl, 0.05% Tween 20) and twice with PNK buffer (70mM Tris/HCl pH 7.5, 10mM MgCl₂, 0.05% NP-40). At this point, high RNase control samples were stored in PNK buffer at 4°C overnight until radioactive labelling.

Step 4: Dephosphorylation and first adapter ligation

All other samples were dephosphorylated in PNK dePPL buffer (5x: 350 mM Tris-HCl pH 6.5, 50 mM MgCl₂, 5 mM DTT) by adding the following mixture to the beads:

4 µl	5x PNK dePPL buffer
0.5 µl	RNaseOUT
0.5 µl	T4 Polynucleotide Kinase
15 µl	DMPC-H ₂ O
<hr/>	
20 µl	total volume

On-bead dephosphorylation reactions were incubated for 20 min at 37°C, 1000 rpm and washed twice with TBS-T 400 (50 mM Tris-HCl pH 7.4, 400 mM NaCl, 0.05% Tween 20) and twice with PNK buffer. Samples were now prepared for ligation of the pre-adenylated first adapter to the 3' end of the RNA. Therefore, the pre-mixed RNA-linker ligation reaction was added to the beads:

2 µl	10x T4 RNA ligase buffer
1 µl	Pre-adenylated L3-App (20 µM)
0.5 µl	RNaseOUT
4 µl	PEG400
1 µl	T4 RNA ligase
11.5 µl	DMPC-H ₂ O
<hr/>	
20 µl	total volume

Ligation was allowed to proceed overnight at 16°C, 1000 rpm. The next day, samples were washed twice with PNK buffer.

Step 5: Radioactive RNA 5'-labelling

RNA of all samples (including those treated with high RNase I concentrations) was 5'-end-labelled with the following [γ -³²P]-ATP containing mixture:

1 µl	10x PNK buffer
1 µl	[γ - ³² P]-ATP (12.33 µM, 800 Ci/mmol)
0.25 µl	RNaseOUT
0.5 µl	T4 Polynucleotide Kinase
7.25 µl	DMPC-H ₂ O
<hr/>	
10 µl	total volume

The mixture was added to the beads and incubated at 37°C for 20 min. Then, beads were washed once with TBS-T 150 and once with PNK buffer.

Step 6: SDS-PAGE and nitrocellulose transfer

Beads were resuspended in 25 µl 1x LDS loading buffer (supplied with reducing agent) and protein-RNA complexes eluted by incubating for 10 min at 70°C, shaking. SDS-PAGE and nitrocellulose transfer were mediated using the NuPAGE Electrophoresis and Blotting System. First, samples were placed on a magnetic rack and supernatants loaded on a 4-12% NuPAGE Bis-Tris gel together with the peqGOLD Protein Marker IV. The gel was run for 2.5 h at 200 V in 1x MOPS SDS running buffer (2.5 mM MOPS, 2.5 mM Tris Base, 0.05 mM EDTA, 0.005 % SDS, pH 7.7). After electrophoresis, protein-RNA complexes were transferred to a nitrocellulose membrane by blotting for 1 h at 30 V in 1x transfer buffer (12.5 mM bicine,

12.5 mM Bis-Tris, 0.05 mM EDTA, 20% (v/v) methanol, pH 7.2). The membrane was wrapped in a plastic bag and exposed to an autoradiography film in a film cassette with intensifying screen for different time intervals at -80°C .

Step 7: RNA isolation

The film was used as a template to cut the regions above the FLAG-IMP3 crosslink band in FLAG-IMP3-IP and c-Myc-IP samples. Proteins were digested by adding 20 μl proteinase K in 400 μl CLIP-PK buffer (100 mM Tris/HCl pH 7.4, 50 mM NaCl, 10 mM EDTA, 1% SDS) to nitrocellulose pieces. After incubation for 20 min at 37°C , 1000 rpm, 400 μl of urea containing PK buffer (PK buffer + 7 M urea) were added and incubated for another 20 min at 55°C . RNA was extracted by adding 800 μl phenol/chloroform, incubating for 5 min at 30°C , 1000 rpm and centrifuging using phase lock heavy gel tubes (21,000 \times g, 5 min, 4°C). The aqueous upper phase was transferred into a new tube and RNA precipitated with 0.1 volumes of 3 M sodium acetate (pH 5.2), 0.7 volumes isopropanol, and 1 μl glycoblue overnight at -80°C . Samples were centrifuged (21,000 \times g, \geq 30 min, 4°C) and pellets washed with 80% ethanol. Air-dried pellets were dissolved in 12 μl DMPC- H_2O .

Step 8: Reverse transcription

To prepare cDNA, RNA is reversed transcribed. In a first step, primer and dNTPs were added:

1 μl	RT1 oligo (0.5 μM)
1 μl	dNTP mix
12 μl	RNA
<hr/>	
14 μl	total volume

Samples were incubated for 5 min at 70°C and then left at room temperature until addition of the remaining reaction mix:

4 μl	5x RT buffer
1 μl	DTT (0.1 M)
0.5 μl	RNaseOUT
0.5 μl	SuperScript III RT
<hr/>	
20 μl	total volume

Reverse transcription was mediated by incubation for 5 min at 25°C , for 20 min at 42°C and 40 min at 50°C . Samples were left at 4°C if not proceeded directly. After reverse transcription, 1.65 μl 1 M NaOH were added and incubated for 20 min at 98°C to hydrolyse RNA. Then, 20 μl 1 M HEPES-NaOH (pH 7.3) were added to ensure elimination of radioactivity.

Step 9: Second adapter ligation

Prior to ligation of the second adapter at the 3' end of the cDNA, cDNA was purified using MyONE Silane beads. For each sample, 10 μ l bead suspension were used. Beads were washed with 500 μ l RLT buffer and resuspended in 125 μ l RLT buffer before the sample was added and mixed to obtain a homogeneous suspension. Then, 150 μ l 100 % ethanol were added, mixed by pipetting and incubated for 10 min with mixing by pipetting after half of the time. Beads were magnetically attracted and the supernatant discarded. Washing of beads was performed three times with 1 ml 80 % ethanol each and change of tubes after the first wash. Beads were air-dried for 5 min at room temperature before the addition of 5 μ l DMPC-treated water. Samples were incubated for 5 min at room temperature before ligation of the second adapter.

The second linker contains also the barcode, which is why different linkers are chosen for each sample. For the two iCLIP replicates, the following linkers were chosen:

	Total	Cytosol	MO	Myc-IP (neg. ctr)
iCLIP 1	L01clip2.0	L02clip2.0	L04clip2.0	L21clip2.0
iCLIP 2	L03clip2.0	L08clip2.0	L10clip2.0	L16clip2.0

Each second adapter was added (2 μ l, 10 μ M) as well as DMSO (1 μ l, 100 %) and the mix heated briefly for 2 min at 75°C with subsequent cooling on ice.

A ligation master-mix was prepared and 12 μ l added to each cDNA-adapter-bead solution:

2 μ l	10x RNA ligase buffer
0.2 μ l	ATP (100 mM)
9 μ l	PEG8000 (50%)
0.5 μ l	T4 RNA ligase (high concentration)
0.3 μ l	DMPC-H ₂ O
<hr/>	
12 μ l	total volume

After thoroughly mixing, an additional 1 μ l RNA ligase was added to each sample and mixed by stirring. The ligation was allowed to proceed overnight at room temperature, stirring at 1100 rpm.

A second clean-up with MyONE Silane beads was performed the next day. For each sample, 5 μ l of bead suspension were used. Beads were washed with 500 μ l RLT buffer and resuspended in 60 μ l RLT buffer before the sample was added. After mixing, 60 μ l 100 % ethanol were added and the suspension mixed again by pipetting. Incubation times and washing was as described for the first MyONE clean-up. Air-dried beads were then resuspended in 23 μ l

DMPC-treated water. The mix was incubated for 5 min at room temperature to elute the cDNA. Beads were magnetically attracted and eluate subjected to the first PCR.

Step 10: First PCR amplification

For cDNA pre-amplification, a first PCR was performed with shorter primers. The following PCR mix was prepared and underwent the described programme:

22.5 µl	cDNA
2.5 µl	Primer mix of P5Solexa_s and P3Solexa_s, 10 µM each
25 µl	2x Phusion HF PCR MasterMix
<hr/>	
50 µl	total volume

98°C	30s	6 cycles
98°C	10s	
72°C	30s	
72°C	3 min	
16°C	Hold	

Step 11: ProNex size selection

Primer dimers were removed through ProNex Size-Selective Chemistry. For each PCR sample (50 µl), 147.5 µl of room temperature equilibrated ProNex Chemistry (beads) were added, corresponding to a 1:2.95 sample to bead ratio. Samples were resuspended and incubated for 10 min at room temperature. Beads were magnetically attracted and supernatant discarded. Washing was performed twice using 300 µl ProNex Wash Buffer with short incubation times (30 – 60 s) each but without removal from the magnetic rack. Samples were air-dried for ca. 8 – 10 min until cracking of the beads started. Beads were resuspended in 23 µl ProNex Elution Buffer and incubated for 5 min at room temperature. Samples were returned to the magnetic stand and eluted cDNA transferred to a new tube.

Step 12: Second PCR amplification

Step 12.a: Analytical PCR

Numbers of PCR cycles must be optimised for each sample individually to obtain a library with sufficient yield but without over-amplification. Therefore, analytical PCRs with two different numbers of cycles were performed to estimate the cycle number needed for the preparative PCR. The following PCR mix was prepared and underwent the following programme:

2 μ l	cDNA
1 μ l	Primer mix of P5/P3Solexa, 10 μ M each
10 μ l	2x Phusion HF PCR MasterMix
7 μ l	DMPC-H ₂ O
<hr/>	
20 μ l	total volume \rightarrow split to 2x 10 μ l reactions

98°C	30s	7 - 13 cycles
98°C	10s	
65°C	30s	
72°C	30s	
72°C	3 min	
16°C	Hold	

Each sample was supplied with 2 μ l 6x DNA loading buffer and 6 μ l loaded on a 7% native PAA-TBE gel. For size comparison, the GeneRuler Low Range DNA Ladder was used. The gel was run for 30 min at 200 V in 1x TBE and stained for 10 min with an ethidium bromide solution (1xTBE, 1:20,000 EtBr). DNA was visualised with a gel documentation system (SynGene) and necessary cycle number estimated according to the signal.

Step 12b: Preparative PCR

Preparative PCR was carried out using the same PCR programme as described for analytical PCR. The reaction setup included now half of the remained cDNA:

10 μ l	cDNA
2 μ l	Primer mix of P5/P3Solexa, 10 μ M each
20 μ l	2x Phusion HF PCR MasterMix
8 μ l	DMPC-H ₂ O
<hr/>	
40 μ l	total volume

For quality control, 5 μ l PCR was supplied with 1 μ l 6x DNA loading buffer and loaded on a 7% native PAA-TBE gel together with the GeneRuler Low Range DNA Ladder. The gel was run, stained and visualised as before (12.a).

Step 13: Second ProNex size selection

For this step, the library of the negative control (c-Myc IP) was excluded as it was not subjected to sequencing. From all three FLAG-IMP3 iCLIP experiments, 1% input was taken, pooled and mixed with 6x DNA loading buffer. The following size selection occurred as before but with a different sample-ProNex ratio of 1:2.4 (v/v) due to the longer primers. Thus, 82.8 μ l of room temperature equilibrated ProNex Chemistry (beads) were added to each sample. Mixing, incubation and washing and drying of beads was performed as in the first ProNex size selection

(step 11). Beads were finally resuspended in 20 µl ProNex Elution Buffer and incubated for 5 min at room temperature for elution. Samples were returned to the magnetic stand and eluted cDNA transferred to a new tube. 0.5 µl of each library was pooled and mixed with 6x DNA loading buffer for analysis of primer removal. 1% of pooled inputs and pooled libraries were loaded on a 7% native PAA-TBE gel together with the GeneRuler Low Range DNA Ladder. The gel was run for 25 min at 200 V in 1x TBE, stained and visualised as before.

Step 14: Next-generation sequencing

iCLIP libraries were additionally examined using the High Sensitivity DNA Kit (Bioanalyzer) and the Qubit dsDNA HS Assay kit. This way, the concentration of each library could be determined and libraries pooled in equimolar amounts. During the library preparation for sequencing, 5 % of a PhiX library were spiked-in as a control according to the manufacturer's instructions. High-throughput sequencing was performed as 150 bp single-reads using the MiSeq Reagent Kit v3.

3.12 Bioinformatic analyses of high-throughput sequencing data

The high-throughput sequencing data analysis was done by my colleague Lee-Hsueh Hung. Methods are described in Schreiner *et al.* (2020) for RNA-seq and Rossbach *et al.* (2014) for iCLIP-seq, applied here for the analysis of IMP3/IGF2BP3.

4 Results

4.1 IMP3 circRNA sponges

CircRNAs have been shown to be efficiently used as sponges for microRNAs, thereby inhibiting their function. We proposed that this mechanism should be also applicable to RNA-binding proteins, given that the RNA-binding motif of the respective protein is known. Previous work from our lab has revealed the RNA-recognition code of the multidomain IMP3 protein by SELEX-seq analysis and confirmed it by multiple validation experiments (Schneider *et al.*, 2019). In this model, CA-rich sequences are bound by RRM1, KH2 and KH3 domains, whereas GGC-rich elements are bound by KH1 and KH4 (Fig. 4.1).

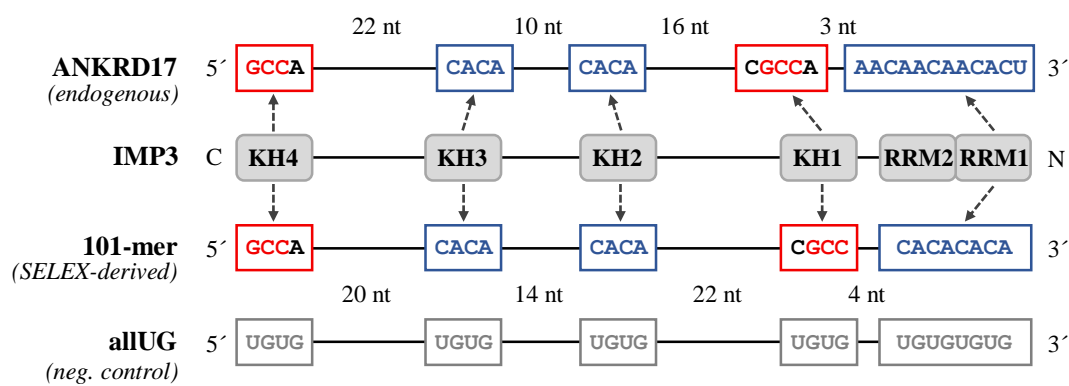


Figure 4.1: RNA-recognition code of IMP3 and constructs used in this thesis.

The RNA-recognition code of IMP3 protein was derived from SELEX-seq and iCLIP data integration (Schneider *et al.*, 2019). The sequences of the motif arrays found within exon 29 of *ANKRD17*, a natural IMP3 target (121 nt), and in the synthetic 101-mer RNA, are shown, both containing the appropriate spaced CA and GGC elements. The specific recognition of these RNA motif elements by the KH- and RRM-domains of IMP3 are indicated. In addition, a mutant derivative of the 101-mer RNA, allUG, in which all binding motifs were converted to UG elements, was used as a negative control. All constructs contain additional, short 5'- and 3'-sequences (not shown).

The motif array was found in multiple targets of IMP3, one of them the endogenous *ANKRD17* mRNA, where it is present in exon 29. Interestingly, there are also two natural circRNAs of this gene, comprised either of exon 29 alone, or of exon 29 and exon 30, and IMP3 is known to bind to these (Schneider *et al.*, 2016). Therefore, the short region (121 nt) of *ANKRD17* exon 29 containing the RNA motif array was used as a positive control and compared to a series of synthetic 101-mers containing either the endogenous motif, with optimal spacing between individual elements, or swapped and/or mutated motifs (Schneider *et al.*, 2019). As these assays revealed in depth insight into the sequence-dependent binding of IMP3 to linear RNAs, we asked whether IMP3 might be also able to bind these RNAs if they were circularised. Given the high stability of circular RNAs, this would be beneficial in developing a potential new tool for

IMP3 inhibition. Therefore, we decided to pick a subset of the described RNAs and examined it further within this thesis. We chose both RNAs containing the full RNA-recognition code, which is the endogenous *ANKRD17* sequence and the synthetic 101-mer construct, and directly compared them. In addition, the mutant derivative of the 101-mer RNA “allUG”, in which all RNA motif elements were converted to UG repeats, was used as a negative control (Fig. 4.1).

4.1.1 IMP3 binds to circRNA sponges with high affinity *in vitro*

In a first step, binding of IMP3 to the described RNAs was assayed *in vitro*. To improve circularisation, a short, terminal stem sequence was attached to all constructs, as circularisation efficiency without the stem was rather low, especially for the *ANKRD17* construct (data not shown). The stem sequence comprises 10 nt: 6 nt for base-pairing and 4 nt as short overhangs (designed by Oliver Roßbach). The influence of the attached stem sequence on the accessibility of the RNA-binding elements was examined by secondary structure predictions (Fig. 4.2). We found no big changes in the overall RNA secondary structure nor on the positioning of the RNA-recognition elements, although the attached stem sequence led to shorter 5' and 3' unpaired sequences, thereby decreasing the flexibility of the ends as desired.

Circular RNAs were generated by T7 polymerase-mediated *in vitro* transcription and ligation by T4 RNA ligase (Fig. 4.3A). Comparison of the ligated transcript to a control ligation reaction without RNA ligase revealed a second, upshifted band in denaturing polyacrylamide gel electrophoresis (Fig. 4.3B). This upshifted band is stronger than the remaining linear transcript band and its exact position dependent on polyacrylamide percentage (data not shown), indicating circularity of the RNA. To further confirm circularity of the transcript, an enzymatic digest with the 3'→5' exoribonuclease RNase R was performed, since this enzyme degrades linear but not circular RNA. All transcripts showed degradation of the linear RNA upon RNase R treatment, whereas the upper bands remained (Fig. 4.3C), supporting circularity.

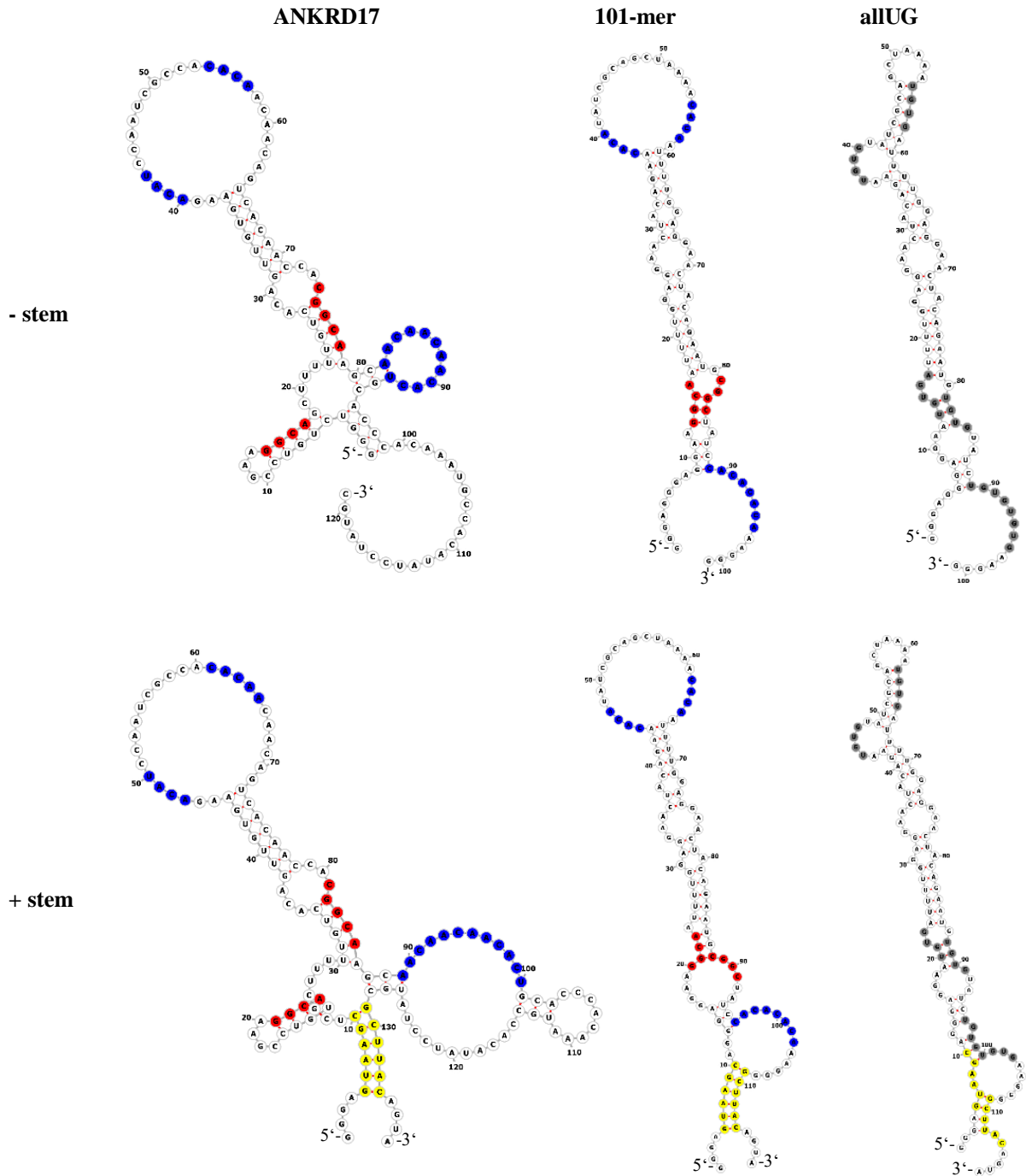


Figure 4.2: Influence of stem sequence on secondary structures of IMP3 sponge constructs.

Predicted RNA secondary structures of ANKRD17, 101-mer and allUG without (top) or with (bottom) stem sequence. Linear sequences without stem have been analysed for IMP3 binding previously (Schneider *et al.*, 2019). Possible influence of the introduced stem sequence on IMP3-binding motifs was examined by RNA secondary structure prediction. CA and GGC motifs recognised by IMP3 are coloured in blue and red, respectively, mutated motifs to UG are denoted in grey. The attached stem sequence to enhance circularisation efficiency is highlighted in yellow.

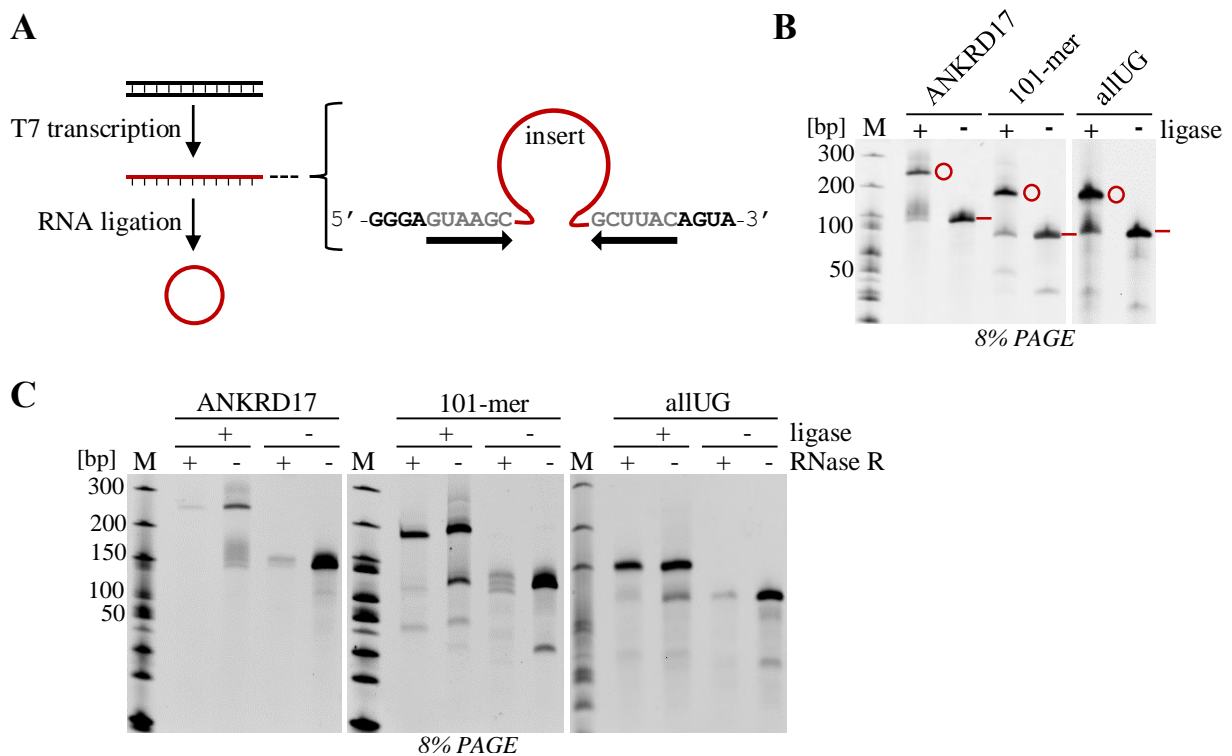


Figure 4.3: Generation of synthetic circular RNAs *in vitro*.

(A) Schematic overview of *in vitro* circularisation of short RNAs. After transcription of a DNA template by T7 polymerase, the resulting RNA is ligated (T4 RNA ligase) to form a covalently closed circle (left). Circularisation was facilitated by addition of a terminal, short stem sequence (arrows), leading to correct positioning of the 5' and 3' ends of the RNA (right).

(B) *In vitro* circularisation of IMP3 sponge RNAs. Circular RNAs were generated as described in (A) and compared to the corresponding linear transcripts. Analysis of ligated RNA shows a characteristic shift of the circular RNA compared to its linear counterpart in denaturing polyacrylamide gel electrophoresis (EtBr staining).

(C) Quality control of *in vitro* generated circRNAs by RNase R treatment. Equal amounts of ligated or non-ligated (+/- ligase) transcripts were treated with or without (+/-) RNase R and analysed by denaturing polyacrylamide gel electrophoresis (EtBr staining).

To be able to examine binding of the circRNAs to IMP3, recombinant IMP3 protein was produced in *E. coli* cells and isolated. Purification occurred via its C-terminal His-tag with Ni-NTA agarose and subsequent elution with imidazole (see Methods section 3.6.4). The procedure was controlled by Coomassie staining after SDS-PAGE and resulted in a clean protein product after elution (E1 and E2, Fig. 4.4 left). Remaining imidazole was removed by dialysis, which did not affect protein stability (E_D, Fig. 4.4 left). The protein concentration was determined by comparing different volumes of protein eluate to a BSA standard and estimated to 140 ng/μl (Fig. 4.4 right).

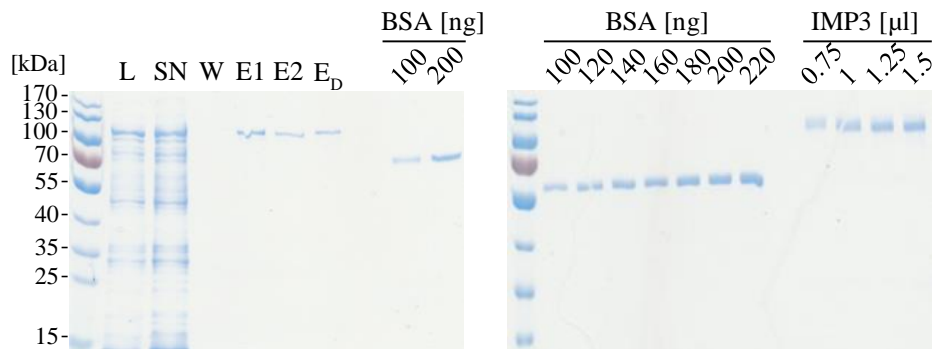


Figure 4.4: Purification of recombinant IMP3.

IMP3 containing a GST- and His-tag was purified from *E. coli* cells and purification controlled by SDS-PAGE and Coomassie staining (left). Samples were taken of lysed cells after removal of cell debris (L), supernatant after incubation with Ni-NTA beads (SN), during washing (W), after both elutions (E1 and E2) as well as after dialysis of the combined eluates (E_D). For a first concentration estimation, defined amounts of BSA were loaded as indicated. Precise concentration of purified IMP3 was determined by comparing different volumes of eluate to a BSA standard in Coomassie stained SDS-PAGE (right).

Finally, *in vitro* binding of IMP3 to circular RNA sponges could be examined by electrophoretic mobility shift assays (EMSAs). For this, transcripts were radioactively labelled with ³²P-UTP. Purified transcripts were either directly tested for binding (linear RNA) or ligated and gel-extracted to yield pure circular RNA. Binding reactions with constant concentrations of RNA, but increasing concentrations of purified IMP3 protein were subjected to native gel electrophoresis (Fig. 4.5A). In all constructs, the formation of a protein-RNA complex was observed that clearly shifted above the unbound RNA. More of the complex was formed at higher protein concentrations. Of note, up to 4-fold higher concentrations of IMP3 were used to examine binding to the negative control. Radioactive signals were quantified and bound fractions calculated (Fig. 4.5B left). Dissociation constants (K_d) were determined by curve fitting and compared between the constructs in their circular and linear isoform (Fig. 4.5B right). The two constructs containing the IMP3 RNA-recognition code, ANKRD17 and 101-mer, were bound with similar high affinities (K_d values between 8.5 – 10.4 nM), whereas the negative control RNA allUG was bound with ~5-7 fold lower affinity by IMP3. In addition, no significant differences in K_d values were found for linear or circularised RNA within each construct (Fig. 4.5B right). We therefore concluded that circular RNAs can be efficiently bound by IMP3 *in vitro* and that they might present a useful tool for IMP3 sponging.

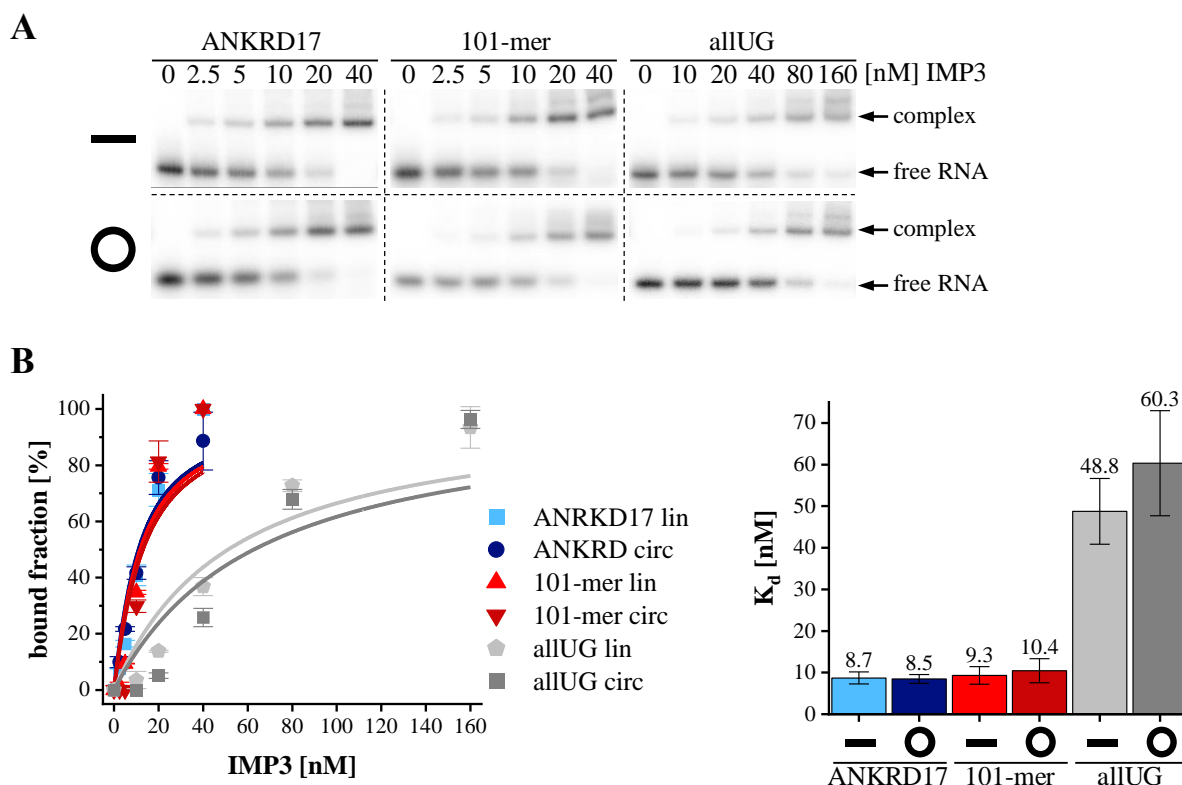


Figure 4.5: IMP3 binds to synthetic circular RNA *in vitro*.

(A) Binding of IMP3 protein to linear (upper) and circular (lower) versions of the three RNAs (natural *ANKRD17* motif array; synthetic 101-mer and allUG mutant derivative). *In vitro* ligated RNAs were gel-extracted to yield only circular RNA. 32 P-labelled RNAs (5 nM) were incubated with recombinant IMP3 protein (0 – 40 nM or 0 – 160 nM range) and binding analysed by EMSA.

(B) Dissociation constants for IMP3-RNA binding derived from EMSA experiments. Curve fits were generated for linear and circular RNA binding using the quadratic binding equation (left). K_d values are depicted with standard deviations of experiments performed in triplicates (right).

4.1.2 Stable expression of circRNA sponges *in vivo*

Next, we asked if our circRNA constructs can also sponge IMP3 *in vivo*. To clarify this, we pursued two different strategies: sponging of IMP3 by stably expressed circRNAs or by transiently overexpressed circRNAs from plasmids (for the latter, see section 4.1.3).

Following the first strategy, we decided to use the Flp-In T-REx system (Invitrogen). In this system, genetically modified cells are used in which the expression of a gene of interest is driven by a tetracycline-inducible CMV promoter (for details, see Methods section 3.3.4). We generated HeLa Flp-In T-REx cells, which stably and inducibly express IMP3 circRNA sponges (Fig. 4.6A). *In vivo* circRNA generation was facilitated by long inverted repeats (IR; ~300 nt) flanking the sponge sequences. Expression of generated constructs after tetracycline induction was tested by RT-PCR using different primer sets: primers detecting the linear and

circular form (“total”, black), outward facing primers detecting only the circular form (“circular”, red) or primers detecting the linear, unspliced transcript (“precursor”, grey) (Fig. 4.6A).

We decided to focus on the ANKRD17 sequence and generated cell lines expressing either one or two repeats of the sequence (1xANKRD17 or 2xANKRD17, respectively), to additionally test the influence of circRNA length and motif repetition on IMP3 binding. Two corresponding control cell lines, 1xallUG and 2xallUG, were also generated. Within cell line generation, several cell clones were tested for circRNA expression after tetracycline induction and the ones with the highest expression picked (data not shown). A time course was performed to assess the optimal time span for tetracycline induction (Fig. 4.6B). Here, tetracycline was added for one, two or three days and the expression of stably integrated sponge constructs examined by RT-PCR. As a control, no tetracycline induction was performed (“0 days”). Construct expression was examined by using the three primer sets described above; *U6* expression served as a loading control. In all four cell lines, expression of the precursor clearly increased with correspondingly longer tetracycline induction (Fig. 4.6B). For both ANKRD17 cell lines, this led also to increased expression of circular RNA. By contrast, the two allUG control cell lines showed almost no circRNA expression, independently of the tetracycline induction time interval. We therefore decided that these cell lines do not represent appropriate negative controls and did not include these in the following experiments.

Furthermore, we asked whether the stable expression of ANKRD17 sponges influenced the expression level of IMP3 or one of its two paralogues IMP1 and IMP2 (Fig. 4.6C). Western blot analysis revealed no differences in any of the protein levels examined between the original HeLa Flp-In cell line or the generated ANKRD17 cell lines, independently of tetracycline induction. The GAPDH loading control confirmed that these constant levels were not due to unequal sample loading. Hence, we concluded that the stable expression of ANKRD17 circRNA sponges is possible *in vivo* and does not modulate IMP3 protein expression.

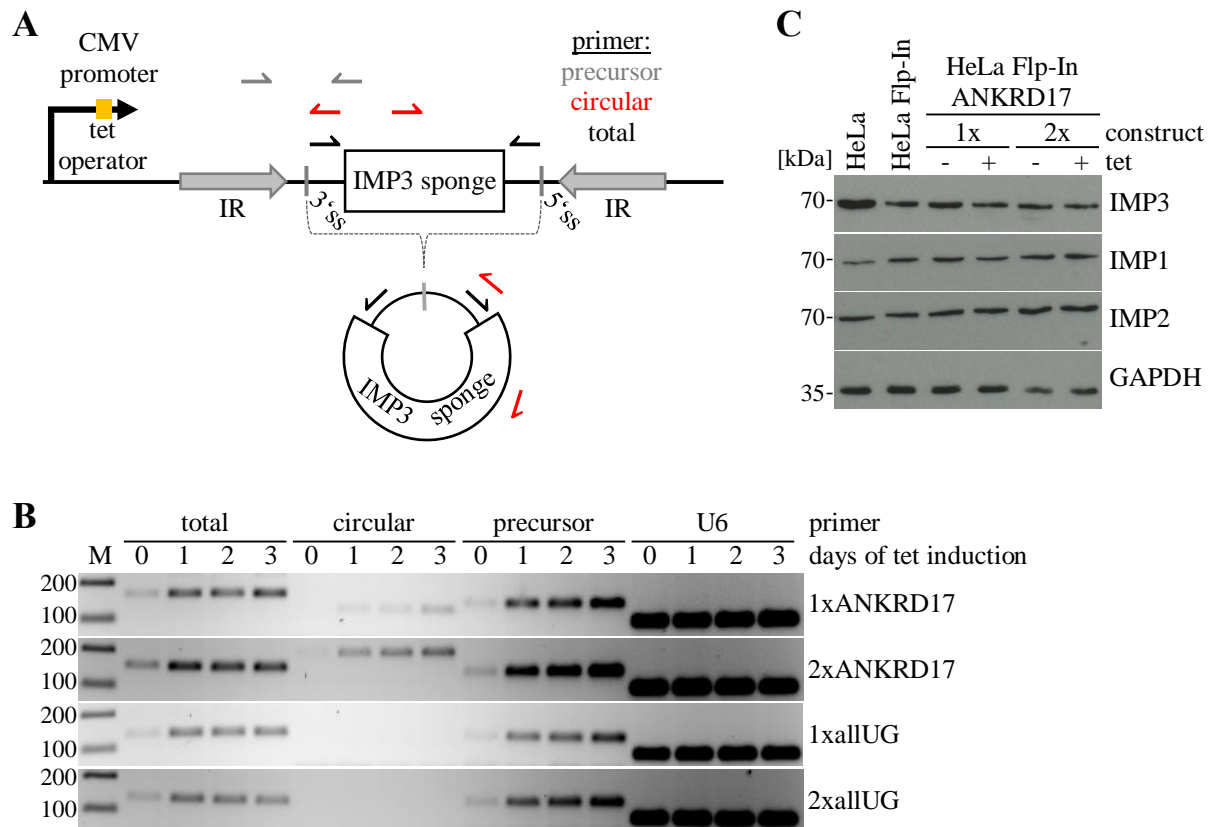


Figure 4.6: CircRNAs can be inducibly and stably expressed *in vivo*.

(A) Schematic of stable circRNA expression in HeLa Flp-In T-REx cells. Transcription is controlled via a tetracycline-inducible CMV promoter. Inverted repeat (IR) sequences facilitate generation of circular RNA by bringing the 3' and 5' splice sites (3'ss / 5'ss) into proximity. IMP3 sponge sequences are flanked by tag sequence for RT-PCR detection; primers for precursor, circular or linear/circular (total) detection are indicated by arrows. The resulting circRNA with the characteristic circ-junction (grey line) is illustrated.

(B) Time course of tetracycline-induced stably expressed IMP3 and control sponge constructs detected by RT-PCR. One (1x) or two (2x) repeats of the IMP3 binding sequence ANKRD17 or the control sequence allUG were stably expressed in HeLa Flp-In T-REx cells. Linear/circular (total), circular and precursor forms were detected, *U6* served as a loading control.

(C) Endogenous IMP3/1/2 level in cell lines stably expressing IMP3 circRNA sponges. Protein levels were examined with (+) or without (-) tetracycline induction. Equal amounts of cell lysates were loaded on SDS-PAGE for Western blot detection. For comparison, HeLa cells and wildtype HeLa Flp-In T-REx cells were loaded. GAPDH served as a loading control.

Finally, we wanted to know if the stable expressed circRNA sponges are bound by IMP3. To examine this, we performed RNA-immunoprecipitation experiments. Cell lysates were prepared, followed by immunoprecipitation with anti-IMP3 antibody, or with anti-IMP1 or anti-FLAG antibodies as specificity controls. Immunoprecipitated RNAs were detected with RT-PCR, using circRNA, total or precursor-specific primer pairs (Fig. 4.7). The quality of the RIP assays was controlled by testing for binding to ferritin light chain (*FTL*) RNA (positive control) and *U6* RNA (negative control). We found that IMP3 bound to circular ANKRD17 sponges,

but hardly to precursor RNA (1.9% or 2.9% compared to 0.1%). Furthermore, this binding was specific for IMP3, since there was no enrichment of ANKRD17 circRNA in the IP of its paralogue IMP1 (0% or 0.4% efficiency, respectively). The negative control *U6* RNA bound IMP3 at low levels (0.9% or 1.3% efficiency). The comparison between the 1xANKRD17 and 2xANKRD17 constructs proved to be difficult given the differences in overall RIP efficiency and background, as seen by differences in the *FTL* and *U6* control. Nevertheless, this confirms that IMP3 binds specifically to synthetic, stably expressed ANKRD17 circRNAs *in vivo*.

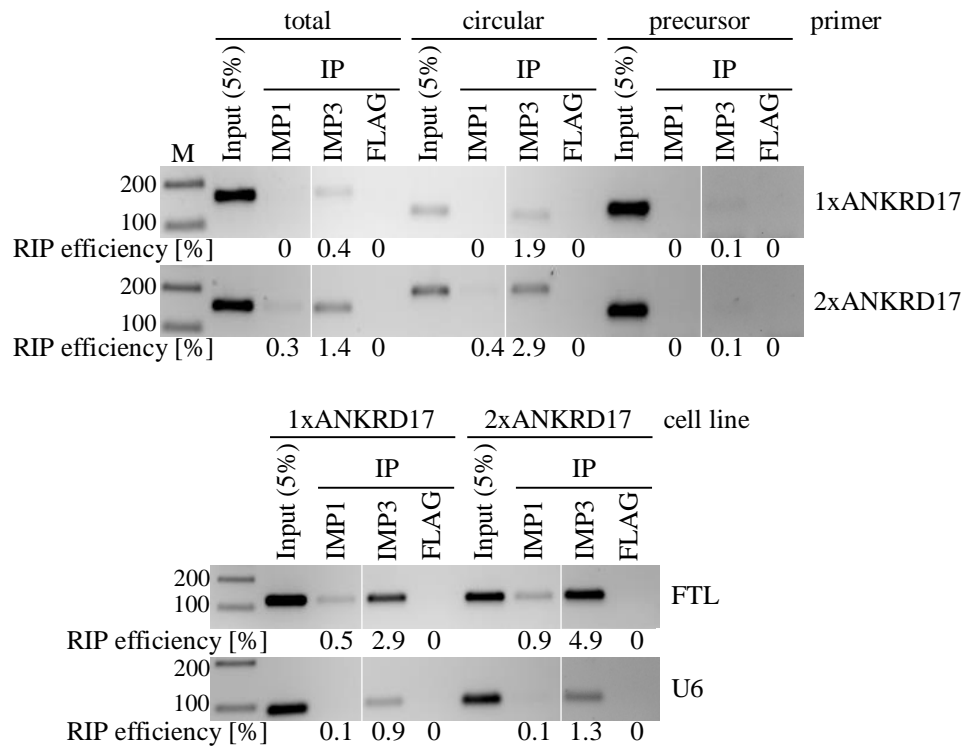


Figure 4.7: Stably expressed circRNA sponges are specifically bound by IMP3 *in vivo*.

RIP experiments of cell lines stably expressing IMP3 sponge constructs were examined by RT-PCR. Expression of ANKRD17 circRNA sponges was induced with tetracycline prior to cell harvest. Specificity of IMP3 sponges was tested by performing RIP experiments with anti-IMP1 and anti-IMP3 antibodies, anti-FLAG antibody served as a negative control. RNA sponge binding was examined by RT-PCR targeting linear/circular (total), circular or precursor form of the sponge constructs. RIP specificity was examined by *FTL* (positive control) and *U6* (negative control). Corresponding samples were loaded together on one gel, but empty lanes in between were removed. RIP efficiency was quantified by densitometry and is shown below each lane.

4.1.3 Transient expression of Tornado circRNA sponges

Following our second strategy, we examined the binding of IMP3 to transiently expressed circRNA sponges. We decided to use the Tornado system (Litke and Jaffrey, 2019) in which circRNAs are transcribed by RNA polymerase III from a transfected plasmid (Fig. 4.8A). The formation of the circRNA occurs via cleavage by two flanking twister ribozymes (5' and 3' ribozyme) and ligation by the endogenous RtcB tRNA ligase. Similar to *in vitro* produced circRNAs, *in vivo* circularisation is enhanced by short, flanking stem sequences. Since this system is more suitable for smaller circRNAs, we decided to use the original three constructs ANKRD17, 101-mer and allUG, each with only single copies of the motifs, resulting in circRNAs not longer than 200 nt. We transfected HeLa cells with the Tornado sponges and examined the expression of our constructs by RT-PCR testing for circular and linear (precursor) RNAs (Fig. 4.8B). The circRNAs were easily detectable, in contrast to the precursor form, which was most likely due to its fast processing not visible. Next, we wanted to know if we can detect the overexpressed Tornado circRNAs in SYBR Gold-stained denaturing polyacrylamide gels of total RNA (Fig. 4.8C). Abundant endogenous small RNAs such as 5S (121 nt) and 5.8S rRNA (157 nt) could be visualised this way. By comparing Tornado-transfected cells to mock-transfected controls, we observed one additional band for each Tornado sponge (Fig. 4.8C, left). This band was at the same height for Tornado-101-mer and Tornado-allUG and just above the 5.8S rRNA, which matched to their length of 144 nt. The additional band in the Tornado-ANKRD17 total RNA ran higher compared to the other two constructs, which was expected due to its larger size. Increase of the acrylamide concentration shifted the respective band to higher molecular weights (Fig. 4.8C, right), which is typical for circular RNAs. Thus, we conclude that circular Tornado sponges are expressed in high amounts *in vivo*.

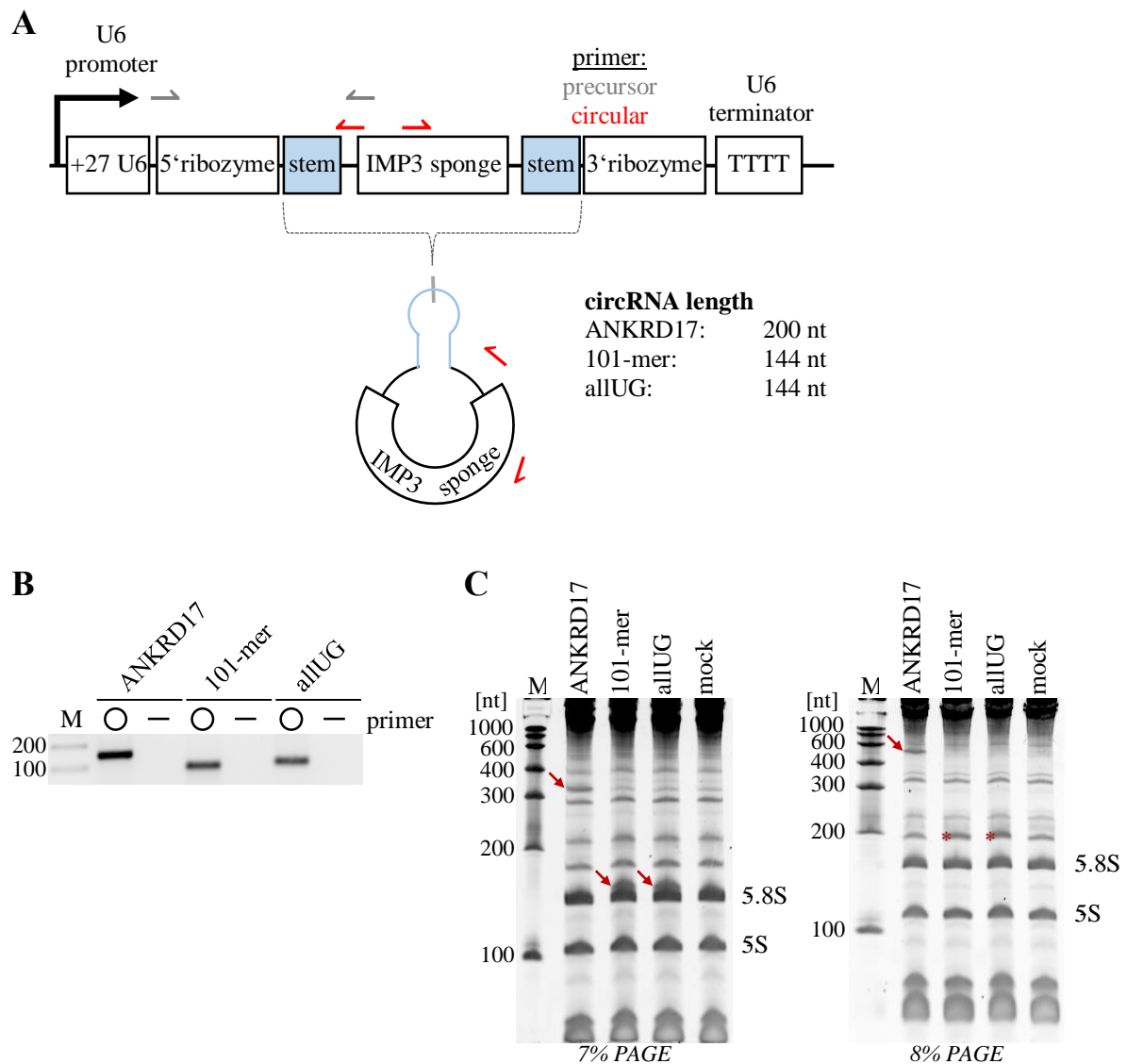


Figure 4.8: Expression of Tornado circRNA sponges.

(A) Schematic of Tornado circRNA expression constructs. Pol III transcription is driven by U6 promoter with the first 27 nucleotides of U6 snRNA. Stem sequences flank the circularising IMP3 sponge sequences to mediate cleavage by the twister ribozymes (5' and 3' ribozymes) and efficient circularisation of the RNA. Pol III transcription is terminated by a T-stretch within the U6 terminator region. The resulting circRNA containing the characteristic circ-junction (grey line) is illustrated and the respective lengths of IMP3 Tornado sponge RNAs indicated. Primers for detection of precursor (linear) and circular RNA are illustrated by arrows.

(B) Detection of IMP3 Tornado sponge RNAs by RT-PCR. HeLa cells were transfected with Tornado constructs and isolated RNA examined for Tornado circRNA (O) and precursor (—) expression.

(C) Visualisation of overexpressed Tornado circRNAs in total RNA. Total RNA (5 μ g) was subjected to denaturing polyacrylamide gel electrophoresis (7% and 8%) and stained with SYBR Gold. Bands corresponding to Tornado circRNAs are indicated by red arrows; asterisks mark putative position of circRNAs.

Due to the expression of Tornado circRNAs from plasmids, the first step in cells is the transcription in the nucleus. Since IMP3 is mainly cytoplasmic, we wondered where the Tornado sponges are localised in cells and whether they influence the localisation of IMP3. We

performed subcellular fractionation with Tornado-transfected or control (mock)-transfected cells into cytoplasmic and nuclear extracts (Fig. 4.9). Prior to cell fractionation, a proportion of the cells were saved as input samples. Examination of the protein distribution in the subcellular fractions showed no visible differences in IMP3 localisation in the presence or absence of Tornado sponges (Fig. 4.9A), as the protein remained in the cytoplasm. The cytosolic protein GAPDH and the predominantly nuclear protein hnRNP A1 localised as expected and thereby validated the fractionation procedure. Furthermore, the RNA distribution was examined by performing RT-qPCR with RNA isolated from the fractions (Fig. 4.9B). As marker RNAs, the cytosolic *GAPDH* mRNA and the nuclear *U78* snoRD were used. Comparison of the relative cytoplasmic to nuclear RNA level showed the expected distribution of the marker RNAs and an enrichment of Tornado circRNA sponges in the cytoplasm. This means that both IMP3 and the Tornado sponges are localised in the cytoplasm, which is beneficial for our purpose, making an interaction of them more likely.

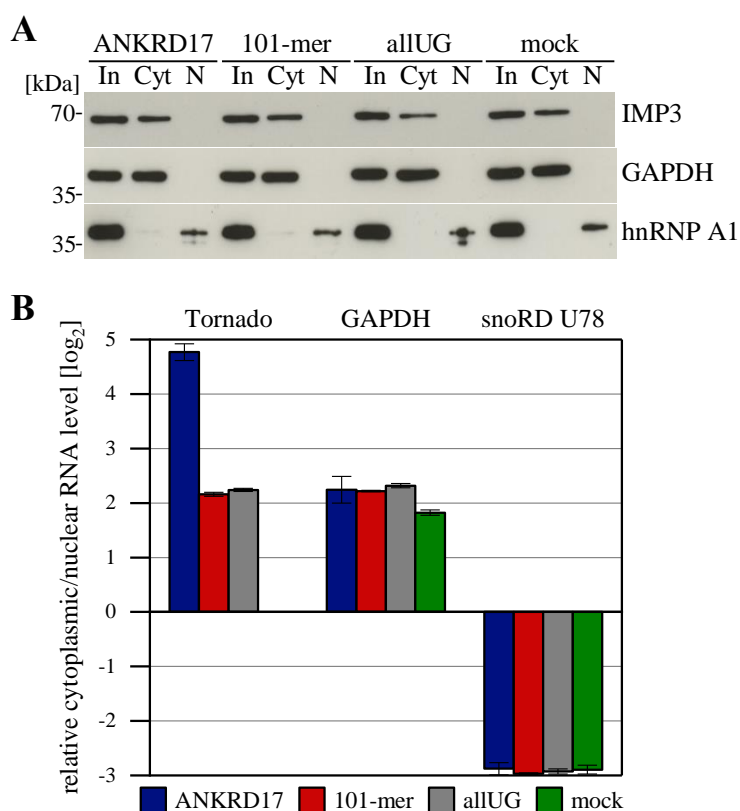


Figure 4.9: Tornado circRNAs are predominantly localised in the cytoplasm.

(A) Detection of IMP3 nuclear/cytoplasmic distribution. HeLa cells were transfected with Tornado IMP3 sponge constructs or mock and harvested 72 h post-transfection. Cells were fractionated into cyt and N extracts. Equivalent lysate amounts of both fractions and input (In) samples were analysed by Western blotting against IMP3, GAPDH (cytosolic marker), and hnRNP A1 (nuclear marker).

(B) RNA distribution analysis of fractionated HeLa cells as described in (A) by RT-qPCR. Equivalent amounts of cytoplasmic and nuclear extracts were taken for RT-qPCR. Levels of the respective Tornado circRNA, *GAPDH* (cytosolic marker) and snoRD *U78* (nuclear marker) were assayed. Data were normalised to input to see cytoplasmic/nuclear distribution. The graph shows combined data obtained from two independent biological replicates with the respective standard deviations.

As a final step, we wanted to know if IMP3 binds to Tornado sponges *in vivo*. To address this question, we performed RIP experiments targeting IMP3 or, as a specificity control, FLAG. Since the Tornado expressed circRNAs are present in high concentrations in cells after 72 h (Fig. 4.8C), presumably exceeding endogenous IMP3 protein concentrations, we performed RIP experiments at three different time points after transfection (8, 24 or 72 h, respectively, Fig. 4.10). Immunoprecipitation was first controlled by Western blotting of input and IP fractions (Fig. 4.10A). IMP3 was successfully precipitated in all samples with comparable efficiency. In addition, IMP3 precipitation was specific as no GAPDH was found in IMP3 precipitated samples and no IMP3 protein was pulled down by anti-FLAG antibody. Next, binding of Tornado sponges was examined by performing RT-qPCR with circular Tornado primers of immunoprecipitated RNAs (Fig. 4.10B). The quality of the RIP assays was controlled by testing for binding to two lowly abundant endogenous circRNAs, *CAMSAP1* (negative control) and *ANKRD17* (large isoform; positive control). Both endogenous control circRNAs confirmed the functionality of the assay, since *circCAMSAP1* was bound at very low efficiency (up to 0.9 % at the 8 h time point) and endogenous *circANKRD17* at high efficiency (up to 28.4 % at the 8 h time point). Regarding Tornado circRNA sponges, we observed an enrichment in all IMP3 IPs compared to FLAG IPs. Further, Tornado-ANKRD17 and Tornado-101-mer were immunoprecipitated with higher efficiencies compared to the negative control Tornado-allUG. For a more detailed view into this enrichment, we calculated the fold change of RIP efficiencies of both Tornado IMP3 binding sponges relative to the negative control allUG sponge (Fig. 4.10C). We found that Tornado-ANKRD17 and Tornado-101-mer were clearly enriched compared to Tornado-allUG and that this enrichment is highest 24 h after transfection (14.3-fold or 15.8-fold enrichment of Tornado-ANKRD17 or Tornado-101-mer, respectively). Overall, we could demonstrate specific binding of IMP3 protein to Tornado circRNA sponges *in vivo*.

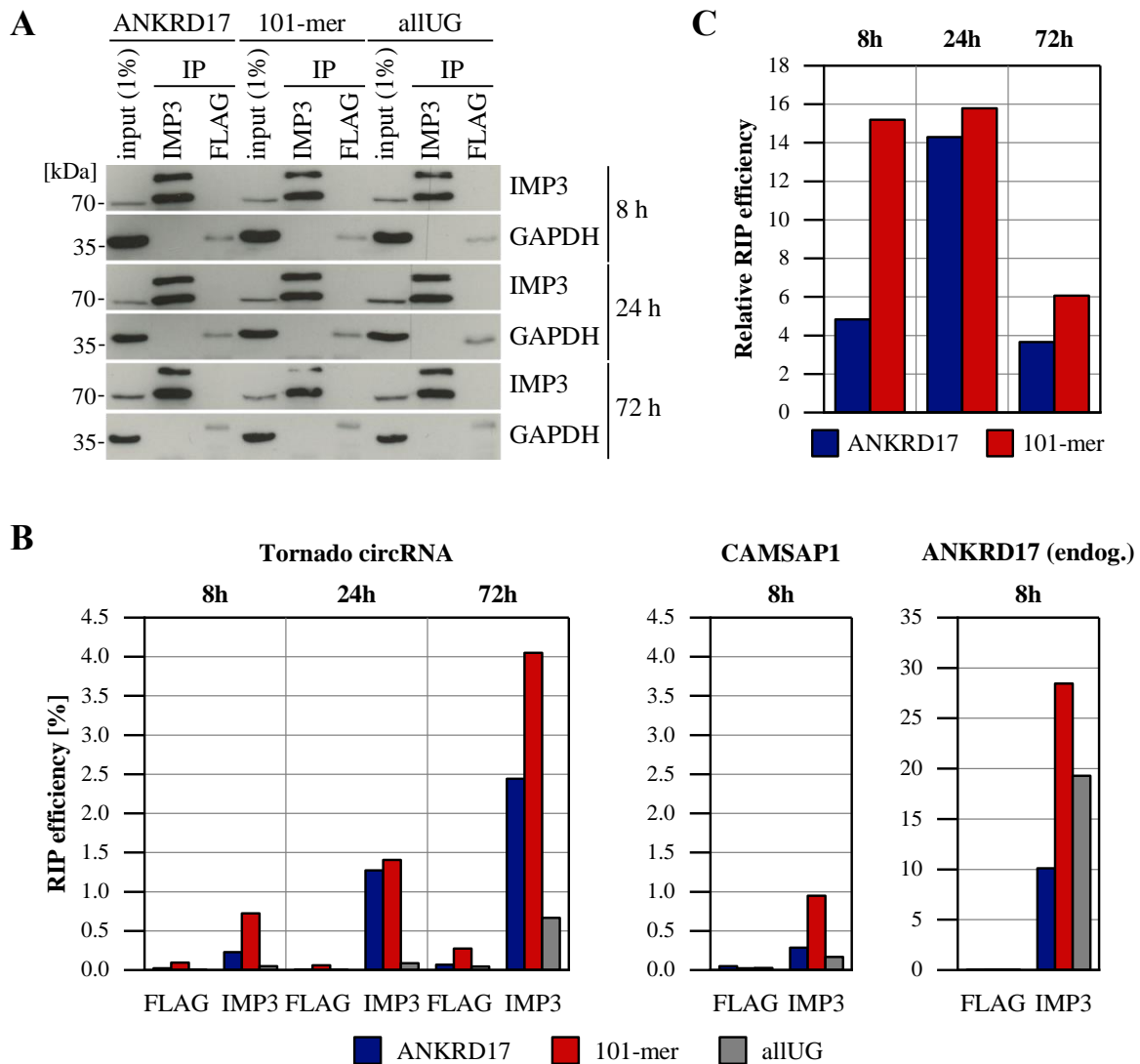


Figure 4.10: IMP3 binds to Tornado circRNA sponges *in vivo*.

(A) Detection of IMP3 and GAPDH protein levels after RIP experiments. HeLa cells were transfected with Tornado constructs and harvested 8, 24 or 72 h after transfection. Cell lysates were incubated with anti-IMP3 or -FLAG (negative control) antibody. Input and both IP samples were then analysed by Western blot with anti-IMP3 and -GAPDH antibodies.

(B) Binding of overexpressed Tornado circRNAs by IMP3. RNA isolation was performed with input and IP samples of RIP experiments and analysed by RT-qPCR to calculate RIP efficiency [%] (left). RIP was controlled by detection of the lowly abundant endogenous circRNAs *CAMSAP1* (negative control, middle) and *ANKRD17* (large isoform, positive control, right) in each experiment and is shown for the 8 h time point.

(C) Fold change enrichment of Tornado-ANKRD17 or -101-mer circRNAs relative to Tornado-allUG in IMP3 RIP experiments. RT-qPCR data shown in (B) were compared to assess specificity of IMP3 binding to Tornado circRNAs.

4.2 Function of IMP3 in RNA localisation

Besides finding a tool for inhibition of IMP3 by circRNA sponging, we further wanted to obtain deeper insights in the endogenous function of this RNA-binding protein and tumour marker. Since several indices hinted at a role of IMP3 in the secretory pathway, we decided to set up experiments to test this hypothesis (Fig. 4.11). For this purpose, we used the ovary carcinoma cell line ES-2, which had previously been established for IMP research (Müller *et al.*, 2018; Schneider *et al.*, 2019), and for which we had a CRISPR/Cas9-mediated IMP3 knockout (k.o.) cell line available. In addition, siRNA-mediated transient IMP3 knockdown (k.d.) and a corresponding control knockdown (ctr k.d.) were established in ES-2 cells. All cells were fractionated into cytosol (cyt) and membrane organelles (MO), followed by extract preparation. Furthermore, total extracts were prepared by standard cell lysis procedures. High-throughput RNA-sequencing was then performed to enable global detection of changes in RNA levels in fractions upon IMP3 depletion. Differentiation between directly or indirectly affected RNAs was possible by performing IMP3 iCLIP experiments in fractionated ES-2 cells (Fig. 4.11). The combination of both RNA-sequencing approaches should reveal direct IMP3 target mRNAs, which display altered levels in the MO fraction upon IMP3 depletion.

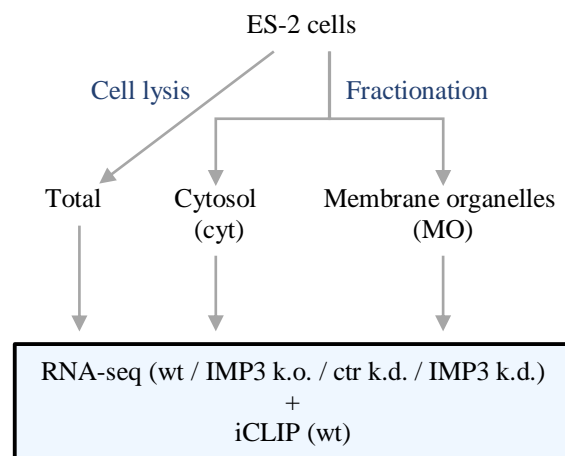


Figure 4.11: Project outline to examine the endogenous function of IMP3.

The human cell line ES-2 was used to test the hypothesis that IMP3 plays a role in the secretory pathway. For this, wildtype (wt) or IMP3 knockout (k.o.) cells were used as well as IMP3 knockdown (k.d.) and corresponding control knockdown (ctr k.d.) cells. All cells were fractionated into cytosol (cyt) and membrane organelles (MO), or lysed to obtain whole cell lysate (total). RNA from all samples was subjected to high-throughput RNA-sequencing and bioinformatically analysed. In addition, iCLIP was performed in fractionated and unfractionated ES-2 wt cells expressing FLAG-tagged IMP3 to identify direct IMP3 targets.

4.2.1 Establishment of the subcellular fractionation procedure

Before the analysis of IMP3's functional role in RNA localisation could begin, a procedure for subcellular fractionation needed to be established. Since many researchers are more interested in the comparison of cytoplasm to nucleus, fractionations into cytoplasm and membrane organelles are less common. Nevertheless, a standard method relies also on detergent-based fractionation. A protocol published by Holden and Horton (2009) was employed for the fractionation procedure and is illustrated in Fig. 4.12. In this set-up, cell membranes are first lysed by incubation with a digitonin-containing buffer. Centrifugation yields cytosol-enriched supernatant, which is transferred to a different tube and preserved. The remaining pellet is further lysed by an NP40-containing buffer. Again, centrifugation after incubation is performed to obtain membrane organelle fractions. The extract is retained and the remaining cell components, comprising nuclei and insoluble components, are dissolved in TRIzol for isolation of RNA. Washing in between the extractions shall insure prevention of contamination between extracts.

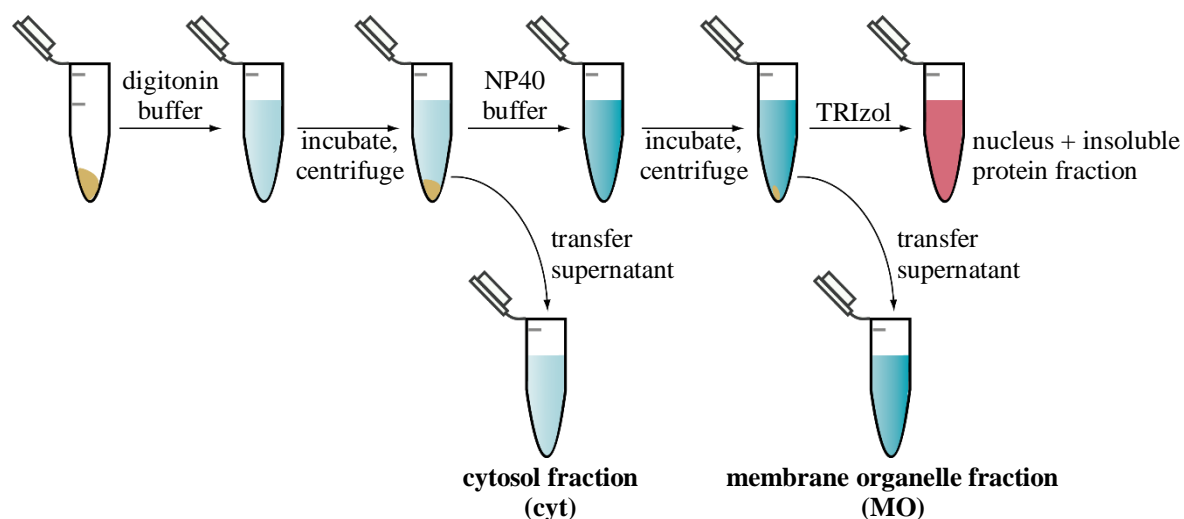


Figure 4.12: Overview of subcellular fractionation of ES-2 cells.

Experimental flowchart of the subcellular fractionation. ES-2 cells were harvested, counted, and equal numbers of cells used for the experiment. Cell pellets were resuspended in digitonin-containing buffer to lyse the cell membrane. After incubation and centrifugation, the supernatant contained the cytosol fraction. The remaining pellet was resuspended in NP40-containing buffer to lyse membranes of organelles. After incubation and centrifugation, the supernatant contained the membrane organelle fraction. RNA was isolated from the remaining pellet, i.e. nuclei and insoluble proteins, as well as from both fractions. In addition, total RNA was extracted from input samples.

Since cell lysis by digitonin depends on the cholesterol content of the cell membrane, the optimal digitonin concentration needs to be determined for each cell line. Therefore, a test fractionation with ES-2 wildtype and ES-2 IMP3 k.o. cells was performed with digitonin concentrations ranging from 0 – 200 $\mu\text{g/ml}$ in the first fractionation buffer. The second NP40-

containing buffer was identical for all samples. The outcome of the experiment was analysed by loading equivalents of fractions on SDS-PAGEs and probing for specific protein markers by Western blot (Fig. 4.13). As control, unfractionated cells were also loaded. The cytosol markers GAPDH and γ -tubulin were shifted in the cytosol fraction with a digitonin concentration $\geq 25 \mu\text{g/ml}$, whereas the endoplasmic reticulum-resident protein calnexin resided in the MO fraction independently of the digitonin concentration. Since IMP3 is mainly cytosolic, it behaved similar to GAPDH and γ -tubulin, but the proportion remaining in the MO fractions was higher compared to the cytosol markers. In conclusion, a digitonin concentration of $25 \mu\text{g/ml}$ was sufficient to extract cytosolic components in ES-2 wt and k.o. cells and was thus used in all further experiments for the fractionation procedure.

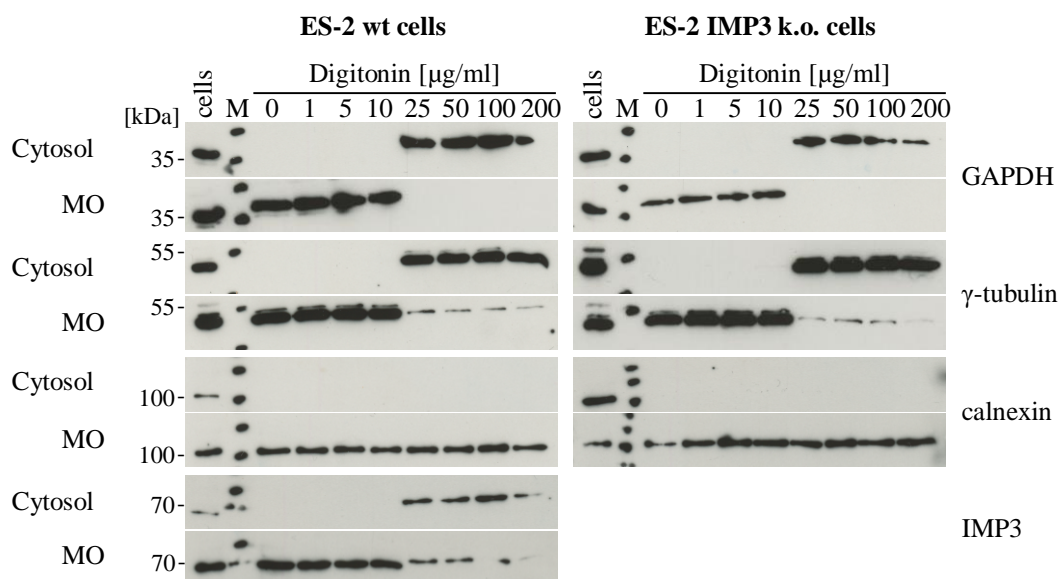


Figure 4.13: Optimisation of digitonin concentration for subcellular fractionation.

ES-2 wt and ES-2 IMP3 k.o. cells were harvested from 12-well plates and lysed in different digitonin-containing buffers with increasing digitonin concentrations (0 – 200 $\mu\text{g/ml}$). The following steps of cell fractionation were identical for all samples. Equivalent lysate amounts of obtained cytosol and membrane organelle fractions were analysed for efficient cell membrane lysis by Western blot. Distribution of GAPDH and γ -tubulin (cytosol markers), calnexin (ER marker), and IMP3 were analysed.

4.2.2 Combined analysis of RNA-seq and iCLIP data reveals target mRNAs

To generate samples for RNA-sequencing, an IMP3 knockdown had to be established first. ES-2 cells were treated with siRNA for three days and transient depletion of IMP3 was controlled by Western blot (Fig. 4.14A). The overexposed Western blot clearly shows that the depletion was very efficient, and there were only low levels of IMP3 protein remaining; the GAPDH blot proves that this was not due to unequal sample loading. Subcellular fractionation was then

conducted with all cells simultaneously and quality-controlled by Western blot (Fig. 4.14B). As expected, the cytosol markers GAPDH and γ -tubulin were located in the cytosol fractions, whereas the ER marker calnexin was found in the MO fractions. IMP3 was detected in cytosol and MO fractions of ES-2 wt and ctr k.d. cells, but not in IMP3 k.d. or ES-2 IMP3 k.o. cells. Moreover, IMP3 levels were higher in cytosol fractions than in MO fractions, with a similar distribution in wt and ctr k.d. cells. Thus, the experiment was found to be suitable for RNA-sequencing. An experimental flowchart of sample preparation is depicted schematically in Fig. 4.14C. For all four cell types, RNA was isolated from cytosol and membrane organelle fractions as well as from unfractionated cells, which were harvested from the same culture, hence referred to as “input”. Before further processing, a commercial RNA spike-in control was added to all samples, which could later be used for normalisation in bioinformatic analyses. Samples were depleted of ribosomal RNAs and libraries prepared. Constructed libraries were quantified and quality-controlled before they were handed to a sequencing facility for high-throughput Illumina sequencing. As an example, quality control by Bioanalyzer measurements of IMP3 k.d. samples are shown (Fig. 4.14D). The electropherograms showed the expected distribution of library fragment sizes with an average size of around 350 bp. Hence, libraries were successfully prepared and sequencing data generated.

Our RNA-sequencing approach cannot reveal differences between direct or indirect effects of RNA-level changes upon IMP3 depletion. Thus, IMP3 iCLIP experiments were performed with fractionated ES-2 wildtype cells to find direct IMP3 RNA targets. Since CLIP assays employ an UV-crosslinking step, the impact of crosslinking to the established fractionation procedure and the optimal UV dosis was first determined. No significant changes in subcellular fractionation were found by using the optimal UV dosis (data not shown). For iCLIP experiments, an N-terminal triple FLAG-tagged IMP3 was used. Thus, subcellular fractionation was again quality-controlled by comparing FLAG-IMP3 expressing cells to mock-transfected cells in Western blot analysis (Fig. 4.15A). Here, the remaining nuclear and insoluble protein fraction was resuspended in SDS-loading buffer and also analysed. The marker proteins showed the expected distribution as before. In addition, the predominantly nuclear protein hnRNP A1 was detected in the nuclear fractions. FLAG-IMP3 distribution was monitored by anti-FLAG and anti-IMP3 antibody, the latter showing both the endogenous and the tagged protein. FLAG-IMP3 distribution between the fractions was comparable to endogenous IMP3 protein, although the protein levels were higher compared to endogenous one. Nevertheless, the same localisation makes FLAG-IMP3 suitable for the following iCLIP procedure. For the iCLIP experiment, volumes of each (sub-)cellular extract were adjusted to achieve similar levels of FLAG-IMP3

in the IP reactions. Due to the different volumes and buffers of the extracts, RNase I concentrations had to be individually adjusted for each sample to obtain RNA fragments of suitable length. For unfractionated (“total”) cells, several controls were included: cells were also non-crosslinked (-UV) or crosslinked but precipitated with c-Myc antibody as a negative control (ctr +UV) (Fig. 4.15B). In addition, all total cell samples were treated with two different RNA concentrations (“H, high” and “M, medium”) as controls. The autoradiograph of the iCLIP membrane showed characteristic smears above ~90 kDa for all preparative samples (Fig. 4.15B top). By contrast, no or low radioactive signal was detected for the control IP and the minus-UV samples. Red boxed regions indicate the areas, which were cut from the membrane and further processed. After cutting, the membrane was probed with anti-FLAG antibody (Fig. 4.15B bottom). Protein signals at the expected height were found in all samples, except for control IP samples, with similar levels of pulled-down protein. Signals around 55 kDa are related to the heavy chains of the antibody and prove the use of an antibody in the control-IP samples. Finally, RNA was isolated from the cut membranes and libraries prepared. Within the library preparation, test PCRs were performed to determine the amount of cycles needed for each sample. Aliquots of preparative PCR reactions were then again controlled by native polyacrylamide gel electrophoresis (Fig. 4.15C). Library fragment sizes were between ~170 and 300 bp for FLAG-precipitated samples, whereas no cDNA was found in the control IP sample. Bands below 50 bp correspond to primer dimers from the PCR reaction and were removed for the sequencing samples after successful quality control. Final libraries were analysed by Qubit and Bioanalyzer measurements (Fig. 4.15D). All samples had a similar concentration and library fragment size distribution with an average of ~260 bp length. Since both adapters and the barcodes are together 134 bp long, this results in an average length of around 126 bp for the insert of an RNA sequence. Thus, libraries were loaded on a MiSeq flow chamber and sequenced.

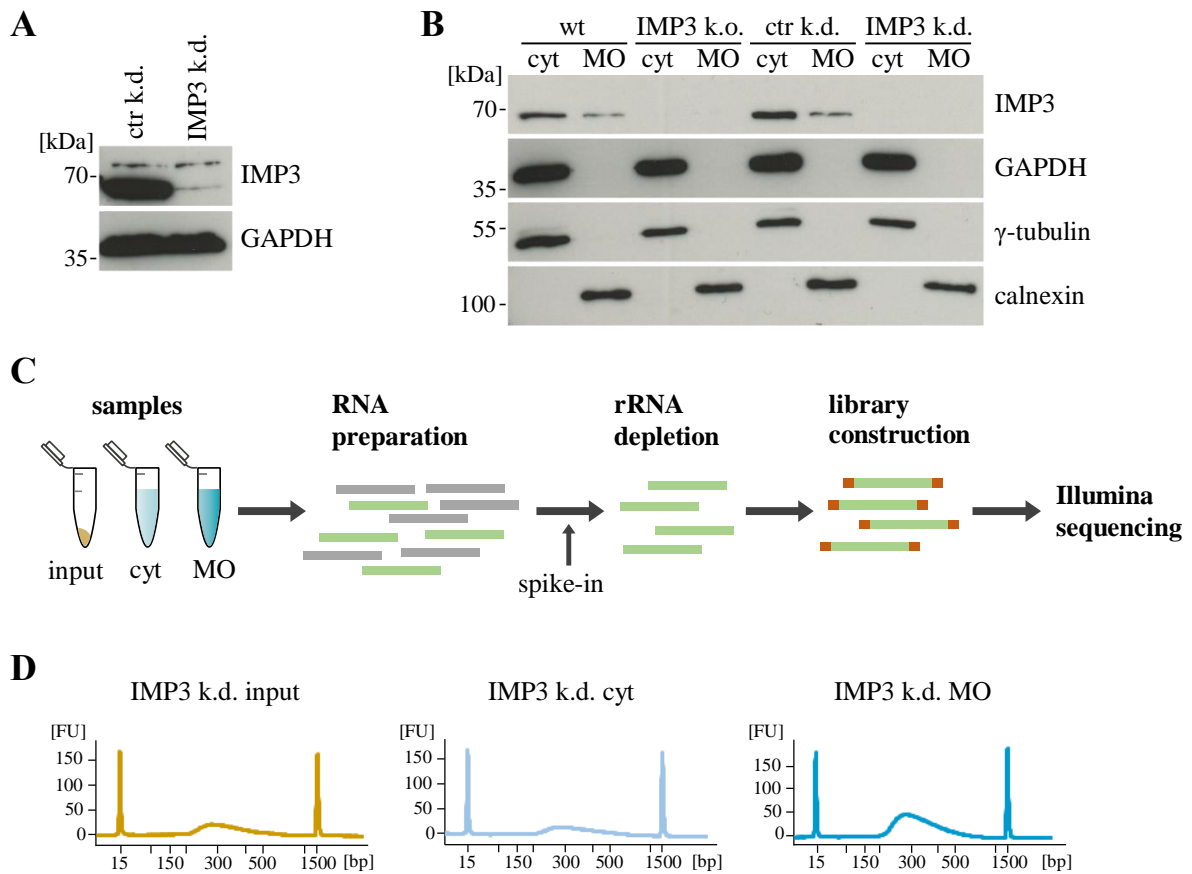


Figure 4.14: Subcellular fractionation of ES-2 cells for RNA-seq.

(A) IMP3 knockdown efficiency in ES-2 cells. Cells were treated with control (ctr; luciferase) or IMP3 siRNA for three days and knockdown efficiency analysed by Western blot. GAPDH served as a loading control.

(B) Quality control of subcellular fractionation. ES-2 wt, IMP3 k.o., or wt cells treated with siRNA (ctr/IMP3) for three days were fractionated and equivalents of fractions examined by Western blotting. GAPDH and γ -tubulin served as cytosolic markers, whereas calnexin represents an ER marker.

(C) Schematic workflow of library preparation for RNA-seq. RNA was isolated from cyt and MO fractions as well as input samples. A spike-in was performed prior to rRNA depletion. Libraries were prepared, quality controlled and subjected to high-throughput Illumina sequencing.

(D) Distribution of library fragment size analysed with Bioanalyzer. As a representative, IMP3 k.d. libraries of input, cyt and MO samples are shown. After successful quality control, libraries were passed to an RNA sequencing facility.

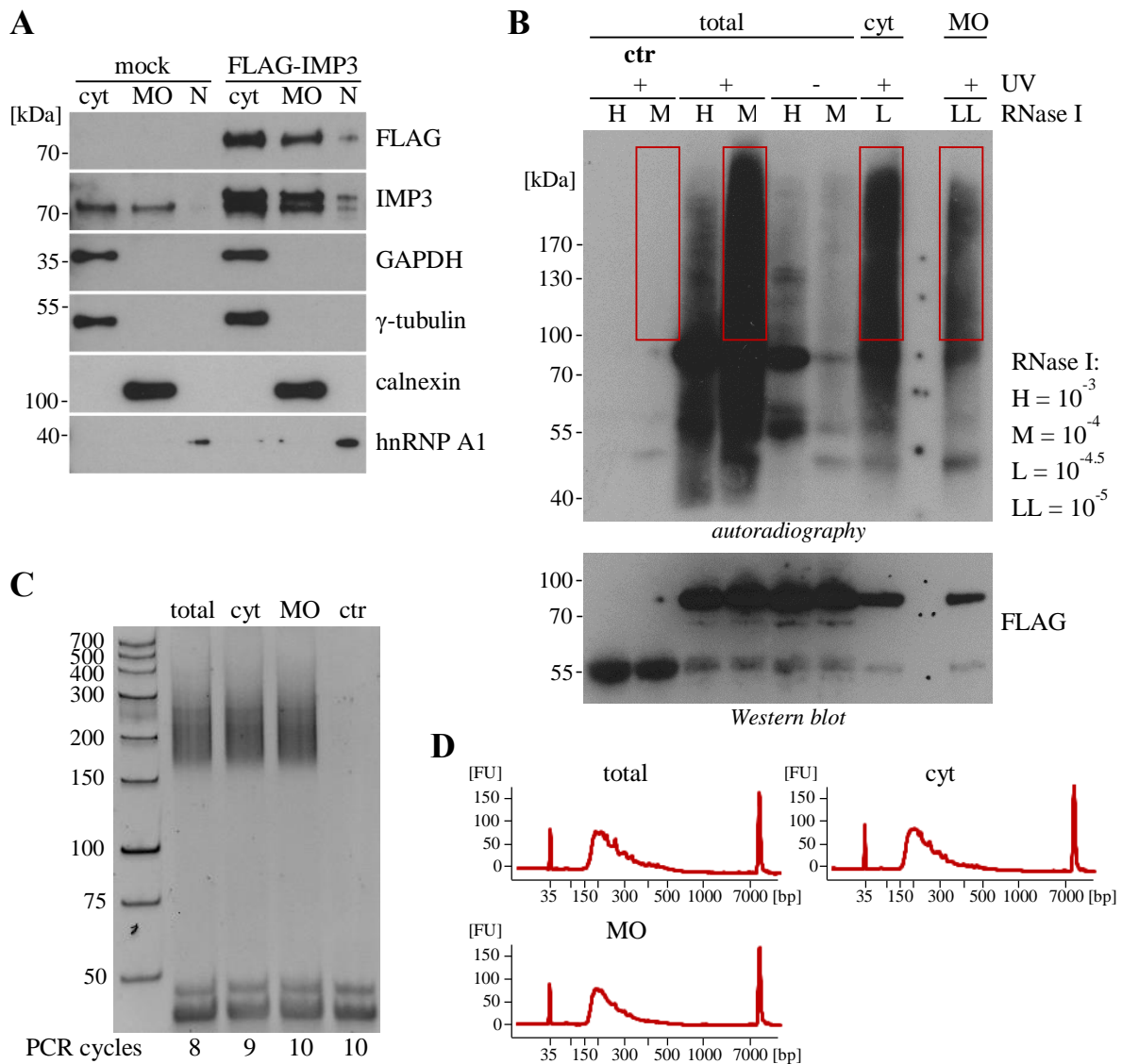


Figure 4.15: Representative FLAG-IMP3 iCLIP experiment.

(A) Protein distribution in fractionated ES-2 cells. ES-2 cells were transfected with FLAG-IMP3 or mock and UV-crosslinked prior to harvest 24 h after transfection. Equivalents of fractions were analysed by Western blotting. Distribution of tagged IMP3 was examined by anti-FLAG and anti-IMP3 antibody. Quality of fractionation was controlled by analysis of GAPDH and γ -tubulin (cytosolic marker), calnexin (ER marker) and hnRNP A1 (nuclear marker) distribution.

(B) Analysis of iCLIP membrane by autoradiography (top) and Western blot (bottom). FLAG-IMP3 immunoprecipitations of ES-2 cell lysates (total), cyt or MO fractions were examined. As controls, cell lysate was precipitated with anti-c-myc antibody (ctr) or not UV-irradiated (-UV). All total samples were treated with high (H) or medium (M) RNase I concentrations as indicated; for cell fractions RNase I concentration was lowered (L or LL). Boxed regions were cut and subjected to RNA isolation and library preparation. After cutting, membrane was analysed by anti-FLAG Western blot. Bands at 55 kDa height represent heavy chain of the antibodies used for IP.

(C) Library preparation from iCLIP samples. Number of PCR cycles was adjusted (indicated on bottom) to yield libraries for high-throughput sequencing and visualised by 7% native PAGE (EtBr staining). Myc-immunoprecipitated material (ctr) was taken as a control for the iCLIP procedure but not subjected to sequencing.

(D) Distribution of library fragment size analysed with Bioanalyzer. Graphs show IMP3-iCLIP samples from (C) after removal of primer dimers.

RNA-seq and iCLIP-seq data were analysed by Lee-Hsueh Hung (see Methods section 3.12). Gene expression correlation between all 12 samples was verified to ensure the quality of the RNA-seq datasets (Fig. 4.16A). As expected, cytosolic and membrane-bound samples have the lowest correlation with a minimum of only 61%. Moreover, MO extracts of ctr k.d. and wt samples were more similar than extracts depleted of IMP3 by knockdown or knockout. The read coverage (RNA-seq) and iCLIP-tag-count (iCLIP-seq) in Chromosome M (Fig. 4.16B/C) further confirmed the validity of the datasets. RNA-seq total samples contained between 2.4 – 3.2% ChrM reads, whereas cytosol extracts were depleted to 0.02 – 0.03% (Fig. 4.16B). By contrast, sequencing data of MO extracts possessed up to 18.5% ChrM reads. For the iCLIP-seq data, the same trend of enrichment and depletion between the extracts was found (Fig. 4.16C). Furthermore, iCLIP tags were mainly found in the 3'UTR (up to 52%) as well as in exonic region (up to 25%) of coding transcripts (data not shown). Since IMP3-bound mRNAs possessed iCLIP tags in all cellular extracts, only iCLIP data of total cells were analysed and normalised with RNA-seq read coverage in ES-2 wt cells for measurement of IMP3 binding.

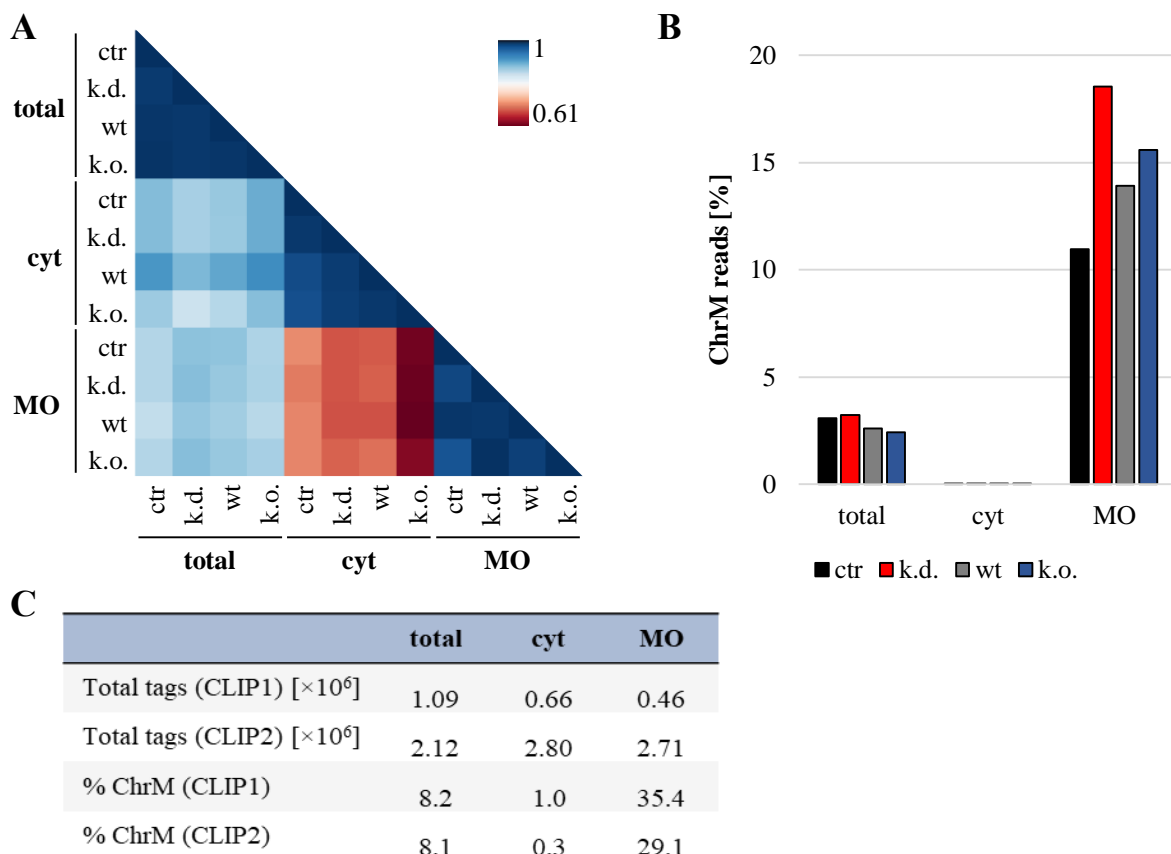


Figure 4.16: Quality analysis of RNA-seq and iCLIP data.

(A) Gene expression correlation (Pearson) between samples.

(B) Percentage of chromosome M (ChrM) reads in RNA-seq samples.

(C) Overview of iCLIP data from two biological replicates. Total tags after filtering as well as percentage of ChrM reads are indicated for each replicate.

All bioinformatic analyses were performed by Lee-Hsueh Hung.

A simplified workflow to reveal IMP3 target RNAs, which show a change in gene expression levels in MO extracts upon IMP3 depletion, is illustrated in Fig. 4.17A. The focus was set on protein-coding transcripts, i.e. mRNAs, because we were interested in the role of IMP3 in the secretory pathway. To find transcripts with gene expression changes in MO extracts, a fold change of minimally factor 1.4 ($\log_2(0.5)$) was set between IMP3 k.o./wt or IMP3 k.d./ctr k.d. MO extracts. This way, around 200 transcripts were found to be up- or down-regulated by comparing IMP3 k.o. to wt extracts, whereas this was the case for around 300 – 400 transcripts in IMP3 k.d./ctr k.d. extracts. In the last step, targets were finally selected. An additional important criterium was applied, which states that the fold change differences between IMP3 k.o./wt or IMP3 k.d./ctr k.d. should be more pronounced in MO extracts than in cytosol extract. Moreover, both iCLIP replicate datasets were combined. The final gene counts showed only few targets which were upregulated in the MO extracts upon IMP3 depletion (0 upon IMP3 k.d., 6 upon IMP3 k.o.). For IMP3 k.o., only slightly more targets were downregulated compared to wt. By contrast, transient IMP3 k.d. yielded 159 target mRNAs, which were downregulated. Therefore, the focus was set to these targets. GO-term enrichment analysis regarding cellular components (<http://geneontology.org>) revealed that the most significant enriched terms are related to membrane/ER/Golgi association (Fig. 4.17B). This mirrors the enrichment of transcripts coding for proteins within the secretory pathway as well as the good quality of the subcellular fractionation procedure.

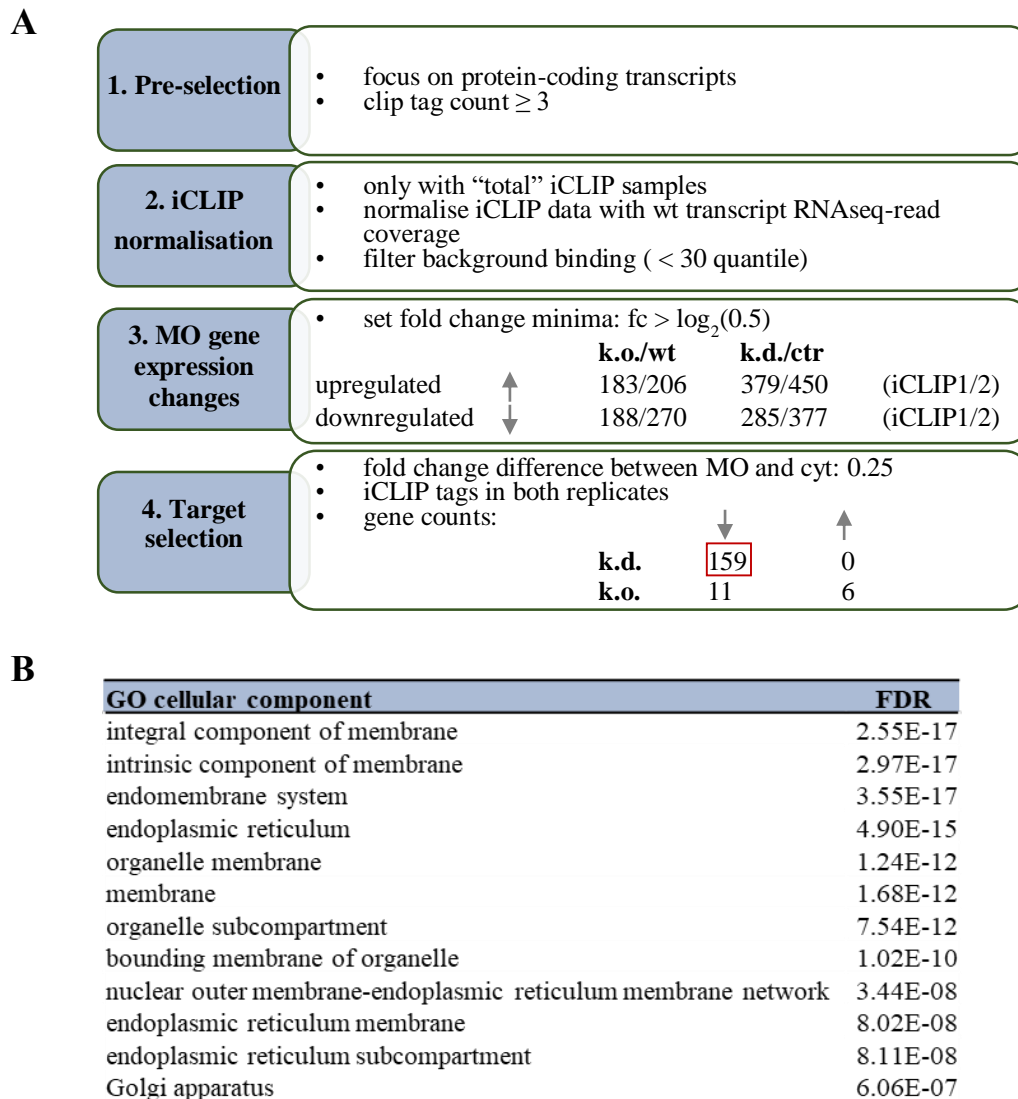


Figure 4.17: Combined bioinformatic analysis of RNA-seq and iCLIP data for target identification.

(A) Simplified workflow of bioinformatic analysis. The focus was directed at the 159 genes bound by IMP3 which were downregulated in the MO fraction upon IMP3 knockdown.

(B) GO term (cellular component) enrichment of IMP3 bound RNAs downregulated in the membrane organelle fraction upon IMP3 knockdown. The most significantly enriched terms are listed (FDR < 1E-06).

All bioinformatic analyses were performed by Lee-Hsueh Hung.

4.2.3 Experimental validation of target mRNAs

Within the 159 bioinformatically found targets, several targets were chosen for biochemical validation. The chosen targets are all part of the secretory pathway, downregulated in the MO fraction upon IMP3 k.d. at least 1.7-fold compared to ctr k.d., and encode proteins in different cellular components with different functions. This way, a broad spectrum should be covered. As a representative, the iCLIP profiles of the two sequenced iCLIP replicates are shown for the

selected target C-X-C motif chemokine 5 (*CXCL5*) (Fig. 4.18A). In all samples, iCLIP tags are located in the exons and in the long 3'UTR. Validation of iCLIP data was conducted by RIP experiments with FLAG-IMP3 and endogenous IMP3. Importantly, no UV-crosslink was used to reflect more physiological conditions. In addition, a control-IP with anti-c-Myc antibody (as in iCLIP experiments for FLAG-IMP3) or anti-FLAG antibody (as in previous RIP assays for endogenous IMP3) was performed. Input as well as IP samples were analysed by Western blot (Fig. 4.18B) and RT-PCR (Fig. 4.18C). (FLAG-)IMP3 was shown to be specifically pulled down by the respective antibody (Fig. 4.18B). Analysis of selected target mRNAs revealed that they were present in the IP of FLAG-IMP3 and endogenous IMP3, but were not found in ctr IP reactions (Fig. 4.18C). The control RNAs *FTL* (positive ctr) and snoRD *U78* (negative ctr) confirmed the quality of the RIP assays.

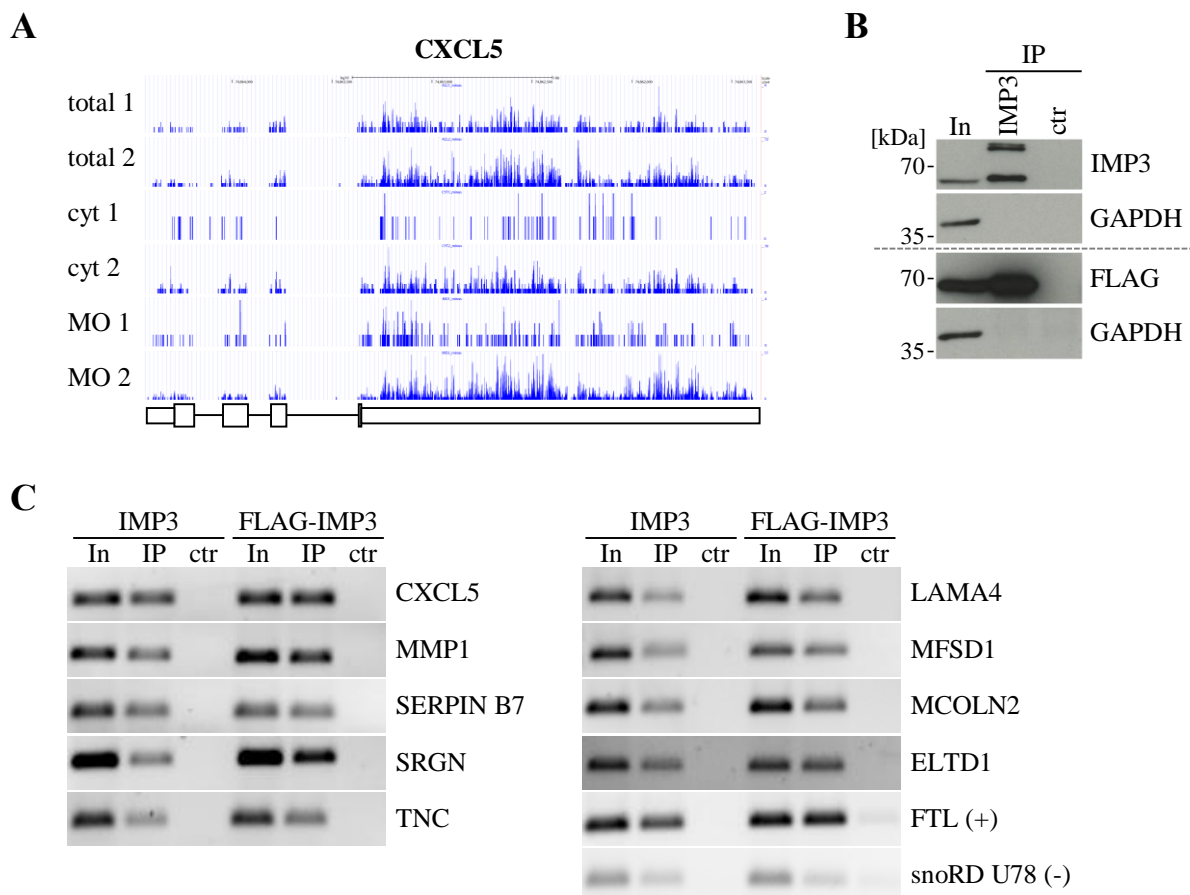


Figure 4.18: IMP3 binds to selected target mRNAs.

(A) iCLIP tags in *CXCL5*. *CXCL5* is downregulated in the MO fraction upon IMP3 knockdown and shown as an example target. iCLIP tags of both replicates are shown in total cells, cytosol and MO fraction, exon/intron structure is shown schematically at the bottom.

(B) (C) Validation of iCLIP targets by RNA immunoprecipitation with endogenous and FLAG-tagged IMP3. Input, (FLAG-)IMP3 IP and ctr IP samples were first analysed by Western blot (B) and then by RT-PCR (C). Binding to selected targets, which are part of the secretory pathway, was tested. The two RNAs *FTL* and snoRD *U78* served as positive (+) or negative (-) control, respectively.

Having IMP3 binding to the selected targets validated, the downregulation in the MO fraction upon IMP3 k.d. should be also biochemically confirmed. For this purpose, RT-qPCR was performed with isolated RNA from three independent subcellular fractionation experiments. RNA levels in IMP3 k.d. fractions were calculated relative to RNA levels in ctr k.d. samples (Fig. 4.19). All targets showed a decrease of RNA levels upon IMP3 depletion, which was significant for eight of the nine selected targets as indicated by the asterisks ($p < 0.05 - p < 0.00005$). In addition, three targets showed an overall downregulation of the RNA level (as can be seen in “input” samples), and two targets a weak significant downregulation in cytosol fractions. In conclusion, IMP3 binding to mRNAs and their downregulation in MO fractions upon IMP3 depletion, as revealed by iCLIP and RNA-seq data, could be experimentally validated.

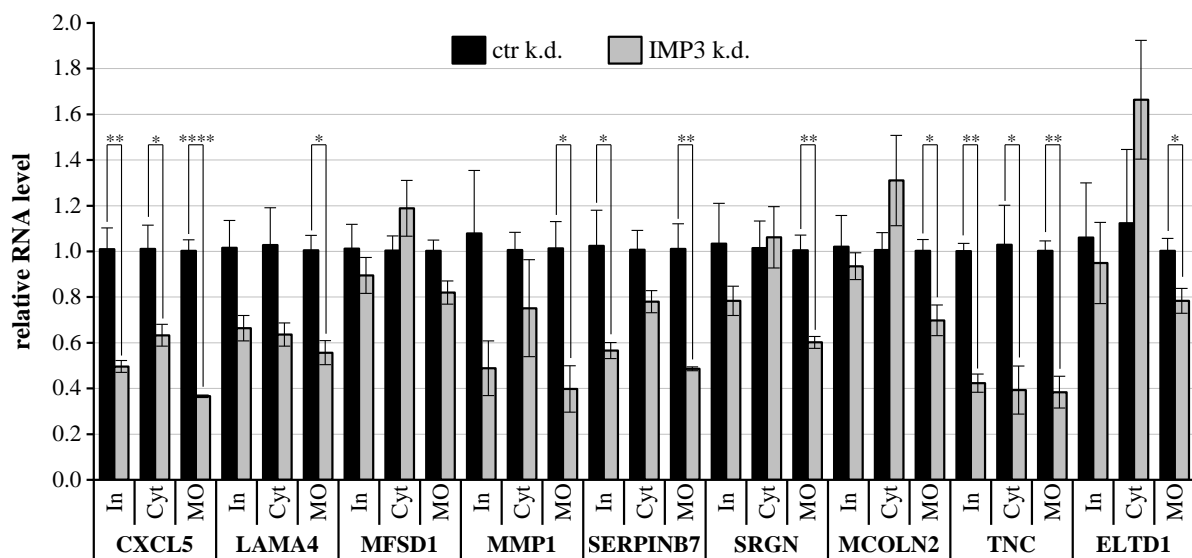


Figure 4.19: IMP3 knockdown leads to downregulation of target mRNAs in MO fractions.

RNA level changes of validated bound targets in input (total), cyt or MO fractions. mRNA levels are shown for IMP3 k.d. relative to ctr k.d. Error bars represent standard errors of mean ($n = 3$ biological replicates, * $p < 0.05$, ** $p < 0.005$, *** $p < 0.0005$, **** $p < 0.00005$).

However, the molecular mechanism of this downregulation remained elusive. Since the IMP family is also known to regulate the stability of RNAs, the observed effect might be explained by decreased stability of target mRNAs upon IMP3 depletion. To clarify this, stability assays with the transcription inhibitor actinomycin D were performed. Again, ctr or IMP3 k.d. was performed and analysed by Western blot and RT-qPCR (Fig. 4.20A + B). Upon knockdown, IMP3 mRNA levels decreased to ~23% compared to ctr k.d. mRNA levels, consistent with the protein levels detected by Western blot. To examine the stability of RNAs, a time course with actinomycin D treatment was performed and cells harvested up to 3 h. Additionally, cells were harvested before actinomycin D was added (“0” time point). Isolated RNA of all time points

was subjected to RT-qPCR and obtained data set relative to RNA levels in the respective “0” time point (Fig. 4.20C + D). As a positive control, *MYC* mRNA, a known IMP3 target with a short half-life of ~1 h (Huang *et al.*, 2018) was used (Fig. 4.20C). Within three hours, *MYC* mRNA levels dropped to 5.6 % or 3.9 % in ctr k.d. or IMP3 k.d. cells, respectively, confirming the functionality of the assay. However, looking at the target mRNAs, no decrease in mRNA levels was observed in ctr k.d. or IMP3 k.d. cells (Fig. 4.20D). This implies that all selected mRNAs have a long half-life *in vivo*. Nevertheless, since we did not see any changes upon IMP3 knockdown, we conclude that IMP3 has no dramatic influence on the stability of the selected target mRNAs.

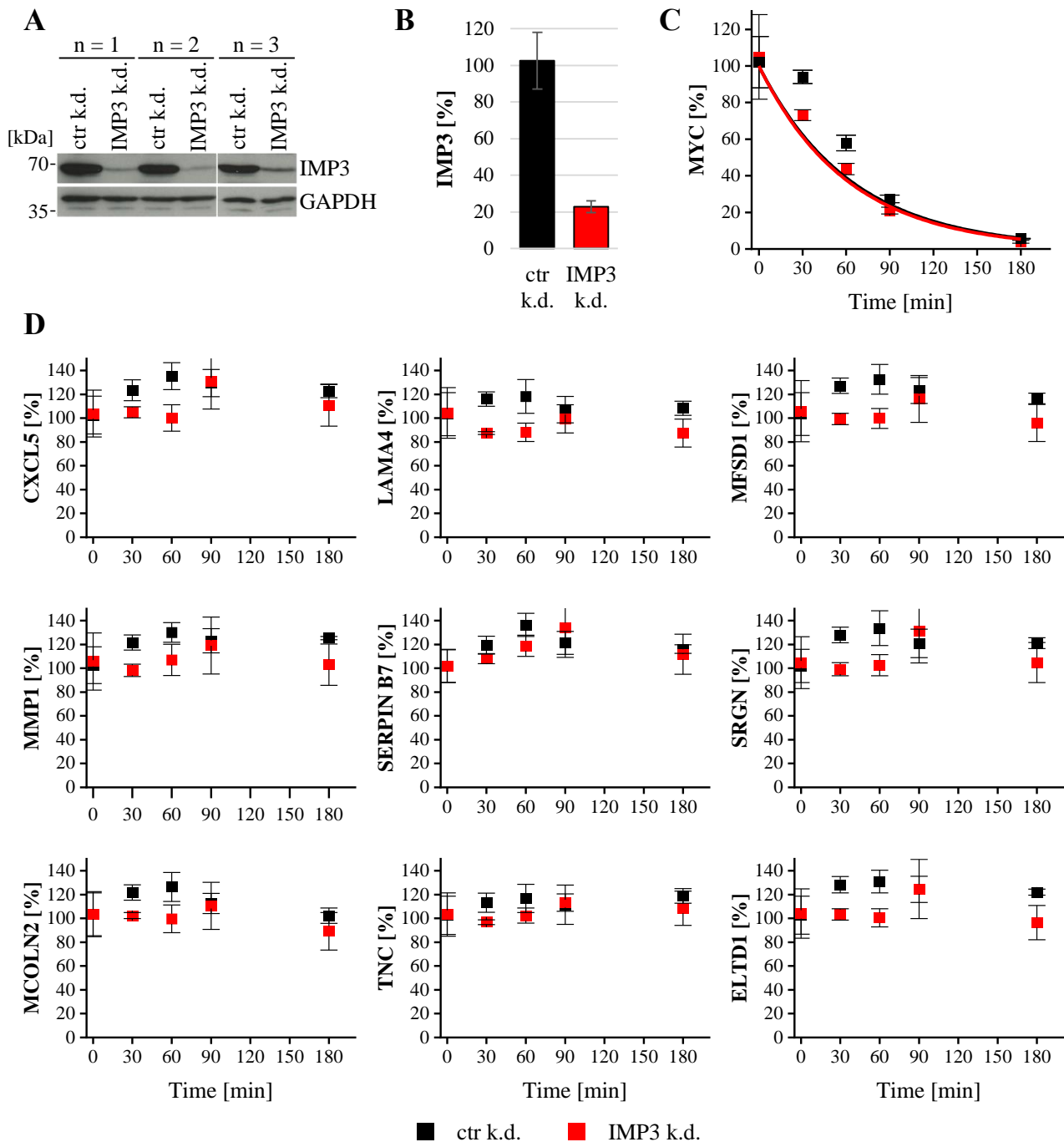


Figure 4.20: IMP3 knockdown does not influence stability of target mRNAs.

(A) (B) Knockdown verification of IMP3 protein level by Western blot (A) or IMP3 mRNA level by RT-qPCR (B). IMP3 k.d. was compared relative to control k.d., the latter was set to 100% in qPCR analysis. Error bars show the standard error of mean of three independent biological replicates. GAPDH served as a loading control for Western blotting.

(C) Changes in *MYC* mRNA levels (positive control) upon actinomycin D treatment. *MYC* mRNA levels were assessed by RT-qPCR upon actinomycin D treatment in ctr k.d. (black) or IMP3 k.d. (red) cells. RNA levels during the time course were calculated corresponding to the respective 0 time point. Error bars show the standard error of mean ($n = 3$). Data were fit with a first-order decay function.

(D) Changes in target mRNA levels upon actinomycin D treatment. mRNA levels were calculated as in (C) and are depicted the same way.

4.2.4 Functional analysis of IMP3 circRNA sponges on target mRNAs

Last but not least, we asked whether our circRNA sponges might have a similar effect on target mRNA levels in MO fractions as an IMP3 knockdown. To clarify this aspect, we pursued two different strategies of sponging: (1) We used again the Tornado system, in which circRNAs are expressed from a transfected plasmid *in vivo*, or (2), directly transfected purified, *in vitro* synthesised circRNAs. For the latter, two different amounts of circRNAs were transfected (1 µg or 4 µg). All sponge constructs possessed one repeat of the ANKRD17, 101-mer or allUG sequence, respectively, with allUG serving again as the negative control. 24 h after transfection of ES-2 cells, cells were fractionated, as controlled by Western blot (data not shown). RNA isolated from the cytosol and MO fractions was examined by testing for the top three target mRNAs by RT-qPCR (Fig. 4.21A). Target RNA levels were set relative to respective allUG samples. In addition to the comparison of the effect of the circRNA sponges, a mock transfection was included in the experiment and depicted in the qPCR graphs. The expected decrease of RNA levels in MO fractions upon the presence of ANKRD17 or 101-mer circRNAs in comparison to allUG circRNA could not be seen for any of the three targets in any of the three different conditions. By contrast, the RNA levels of *CXCL5* were strongly increased upon transfection of purified ANKRD17 and 101-mer circRNAs (Fig. 4.21A, upper left). However, the transfection itself seemed to have an influence on target RNA levels, since these were mostly overall lower in mock-transfected cells, with again *CXCL5* showing the strongest discrepancy between mock transfection and transfection of circRNA sponges (up to 7-fold higher RNA levels). Trying to understand this effect, we wondered where the sponges are located within the cells. We therefore performed RT-qPCR on the circRNA sponges and calculated their relative cytoplasmic/membrane organelle distribution (Fig. 4.21B). All three Tornado sponges were predominantly located in the cytoplasm. Concerning the transfected circRNAs, their localisation was less distinct, with a tendency towards the cytoplasm. To sum up, we could not reproduce the effect on target mRNA levels with circRNA sponging as for IMP3 knockdown. However, this might be due to technical issues (see discussion).

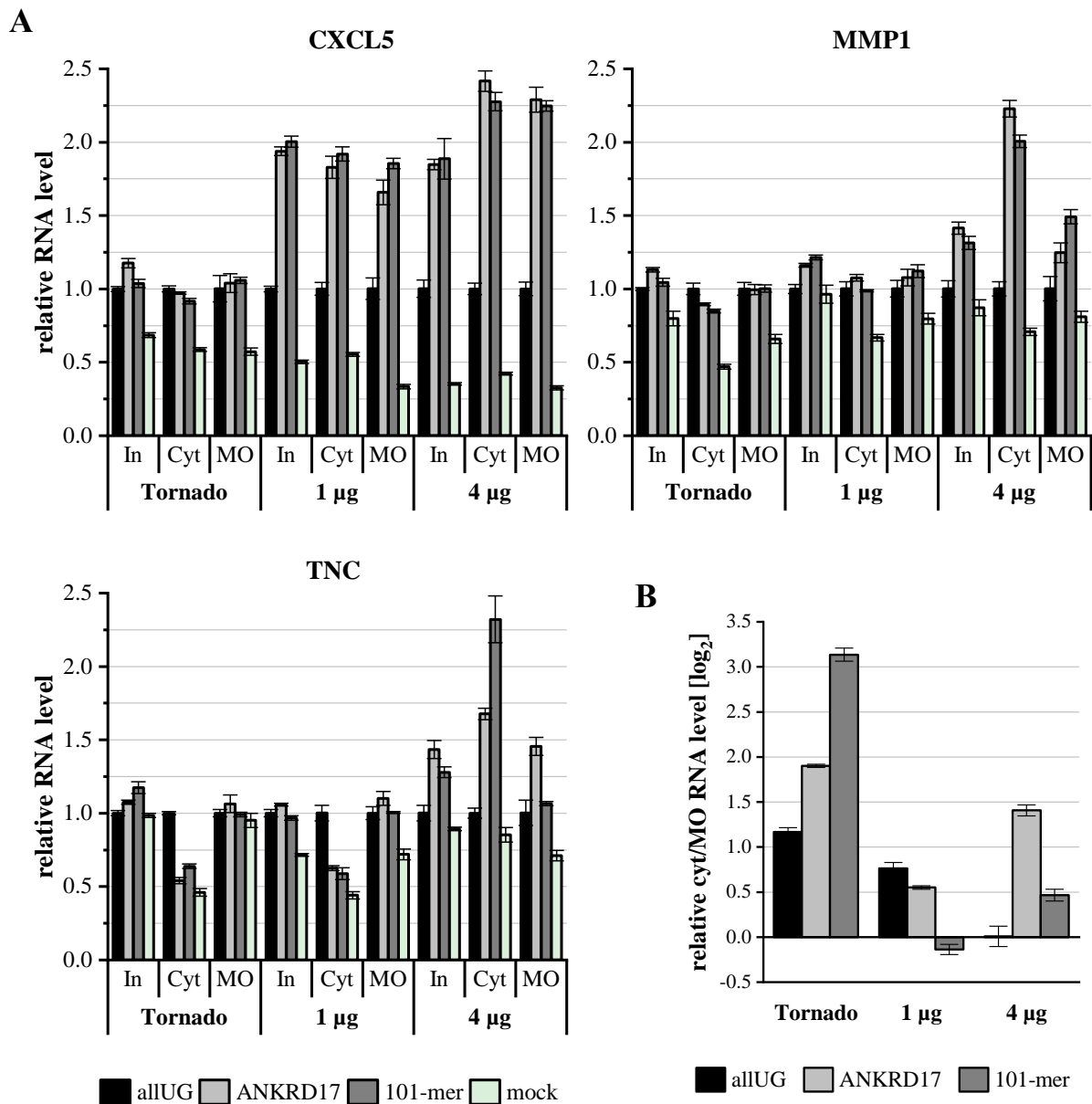


Figure 4.21: Influence of IMP3 circRNA sponges on target mRNA regulation.

(A) RNA levels of *CXCL5*, *MMP1* and *TNC* in input, cyt or MO fractions upon presence of IMP3 sponges allUG, ANKRD17 or 101-mer. Plasmids encoding Tornado circRNAs, 2 different amounts (1 or 4 μg) of *in vitro* produced circRNAs or mock control were transfected in ES-2 cells. Cells were harvested 24 h after transfection and subcellular fractionated. Effect of sponges on three selected target mRNAs was examined by RT-qPCR. RNA levels are shown relative to corresponding allUG transfection. Error bars represent standard deviations (n = 3 technical replicates).

(B) IMP3 sponge circRNA distribution analysis of fractionated ES-2 cells from (A) by RT-qPCR. Levels of the respective Tornado circRNA or *in vitro* produced circRNA were assessed. Data were normalised to input to see cytoplasmic/membrane organelle distribution. Error bars show standard deviations (n = 3 technical replicates).

5 Discussion

5.1 Designer circRNAs function as IMP3 sponges

5.1.1 *In vitro* interaction of IMP3 with circRNA sponges

CircRNAs have great potential to be used as a tool in biotechnological and molecular-medical applications. Thus, we investigated whether a relevant RNA-binding protein could be sponged by designer circRNAs, thereby inhibiting its binding to endogenous target RNAs. We focussed on IMP3, an RBP upregulated in a variety of cancers and hence classified tumour marker, for which previous work from our lab revealed a defined RNA-binding motif (Schneider *et al.*, 2019; Fig. 1.2). We selected two constructs possessing the full-length CA- and GGC-rich IMP3 binding motifs, which were either extracted from the natural ANKRD17 sequence or from SELEX-seq analysis (“101-mer”; Fig. 4.1). A construct, in which all binding motifs were converted to UG-repeats (“allUG”), served as a negative control. Since these constructs had previously been analysed for IMP3 binding *in vitro* as linear RNAs (Schneider *et al.*, 2019), we asked whether their binding properties are similar for RNAs in a circular configuration.

A stem sequence was attached to all constructs to restrict flexibility of the 5' and 3' ends and thereby enhance circularisation efficiency, a well-known strategy for circRNA synthesis (Breuer and Rossbach, 2020; Müller and Appel, 2017). The stem sequence did not alter positioning of the IMP3 RNA-binding motifs in RNA secondary structure predictions (Fig. 4.2), making it usable for *in vitro* circRNA generation. Analysis of ligated transcripts revealed the presence of a second upshifted band (Fig. 4.3B), which was stronger than the band representing the linear transcript and changed its position respective to linear markers depending on the polyacrylamide concentration of the gel (data not shown). This altered migration in polyacrylamide gels is a typical feature of circRNAs (Jeck and Sharpless, 2014). Another circRNA characteristic is their resistance to the exoribonuclease RNase R, which is commonly used for validation of circularity (Hansen *et al.*, 2013a; Jeck *et al.*, 2013; Memczak *et al.*, 2013; Salzman *et al.*, 2012). Only ANKRD17 circRNA was not fully resistant to RNase R treatment, but showed increased stability compared to its linear counterpart (Fig. 4.3C). Since some circRNAs were reported to be RNase R sensitive (Szabo and Salzman, 2016), we propose that ANKRD17 belongs to this group.

Binding of IMP3 to circRNA sponges was examined by EMSAs using radioactively labelled RNAs. EMSA assays have been performed with biotinylated circular RNAs before (Li *et al.*, 2019a), but to our knowledge neither with radioactively labelled circRNAs nor, more

importantly, in a direct comparison of the circRNA to its linear counterpart. IMP3-RNA complexes were visualised after gel electrophoresis and showed one distinct band representing the bound RNA (Fig. 4.5A), suggesting a 1:1 stoichiometry of protein and RNA, consistent with the literature (Schneider *et al.*, 2019). Dissociation constants of ANKRD17 and 101-mer were similar and demonstrated high affinity of IMP3 binding to linear and circular RNA (Fig. 4.5B). The negative control RNA allUG was bound with ~5-7 fold lower affinity by IMP3, with again no relevant difference in binding affinity for the linear or circular RNA isoform. The obtained K_d values were in the same range as has been reported for the linear RNA constructs without stem sequence (Schneider *et al.*, 2019). Linear RNAs containing the full-length IMP3 recognition motif seemed to be less tightly bound upon presence of the stem sequence (ANKRD17 $-/+$ stem: K_d 1.6 nM / 8.7 nM; 101-mer $-/+$ stem: K_d 3.5 nM / 9.3 nM), whereas the negative control showed a slightly higher affinity upon presence of the stem (allUG $-/+$ stem: K_d 61.1 nM / 48.8 nM) (K_d values of linear RNAs without stem from Schneider *et al.*, 2019). Thus, no clear influence of the stem structure on IMP3 binding could be observed. However, these small differences are likely not biologically relevant and might result from differences within the experiment, for example the usage of a different purified protein batch. We therefore concluded that the attached stem sequence has no influence on IMP3 binding and that circular RNA sponges are bound with affinities comparable to their linear counterparts *in vitro*. The here obtained results are promising that circRNAs can be used as a tool for RBP sponging.

5.1.2 *In vivo* sponging of IMP3

Going one step further, we examined binding of IMP3 to circRNA sponges *in vivo*. In the first strategy, we genomically integrated the circRNA sponge sequences in HeLa Flp-In T-REx cells. *In vivo* backsplicing should be facilitated by using inverted repeat sequences from the *ZKSCAN1* gene, as has been previously shown to transiently generate circRNAs after plasmid transfection (Liang and Wilusz, 2014). Addition of tetracycline led to induced expression of precursor RNAs for all constructs and this increased steadily over three days (Fig. 4.6B). The two ANKRD17 constructs containing either one (1xANKRD17) or two (2xANKRD17) repeats of the full-length IMP3 binding motif showed also increased expression of the corresponding circRNAs, in contrast to the negative controls 1xallUG and 2xallUG. For the latter, circRNA expression was not visible independent of the time interval of induction. It was observed before that the circularisation efficiency of this vector depends on the collaboration of the exon and intron sequences, i.e. exon length and sequence are decisive factors (Liang and Wilusz, 2014).

Since the length of the allUG and ANKRD17 constructs was almost identical, we assume that the sequence must be pivotal in this case. Further, as we detected allUG circRNA expression from transiently transfected ZKSCAN1 vectors (data not shown), it seems like the genomic integration plays a role, presumably by reducing the overall expression of the constructs. Regardless of the reason, we decided that our allUG cell lines do not represent appropriate negative controls and did not use them in the following experiments.

RNA-immunoprecipitation experiments in ANKRD17 stable cell lines revealed specific binding of IMP3 to the circRNA and not to the precursor (Fig. 4.7). This was also observed for the splicing regulator hnRNP L, as it bound to an identical genomically integrated circRNA sponge with higher efficiency than to its precursor form (Schreiner *et al.*, 2020). Considering the higher expression of the precursor compared to the circRNA, as suggested by experiments (Fig. 4.6B) and the literature (Liang and Wilusz, 2014), the preference of IMP3 for the circRNA isoform is especially remarkable. However, it cannot be concluded whether the 1xANKRD17 or the 2xANKRD17 circRNA sponges sequester IMP3 better, since the overall RIP efficiency and background varied slightly (as indicated by the FTL positive and U6 negative RNA control). In sum, we conclude from these experiments that stable and inducible expression of circRNAs is sequence dependent, but generally possible, and that IMP3 specifically binds to these.

Testing a second strategy, we transiently overexpressed circRNA sponges using the Tornado system (Litke and Jaffrey, 2019). Here, one copy of each sponge sequence was inserted, since polymerase III is specialised in synthesizing short RNAs. Tornado circRNA sponges could be detected by RT-PCR in contrast to the linear precursor form (Fig. 4.8B), which is of low abundance in this expression system (Litke and Jaffrey, 2019). In addition, detection of Tornado circRNAs was possible by SYBR Gold staining of total RNA separated by PAGE and the circRNA position changed with the polyacrylamide percentage of the gel, representing a typical circRNA migration behaviour (Fig. 4.8C). Tornado circRNA band intensities were just below those of 5S and 5.8S RNA, indicating high expression of the sponges. Indeed, expression of a Tornado Broccoli aptamer containing circRNA (96 nt) was estimated to achieve a concentration of 16 μM in HeLa cells (Litke and Jaffrey, 2019) and Tornado circRNAs with varying length and sequence were calculated to reach $\sim 10^5 - 10^7$ copies per cell (Schreiner *et al.*, 2020). Further characterisation of Tornado circRNA sponges showed that they were enriched in the cytoplasm, as expected (Fig. 4.9B; Litke and Jaffrey, 2019). Expression of circRNAs did not disturb

subcellular localisation of IMP3, which is also cytoplasmic (Fig. 4.9A; Nielsen *et al.*, 1999). Hence, both IMP3 and Tornado circRNA sponges are present in the cytoplasm.

RIP experiments demonstrated an enrichment of Tornado-ANKRD17 and Tornado-101-mer sponges in IMP3 IPs compared to control FLAG IPs (Fig. 4.10B). In comparison to the lowly abundant endogenous *circANKRD17* target, RIP efficiencies of Tornado sponges were rather low. We assume that this is due to the high copy number of the sponges present in the cells, probably exceeding IMP3 cellular concentration, as the latter is estimated to be present in the high nanomolar range in HeLa cells (Itzhak *et al.*, 2016). Interestingly, also RIP efficiencies of Tornado circRNA sponges targeting hnRNP L were rather low (3.8 – 10.7%), in contrast to RIP efficiencies previously obtained with different generated circRNAs (up to ~82%) (Schreiner *et al.*, 2020). This suggests that hnRNP L is also a limiting factor, although its cellular concentration is estimated to be 5.5-fold higher than IMP3 in HeLa cells (~4.1 μ M, Itzhak *et al.*, 2016). Since Tornado circRNA levels were reported to reach their maximum after 72 h (Litke and Jaffrey, 2019), we performed RIP experiments after shorter expression of Tornado sponges. Overall obtained RIP efficiencies for Tornado circRNAs were not higher (Fig. 4.10B), but comparison of the Tornado-ANKRD17 and -101-mer circRNAs to the negative control circRNA Tornado-allUG revealed the highest RIP efficiency after 24 h (Fig. 4.10C). In sum, we conclude that Tornado circRNA sponges are specifically bound by IMP3 and that the relative abundances of protein and circRNA has to be considered, when using this system.

Both *in vivo* applied methods for the generation of circRNA sponges demonstrated specific binding of IMP3. When deciding for one method, the benefits and drawbacks should be considered. The usage of a pol II expression system in which the circRNA sequence is flanked by inverted repeat sequences facilitates the generation of a circRNA similar to the natural context, meaning in turn that the backsplicing efficiency is rather low and the predominant outcome is a linear RNA. Thus, the circRNA will be present in a low copy number and might be the limiting factor for the desired circRNA-RBP interaction. By contrast, Tornado circRNAs are massively overexpressed in the cell. This relies partly on the pol III-based expression used, which is known to be more efficient in generating small circRNAs in comparison to pol II-based systems (Noto *et al.*, 2017). Usage of pol III expression also requires the circRNA sequences to be carefully controlled for polyU stretches, since four or more consecutive thymidines lead to transcription termination (Richard and Manley, 2009). This can make the introduction of sequence modifications necessary. Moreover, it should be considered that the targeted binding protein of the Tornado circRNA will likely be the limiting factor in this system.

Hence, a circRNA expression system should be chosen dependent on the introduced circRNA sequence properties and the purpose of the experiment.

5.2 IMP3 functions in RNA localisation

5.2.1 RNA-seq and iCLIP experiments reveal a subset of target mRNAs

The IMP family is known to regulate RNAs in terms of localisation, stability and translation. We wanted to obtain further insights in the role of IMP3 in RNA localisation, since there is currently only literature available for IMP1/ZBP1 or the IMP3 frog orthologue Vg1RBP in regulating RNA localisation. In addition, preliminary data from our lab suggested that IMP3 might function in the secretory pathway. We decided to employ a subcellular fractionation technique to enable separate analysis of cytosol and membrane organelle fractions (Fig. 4.12). For this purpose, cytosol fractions were obtained by a digitonin-based extraction, a procedure commonly used (Holden and Horton, 2009; Wang *et al.*, 2012). The non-ionic detergent digitonin interacts with cholesterol in membranes and this binding is linearly dependent on the cholesterol content (Nishikawa *et al.*, 1984). Since the cholesterol content of the plasma membrane is higher than that of membrane organelles such as mitochondria or the ER (Mesmin and Maxfield, 2009), digitonin can be used to extract the cytosol without perturbation of membrane organelles, provided that the concentration was optimised beforehand. In this procedure, the separation of components relies on their biochemical properties, which in turn means that also spatially distinct regions may co-purify into the same fraction (Taliaferro, 2019). However, biochemical fractionation has been successfully applied to reveal asymmetric distribution of (non)coding RNAs in *Drosophila* and human cells or to examine the role of muscleblind-like proteins in mRNA localisation (Benoit Bouvrette *et al.*, 2018; Wang *et al.*, 2012).

For ES-2 cells, a digitonin concentration of 25 µg/ml in the first fractionation buffer was found to be optimal (Fig. 4.13). This is in agreement with the literature, since cytosol extracts of other human cell lines as HEK293 or HeLa cells were prepared by applying 25 µg/ml or 100 µg/ml digitonin, respectively (Holden and Horton, 2009). Subcellular fractionation of ES-2 wt and ES-3 IMP3 k.o. cells as well as ES-2 wt cells treated with siRNAs was performed. All marker proteins showed the expected distribution, since GAPDH and γ -tubulin were found in the cytoplasm whereas the ER-resident protein calnexin was present in the membrane organelle fraction (Fig. 4.14A,B). IMP3 was enriched in the cytoplasm, but also clearly present in the

MO fraction, in agreement with its perinuclear localisation (Nielsen *et al.*, 1999; Fig. 1.4). A similar distribution was observed for transiently expressed FLAG-IMP3, suggesting that its slightly stronger expression compared to endogenous IMP3 does not impede its function (Fig. 4.15A). In addition, the applied UV-crosslinking of the cells expressing FLAG-IMP3 prior to fractionation did not interfere with the fractionation procedure, as displayed by the marker proteins. In the iCLIP experiments, an optimised RNase I concentration was used to achieve a partial RNA digest (Fig. 4.15B). Optimising this step is crucial to obtain RNA sizes suitable for library preparation, which correspond to RNAs of 50 nt to 300 nt length (Huppertz *et al.*, 2014). Total cell lysates were additionally treated with high RNase I concentrations as controls. In these samples, the pulled-down protein will be bound to short RNAs and migrate at approximately 5 kDa above the expected molecular weight of the protein alone (Buchbender *et al.*, 2020). Unexpectedly, we observed this effect also in non-crosslinked FLAG-IMP3 iCLIP samples (Fig. 4.15B), although the overall radioactive signal was strongly reduced compared to crosslinked samples. Since FLAG-IMP3 was pulled down in all iCLIP samples incubated with anti-FLAG antibody (Fig. 4.15B, bottom), one possible explanation could be strong binding of FLAG-IMP3 to some RNAs, which were not removed through stringent washing and thus labelled. An additional possibility is the co-purification of a kinase, which could label the protein radioactively during the iCLIP procedure (Oliver Roßbach, personal communication). However, since all UV-crosslinked samples showed the expected radioactive smear on the membrane, iCLIP libraries were generated.

Bioinformatic analysis of iCLIP and RNA-seq datasets revealed mRNAs bound by IMP3, which showed altered gene expression upon IMP3 depletion in MO extracts. The final selection revealed only a few upregulated targets in MO extracts upon IMP3 depletion (Fig. 4.17A). Looking at the downregulated targets, we found 11 mRNAs in IMP3 k.o. samples and 159 mRNAs in IMP3 k.d. samples. Discrepancies between gene knockdown and gene knockout has been observed in a variety of studies in different model organisms, ranging from plants to humans (summarised in El-Brolosy and Stainier, 2017). In these studies, knockout/mutants showed now or only little phenotypes in contrast to knockdowns, which is consistent with our observations. A possible explanation is genetic compensation upon knockout, i.e. changes in other protein levels that counterbalance the loss of function of the target protein (El-Brolosy and Stainier, 2017). This might be facilitated by the upregulation of a paralogue or other related protein. In our case, ES-2 IMP3 knockout cells seemed not to possess an increased expression of IMP1 or IMP2, as indicated by Western blot (Schneider *et al.*, 2019). However, this does not exclude the compensation by other factors within a regulatory network. By contrast, siRNA-

mediated knockdown leads to transient depletion of a protein without large compensatory effects. We therefore hypothesise that IMP3 k.d. and IMP3 k.o. cells have different properties, which lead to the discrepancy in target numbers. We decided to focus on IMP3 knockdown targets, since the knockdown cells might be physiologically closer to the natural ES-2 wt cells. Gene ontology analysis showed that selected targets were associated with cellular membranes or membrane organelles (Fig. 4.17B). This confirms the quality of the subcellular fractionation procedure and is in agreement with an enrichment of transcripts encoding proteins that undergo the secretory pathway.

5.2.2 Biochemical validation of target mRNAs

Experimental validation of bioinformatically predicted targets is crucial, since more and different biological replicates as used in the RNA-seq experiments verify the biological conclusion (discussed in Fang and Cui, 2011). Therefore, we chose a subset of the 159 bioinformatically found downregulated targets for validation by RIP experiments and RT-qPCR. The selected subset contained mRNAs encoding for proteins localised in different cellular components with different functions, but all mRNAs entered the secretory pathway and were downregulated in the MO fraction upon IMP3 k.d. at least 1.7 fold compared to ctr k.d.. Some of the target mRNAs have been also reported in context with IMP3 before, e.g. *CXCL5* was among the most downregulated genes in a hepatocellular carcinoma cell line depleted of IMP3, as revealed by microarray analysis (Jeng *et al.*, 2008). Similarly, microarray studies revealed *MMP1* to be downregulated upon simultaneous knockdown of IMP1 and IMP3 in HeLa cells (Vikesaa *et al.*, 2006).

IMP3 iCLIP tags were located in the exons and the 3'UTR of targets, as shown for *CXCL5* (Fig. 4.18A). Other CLIP studies have also found IMP3 to bind preferentially in these regions (Ennajdaoui *et al.*, 2016; Hafner *et al.*, 2010; Huang *et al.*, 2018; Palanichamy *et al.*, 2016). RIP experiments to experimentally verify binding of IMP3 to the targets were performed with transiently expressed FLAG-IMP3 and endogenous IMP3, as we wanted to exclude that the observed iCLIP tags were artefacts from FLAG-IMP3 expression. Moreover, no UV-crosslinking was applied in these experiments. Consequences of this are, first, potential co-immunoprecipitations of other bound proteins resulting in the capture of other, indirectly bound RNAs and, second, loss of transient/weak interacting RNAs during the RIP procedure (Riley and Steitz, 2013). We think that omitting the crosslinking step can be considered as a complementary method to iCLIP, since UV-crosslinking introduces biases of its own (Wheeler

et al., 2018). All nine selected targets could be validated by RIP experiments for both endogenous IMP3 and FLAG-IMP3, as shown for a representative biological replicate (Fig. 4.18C). Moreover, they were specific as seen by immunoprecipitations with control antibodies. We therefore considered the validation of the iCLIP experiments to be successful and continued with verifying the RNA-seq data.

RNA was isolated from extracts resulting of three independent subcellular fractionation experiments and analysed. For eight of the nine selected targets, the downregulation in the MO fraction upon IMP3 k.d. compared to ctr k.d. was found to be significant (Fig. 4.19). This reinforces the RNA-seq data and the reproducibility of the experiment. The three targets *CXCL5*, *SERPIN B7* and *TNC* displayed overall reduced RNA levels upon IMP3 k.d. (see “input” samples) with *CXCL5* and *TNC* being additionally downregulated in the cytosol fraction. In our hypothesis, RNA levels of the targets are reduced in the MO fraction upon IMP3 depletion because they are less efficiently targeted to the ER membrane for translation. If the RNA level is overall decreased, this could potentially arise as a consequence of a feedback loop upon less efficient RNA localisation. However, another possibility is that the RNA becomes destabilised upon IMP3 knockdown. To examine the latter aspect, stability assays with the transcription inhibitor actinomycin D were performed. ES-2 cells treated with siRNA targeting luciferase (control) or IMP3 were supplemented with actinomycin D for up to three hours. This time interval was chosen to avoid secondary effects of cytotoxicity arising from longer treatment with actinomycin D (Lai *et al.*, 2019). For all nine targets, no reduction in RNA levels was observed for ctr k.d. or IMP3 k.d. cells (Fig. 4.20D). The general functionality of the assay was proven by examining *MYC* mRNA, a known IMP3 target with a short half-life ~1 h (Huang *et al.*, 2018), which displayed the expected decrease upon actinomycin D treatment (Fig. 4.20C). Thus, we conclude that the chosen RNA targets possess relatively long half-lives of more than 6 h, which would require an extension of the time interval of actinomycin D treatment to non-recommended periods (Lai *et al.*, 2019). An alternative way to measure RNA stability is *in vivo* labelling of RNA transcripts with uracil analogues (Wada and Becskei, 2017). Most commonly used analogues are 4-thiouridine (4sU) and 5-bromouridine (BrU), with the latter displaying a less general toxic effect than 4sU (Wolfe *et al.*, 2019). However, incorporation of modified nucleotides might alter RNA turnover, for example by influencing RNA structure (Wada and Becskei, 2017; Wolfe *et al.*, 2019). In addition, the labelled RNAs need to be specifically captured after harvesting of the cells, which means elaborate handling times and higher risks of greater variability in the results. Thus, RNA half-lives measured by different techniques were not shown to correlate well (Wada and Becskei, 2017; Wolfe *et al.*, 2019).

In conclusion, we could demonstrate that in the chosen time interval of actinomycin D treatment, we did not see an effect of IMP3 depletion on RNA stability. We therefore suggest that IMP3 functions in RNA localisation and propose the following model (Fig. 5.1): Multiple IMP3 proteins bind to the 3'UTR of mRNAs and serve as an additional factor to localise these mRNAs. Upon the start of translation, other factors such as the signal recognition particle recognise a signal sequence in the nascent polypeptide chain and help to guide the mRNA to the ER membrane by interacting with the SRP receptor. Translation of the mRNA continues with the polypeptide chain being directly translocated into the ER lumen. During the whole process, IMP3 likely interacts also with other proteins within mRNP complexes.

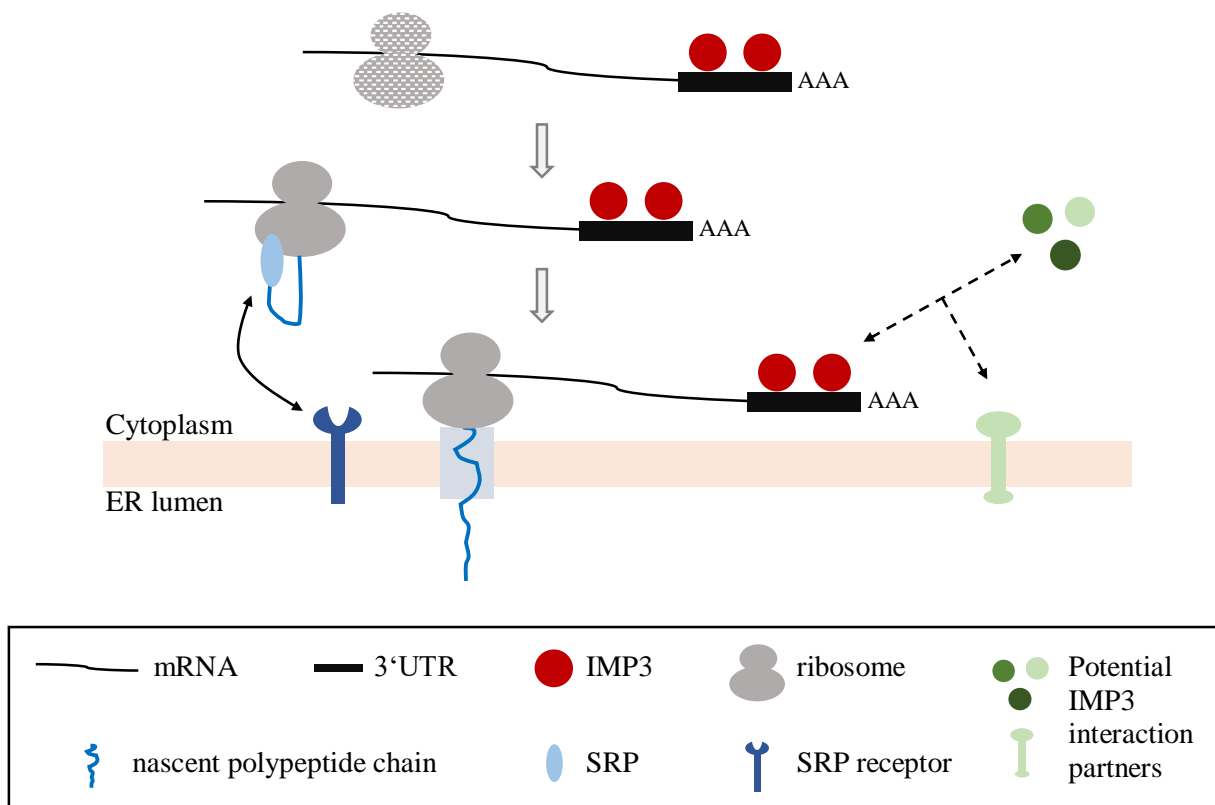


Figure 5.1: Model of IMP3 participation in mRNA localisation.

IMP3 binds to the 3'UTR of mRNAs coding for proteins that undergo the secretory pathway. IMP3 helps to localise these mRNAs to the ER membrane for translation and serves as an additional factor to e.g. the signal recognition particle, which binds to an N-terminal signal sequence on the nascent polypeptide chain of ribosomes and temporarily stalls translation. Targeting to the ER membrane is facilitated by protein-protein interactions of SRP with the SRP receptor, and of IMP3 with other cytoplasmic or membrane proteins.

5.2.3 Effect of circRNA sponges on target mRNA localisation

In a last step, we asked if our IMP3 circRNA sponges affect target mRNA levels similar as a siRNA-mediated IMP3 knockdown. Our lab had previously shown that alternative splicing

patterns of hnRNP L target transcripts were comparably influenced by transfected circRNA sponges as upon hnRNP L knockdown (Schreiner *et al.*, 2020). To examine the effect on IMP3 mRNA target localisation, we transfected Tornado circRNA-encoding plasmids or *in vitro* produced circRNA sponges in ES-2 cells and performed subcellular fractionation 24 h afterwards. All circRNA sponges were preferentially localised in the cytoplasm compared to the membrane organelle fraction (Fig. 4.21B). For the three Tornado sponge constructs, the cytoplasmic localisation was most pronounced, in agreement with the reported cytoplasmic/nuclear distribution and previous results (Litke and Jaffrey, 2019; Fig. 4.9B). The transfected circRNAs showed a less clear distribution profile, but possessed also a tendency towards the cytoplasm. In general, no uniform cellular localisation was reported for transfected circRNAs, as some were enriched in the cytoplasm, others in the nucleus, or evenly distributed between both compartments (Chen *et al.*, 2017; Jost *et al.*, 2018; Schreiner *et al.*, 2020). Hence, circRNA localisation is likely dependent on their intracellular interactions e.g. with RBPs, and thus sequence dependent (Schreiner *et al.*, 2020). All in all, since IMP3 is mainly found in the cytoplasmic fraction, we conclude that the localisation of the here examined circRNAs is beneficial for IMP3 sponging.

Furthermore, RNA levels of the top three targets were examined and are displayed relative to the allUG control (Fig. 4.21A). In short, we did not see a reduction of target mRNAs in the MO fraction upon presence of the ANKRD17 or 101-mer sponge, as we observed before upon IMP3 knockdown (Fig. 4.19). Moreover, there was a remarkable difference in RNA levels between allUG sponge transfections and mock transfection, with mock transfection showing overall lower RNA levels. This suggests an influence of the transfection itself. Indeed, a cytotoxic effect was observed for all transfected cells resulting in a lower cell confluence compared to mock-transfected cells (not shown). This lower cell confluence was not obtained in the previous siRNA-mediated IMP3 knockdown experiments, in which siRNA was transfected three days prior to subcellular fractionation. The changed cell confluence results in a different average cell proliferation state, since confluence is accompanied by contact-induced inhibition and cell cycle arrest (McClatchey and Yap, 2012). The here made observations might therefore also result from cell-cycle dependent gene expression changes. Besides, transfection reagents can induce transcriptome changes (discussed in Stepanenko and Heng, 2017). In general, it seems like the transfection of 4 µg purified ANKRD17 or 101-mer circRNA induces an increase of all three target RNAs in all cellular extracts compared to allUG circRNA. For *CXCL5*, this effect is the strongest and already present when 1 µg circRNA was transfected. One possible explanation for this observation might be a stimulation of the immune system, since introduction of any

vector or nucleic acid can generally lead to such effects (Chen *et al.*, 2003). Interestingly, the upregulation seems to be sequence- and/or structure-dependent and not only based on the introduction of circRNA, as the effects for the more sequence similar ANKRD17 and 101-mer are comparable with each other but not to allUG. Taking a closer look at *CXCL5*, the discrepancy of allUG to mock transfection is the largest. *CXCL5* is a chemokine known to activate neutrophils, which in turn mediate first responses to microbial infection and tissue injury (Rajaratnam *et al.*, 2019). Thus, the transfection might have triggered an immune response, which led to enhanced chemokine production. However, whether foreign circRNAs truly trigger immune responses is currently highly debated in the field. Whereas an activation of the intracellular immune receptor RIG-I (retinoic acid-inducible gene I) was first suggested (Chen *et al.*, 2017), later evidences indicated that the observed effects did not depend on the circRNA itself, but on by-products created during the circRNA synthesis procedure such as structured linear (5'-triphosphorylated) RNAs (Wesselhoeft *et al.*, 2019). Since the circRNAs used in this work were gel-purified, by-products should have been removed. To exclude that the observed effects are not due to impurities, another purification of the synthesised circRNAs could be tested as e.g. HPLC purification in combination with phosphatase treatment to remove RNAs with 5'-triphosphates (Wesselhoeft *et al.*, 2019). However, concerning that all three target mRNA levels were upregulated, the observed phenomenon might reflect a more general cellular stress response. Cellular stress can lead to the formation of stress granules, in which IMP3 has been shown to be part of (Huang *et al.*, 2018; Taniuchi *et al.*, 2014a; Wächter *et al.*, 2013; Zeng *et al.*, 2020). Under stress conditions, IMP3 stabilises target mRNAs. The increase in mRNA target levels observed here could therefore also potentially arise from a transfection-induced stress response, in which IMP3 tightly associates with its target mRNAs in stress granules.

In conclusion, circRNA sponges did not affect target mRNA levels as IMP3 knockdown. However, this is likely due to the transfection procedure. Therefore, a change in the experimental setup by employing e.g. stable inducible expression of circRNA sponges might lead to a different outcome. Further research would be necessary to finally clarify the effect of IMP3 circRNA sponging.

5.3 Future perspectives

IMP3 is a tumour marker with an upregulated expression in a variety of cancer types, leading to poor prognosis for patients. Understanding its biological function will therefore also contribute in developing anti-cancer strategies. In this thesis, insights into IMP3's function in RNA localisation were obtained. The data suggest that IMP3 plays a role in the secretory pathway and helps to guide mRNAs to the endoplasmic reticulum for translation. However, the exact mechanism and potential interaction partners remain unknown and need to be clarified in further research. Potential questions could address if IMP3 interacts with different proteins in cytosolic or membrane organelle extracts as well as the role of post-translational modifications, e.g. phosphorylation, of IMP3. High-resolution microscopy approaches could also reveal the exact cellular localisation of IMP3 with target RNAs and, together with biochemical approaches, the stoichiometry of the interaction.

Despite getting insights into the function of IMP3, circRNA sponge strategies were employed to inhibit IMP3. In general, the elevated stability of circRNAs makes them a promising tool in molecular medicine approaches. Here, we generated evidence that designer circRNA sponges can bind IMP3 *in vitro* and *in vivo*. Further, it would be interesting to see if this is also true in more complex cellular systems such as spheroids or in model organisms. Here, anti-cancer effects of the IMP3 circRNA sponges as for example reduced migration and metastasis could be directly monitored. This would also give additional insights in the general application of circRNAs in therapeutic strategies.

6 References

- Abdelmohsen, K.; Panda, A. C.; Munk, R.; Grammatikakis, I.; Dudekula, D. B.; De, S.; Kim, J.; Noh, J. H.; Kim, K. M.; Martindale, J. L.; Gorospe, M. (2017). Identification of HuR target circular RNAs uncovers suppression of PABPN1 translation by CircPABPN1. *RNA biology* 14(3), 361–369. DOI: 10.1080/15476286.2017.1279788.
- Aktaş, T.; Avşar Ilık, İ.; Maticzka, D.; Bhardwaj, V.; Pessoa Rodrigues, C.; Mittler, G.; Manke, T.; Backofen, R.; Akhtar, A. (2017). DHX9 suppresses RNA processing defects originating from the Alu invasion of the human genome. *Nature* 544(7648), 115–119. DOI: 10.1038/nature21715.
- Altschuler, S. E.; Lewis, K. A.; Wuttke, D. S. (2013). Practical strategies for the evaluation of high-affinity protein/nucleic acid interactions. *Journal of nucleic acids investigation* 4(1), 19–28. DOI: 10.4081/jnai.2013.e3.
- Ashwal-Fluss, R.; Meyer, M.; Pamudurti, N. R.; Ivanov, A.; Bartok, O.; Hanan, M.; Evtantal, N.; Memczak, S.; Rajewsky, N.; Kadener, S. (2014). circRNA biogenesis competes with pre-mRNA splicing. *Molecular cell* 56(1), 55–66. DOI: 10.1016/j.molcel.2014.08.019.
- Atlas, R.; Behar, L.; Elliott, E.; Ginzburg, I. (2004). The insulin-like growth factor mRNA binding-protein IMP-1 and the Ras-regulatory protein G3BP associate with tau mRNA and HuD protein in differentiated P19 neuronal cells. *Journal of neurochemistry* 89(3), 613–626. DOI: 10.1111/j.1471-4159.2004.02371.x.
- Atlas, R.; Behar, L.; Sapoznik, S.; Ginzburg, I. (2007). Dynamic association with polysomes during P19 neuronal differentiation and an untranslated-region-dependent translation regulation of the tau mRNA by the tau mRNA-associated proteins IMP1, HuD, and G3BP1. *Journal of neuroscience research* 85(1), 173–183. DOI: 10.1002/jnr.21099.
- Aviram, N.; Schuldiner, M. (2017). Targeting and translocation of proteins to the endoplasmic reticulum at a glance. *Journal of cell science* 130(24), 4079–4085. DOI: 10.1242/jcs.204396.
- Baek, J.; Kang, S.; Min, H. (2014). MicroRNA-targeting therapeutics for hepatitis C. *Archives of pharmacal research* 37(3), 299–305. DOI: 10.1007/s12272-013-0318-9.
- Baltz, A. G.; Munschauer, M.; Schwanhäusser, B.; Vasile, A.; Murakawa, Y.; Schueler, M.; Youngs, N.; Penfold-Brown, D.; Drew, K.; Milek, M.; Wyler, E.; Bonneau, R.; Selbach, M.; Dieterich, C.; Landthaler, M. (2012). The mRNA-bound proteome and its global occupancy profile on protein-coding transcripts. *Molecular cell* 46(5), 674–690. DOI: 10.1016/j.molcel.2012.05.021.
- Balzeau, J.; Menezes, M. R.; Cao, S.; Hagan, J. P. (2017). The LIN28/let-7 Pathway in Cancer. *Frontiers in genetics* 8, 31. DOI: 10.3389/fgene.2017.00031.
- Barrett, S. P.; Wang, P. L.; Salzman, J. (2015). Circular RNA biogenesis can proceed through an exon-containing lariat precursor. *eLife* 4, e07540. DOI: 10.7554/eLife.07540.
- Bell, J. L.; Wächter, K.; Mühleck, B.; Pazaitis, N.; Köhn, M.; Lederer, M.; Hüttelmaier, S. (2013). Insulin-like growth factor 2 mRNA-binding proteins (IGF2BPs): post-transcriptional

- drivers of cancer progression? *Cellular and molecular life sciences* 70(15), 2657–2675. DOI: 10.1007/s00018-012-1186-z.
- Benoit Bouvrette, L. P.; Cody, N. A. L.; Bergalet, J.; Lefebvre, F. A.; Diot, C.; Wang, X.; Blanchette, M.; Lécuyer, E. (2018). CeFra-seq reveals broad asymmetric mRNA and noncoding RNA distribution profiles in *Drosophila* and human cells. *RNA* 24(1), 98–113. DOI: 10.1261/rna.063172.117.
- Berkovits, B. D.; Mayr, C. (2015). Alternative 3' UTRs act as scaffolds to regulate membrane protein localization. *Nature* 522(7556), 363–367. DOI: 10.1038/nature14321.
- Bernstein, P. L.; Herrick, D. J.; Prokipcak, R. D.; Ross, J. (1992). Control of c-myc mRNA half-life in vitro by a protein capable of binding to a coding region stability determinant. *Genes & development* 6(4), 642–654. DOI: 10.1101/gad.6.4.642.
- Béthune, J.; Jansen, R.-P.; Feldbrügge, M.; Zarnack, K. (2019). Membrane-associated RNA-binding proteins orchestrate organelle-coupled translation. *Trends in cell biology* 29(2), 178–188. DOI: 10.1016/j.tcb.2018.10.005.
- Biswas, J.; Patel, V. L.; Bhaskar, V.; Chao, J. A.; Singer, R. H.; Eliscovich, C. (2019). The structural basis for RNA selectivity by the IMP family of RNA-binding proteins. *Nature communications* 10(1), 4440. DOI: 10.1038/s41467-019-12193-7.
- Bley, N.; Lederer, M.; Pfalz, B.; Reinke, C.; Fuchs, T.; Glaß, M.; Möller, B.; Hüttelmaier, S. (2015). Stress granules are dispensable for mRNA stabilization during cellular stress. *Nucleic acids research* 43(4), e26. DOI: 10.1093/nar/gku1275.
- Breuer, J.; Rossbach, O. (2020). Production and purification of artificial circular RNA sponges for application in molecular biology and medicine. *Methods and protocols* 3(2). DOI: 10.3390/mps3020042.
- Buchbender, A.; Mutter, H.; Sutandy, F. X. R.; Körtel, N.; Hänel, H.; Busch, A.; Ebersberger, S.; König, J. (2020). Improved library preparation with the new iCLIP2 protocol. *Methods* 178, 33–48. DOI: 10.1016/j.ymeth.2019.10.003.
- Burd, C. E.; Jeck, W. R.; Liu, Y.; Sanoff, H. K.; Wang, Z.; Sharpless, N. E. (2010). Expression of linear and novel circular forms of an INK4/ARF-associated non-coding RNA correlates with atherosclerosis risk. *PLoS genetics* 6(12), e1001233. DOI: 10.1371/journal.pgen.1001233.
- Busch, B.; Bley, N.; Müller, S.; Glaß, M.; Misiak, D.; Lederer, M.; Vetter, M.; Strauß, H.-G.; Thomssen, C.; Hüttelmaier, S. (2016). The oncogenic triangle of HMG2, LIN28B and IGF2BP1 antagonizes tumor-suppressive actions of the let-7 family. *Nucleic acids research* 44(8), 3845–3864. DOI: 10.1093/nar/gkw099.
- Capel, B.; Swain, A.; Nicolis, S.; Hacker, A.; Walter, M.; Koopman, P.; Goodfellow, P.; Lovell-Badge, R. (1993). Circular transcripts of the testis-determining gene *Sry* in adult mouse testis. *Cell* 73(5), 1019–1030. DOI: 10.1016/0092-8674(93)90279-y.
- Castello, A.; Fischer, B.; Eichelbaum, K.; Horos, R.; Beckmann, B. M.; Strein, C.; Davey, N. E.; Humphreys, D. T.; Preiss, T.; Steinmetz, L. M.; Krijgsveld, J.; Hentze, M. W. (2012). Insights into RNA biology from an atlas of mammalian mRNA-binding proteins. *Cell* 149(6), 1393–1406. DOI: 10.1016/j.cell.2012.04.031.

- Chang, P.; Torres, J.; Lewis, R. A.; Mowry, K. L.; Houliston, E.; King, M. L. (2004). Localization of RNAs to the mitochondrial cloud in *Xenopus* oocytes through entrapment and association with endoplasmic reticulum. *Molecular biology of the cell* 15(10), 4669–4681. DOI: 10.1091/mbc.e04-03-0265.
- Chao, J. A.; Patskovsky, Y.; Patel, V.; Levy, M.; Almo, S. C.; Singer, R. H. (2010). ZBP1 recognition of beta-actin zipcode induces RNA looping. *Genes & development* 24(2), 148–158. DOI: 10.1101/gad.1862910.
- Chen, C. Y.; Sarnow, P. (1995). Initiation of protein synthesis by the eukaryotic translational apparatus on circular RNAs. *Science* 268(5209), 415–417. DOI: 10.1126/science.7536344.
- Chen, D.; Murphy, B.; Sung, R.; Bromberg, J. S. (2003). Adaptive and innate immune responses to gene transfer vectors: role of cytokines and chemokines in vector function. *Gene therapy* 10(11), 991–998. DOI: 10.1038/sj.gt.3302031.
- Chen, R.-X.; Chen, X.; Xia, L.-P.; Zhang, J.-X.; Pan, Z.-Z.; Ma, X.-D.; Han, K.; Chen, J.-W.; Judde, J.-G.; Deas, O.; Wang, F.; Ma, N.-F.; Guan, X.; Yun, J.-P.; Wang, F.-W.; ... Dan, X. (2019). N6-methyladenosine modification of circNSUN2 facilitates cytoplasmic export and stabilizes HMGA2 to promote colorectal liver metastasis. *Nature communications* 10(1), 4695. DOI: 10.1038/s41467-019-12651-2.
- Chen, Y. G.; Kim, M. V.; Chen, X.; Batista, P. J.; Aoyama, S.; Wilusz, J. E.; Iwasaki, A.; Chang, H. Y. (2017). Sensing self and foreign circular RNAs by intron identity. *Molecular cell* 67(2), 228-238.e5. DOI: 10.1016/j.molcel.2017.05.022.
- Cléry, A.; Blatter, M.; Allain, F. H.-T. (2008). RNA recognition motifs: boring? Not quite. *Current opinion in structural biology* 18(3), 290–298. DOI: 10.1016/j.sbi.2008.04.002.
- Cocquerelle, C.; Daubersies, P.; Majérus, M. A.; Kerckaert, J. P.; Bailleul, B. (1992). Splicing with inverted order of exons occurs proximal to large introns. *The EMBO journal* 11(3), 1095–1098.
- Cocquerelle, C.; Mascrez, B.; Héтуin, D.; Bailleul, B. (1993). Mis-splicing yields circular RNA molecules. *FASEB journal: official publication of the Federation of American Societies for Experimental Biology* 7(1), 155–160. DOI: 10.1096/fasebj.7.1.7678559.
- Conn, S. J.; Pillman, K. A.; Toubia, J.; Conn, V. M.; Salmanidis, M.; Phillips, C. A.; Roslan, S.; Schreiber, A. W.; Gregory, P. A.; Goodall, G. J. (2015). The RNA binding protein quaking regulates formation of circRNAs. *Cell* 160(6), 1125–1134. DOI: 10.1016/j.cell.2015.02.014.
- Conway, A. E.; van Nostrand, E. L.; Pratt, G. A.; Aigner, S.; Wilbert, M. L.; Sundararaman, B.; Freese, P.; Lambert, N. J.; Sathe, S.; Liang, T. Y.; Essex, A.; Landais, S.; Burge, C. B.; Jones, D. L.; Yeo, G. W. (2016). Enhanced CLIP uncovers IMP protein-RNA targets in human pluripotent stem cells important for cell adhesion and survival. *Cell reports* 15(3), 666–679. DOI: 10.1016/j.celrep.2016.03.052.
- Corbett, A. H. (2018). Post-transcriptional regulation of gene expression and human disease. *Current opinion in cell biology* 52, 96–104. DOI: 10.1016/j.ceb.2018.02.011.
- Corley, M.; Burns, M. C.; Yeo, G. W. (2020). How RNA-binding proteins interact with RNA: Molecules and mechanisms. *Molecular cell* 78(1), 9–29. DOI: 10.1016/j.molcel.2020.03.011.

- Costello, A.; Lao, N. T.; Barron, N.; Clynes, M. (2020). Reinventing the wheel: Synthetic circular RNAs for mammalian cell engineering. *Trends in biotechnology* 38(2), 217–230. DOI: 10.1016/j.tibtech.2019.07.008.
- Cui, X. A.; Zhang, H.; Palazzo, A. F. (2012). p180 promotes the ribosome-independent localization of a subset of mRNA to the endoplasmic reticulum. *PLoS biology* 10(5), e1001336. DOI: 10.1371/journal.pbio.1001336.
- Dagil, R.; Ball, N. J.; Ogrodowicz, R. W.; Hobor, F.; Purkiss, A. G.; Kelly, G.; Martin, S. R.; Taylor, I. A.; Ramos, A. (2019). IMP1 KH1 and KH2 domains create a structural platform with unique RNA recognition and re-modelling properties. *Nucleic acids research* 47(8), 4334–4348. DOI: 10.1093/nar/gkz136.
- Dai, N.; Christiansen, J.; Nielsen, F. C.; Avruch, J. (2013). mTOR complex 2 phosphorylates IMP1 cotranslationally to promote IGF2 production and the proliferation of mouse embryonic fibroblasts. *Genes & development* 27(3), 301–312. DOI: 10.1101/gad.209130.112.
- Dai, N.; Rapley, J.; Angel, M.; Yanik, M. F.; Blower, M. D.; Avruch, J. (2011). mTOR phosphorylates IMP2 to promote IGF2 mRNA translation by internal ribosomal entry. *Genes & development* 25(11), 1159–1172. DOI: 10.1101/gad.2042311.
- Daiko, H.; Marafioti, T.; Fujiwara, T.; Shirakawa, Y.; Nakatsura, T.; Kato, K.; Puccio, I.; Hikichi, T.; Yoshimura, S.; Nakagawa, T.; Furukawa, M.; Stoeber, K.; Nagira, M.; Ide, N.; Kojima, T. (2020). Exploratory open-label clinical study to determine the S-588410 cancer peptide vaccine-induced tumor-infiltrating lymphocytes and changes in the tumor microenvironment in esophageal cancer patients. *Cancer immunology, immunotherapy* 69(11), 2247–2257. DOI: 10.1007/s00262-020-02619-3.
- Degrauwe, N.; Schlumpf, T. B.; Janiszewska, M.; Martin, P.; Cauderay, A.; Provero, P.; Riggi, N.; Suvà, M.-L.; Paro, R.; Stamenkovic, I. (2016a). The RNA binding protein IMP2 preserves glioblastoma stem cells by preventing let-7 target gene silencing. *Cell reports* 15(8), 1634–1647. DOI: 10.1016/j.celrep.2016.04.086.
- Degrauwe, N.; Suvà, M.-L.; Janiszewska, M.; Riggi, N.; Stamenkovic, I. (2016b). IMPs: an RNA-binding protein family that provides a link between stem cell maintenance in normal development and cancer. *Genes & development* 30(22), 2459–2474. DOI: 10.1101/gad.287540.116.
- Deshler, J. O.; Highett, M. I.; Abramson, T.; Schnapp, B. J. (1998). A highly conserved RNA-binding protein for cytoplasmic mRNA localization in vertebrates. *Current Biology* 8(9), 489–496. DOI: 10.1016/S0960-9822(98)70200-3.
- Deshler, J. O.; Highett, M. I.; Schnapp, B. J. (1997). Localization of *Xenopus* Vg1 mRNA by Vera protein and the endoplasmic reticulum. *Science* 276(5315), 1128–1131. DOI: 10.1126/science.276.5315.1128.
- Dominguez, D.; Freese, P.; Alexis, M. S.; Su, A.; Hochman, M.; Palden, T.; Bazile, C.; Lambert, N. J.; van Nostrand, E. L.; Pratt, G. A.; Yeo, G. W.; Graveley, B. R.; Burge, C. B. (2018). Sequence, structure, and context preferences of human RNA binding proteins. *Molecular cell* 70(5), 854–867.e9. DOI: 10.1016/j.molcel.2018.05.001.

- Dube, U.; Del-Aguila, J. L.; Li, Z.; Budde, J. P.; Jiang, S.; Hsu, S.; Ibanez, L.; Fernandez, M. V.; Farias, F.; Norton, J.; Gentsch, J.; Wang, F.; Salloway, S.; Masters, C. L.; Lee, J.-H.; ... Cruchaga, C. (2019). An atlas of cortical circular RNA expression in Alzheimer disease brains demonstrates clinical and pathological associations. *Nature neuroscience* 22(11), 1903–1912. DOI: 10.1038/s41593-019-0501-5.
- El-Brolosy, M. A.; Stainier, D. Y. R. (2017). Genetic compensation: A phenomenon in search of mechanisms. *PLoS genetics* 13(7), e1006780. DOI: 10.1371/journal.pgen.1006780.
- Eliscovich, C.; Shenoy, S. M.; Singer, R. H. (2017). Imaging mRNA and protein interactions within neurons. *Proceedings of the National Academy of Sciences of the United States of America* 114(10), E1875-E1884. DOI: 10.1073/pnas.1621440114.
- Ennajdaoui, H.; Howard, J. M.; Sterne-Weiler, T.; Jahanbani, F.; Coyne, D. J.; Uren, P. J.; Dargyte, M.; Katzman, S.; Draper, J. M.; Wallace, A.; Cazarez, O.; Burns, S. C.; Qiao, M.; Hinck, L.; Smith, A. D.; ... Sanford, J. R. (2016). IGF2BP3 modulates the interaction of invasion-associated transcripts with RISC. *Cell reports* 15(9), 1876–1883. DOI: 10.1016/j.celrep.2016.04.083.
- Enuka, Y.; Lauriola, M.; Feldman, M. E.; Sas-Chen, A.; Ulitsky, I.; Yarden, Y. (2016). Circular RNAs are long-lived and display only minimal early alterations in response to a growth factor. *Nucleic acids research* 44(3), 1370–1383. DOI: 10.1093/nar/gkv1367.
- Errichelli, L.; Dini Modigliani, S.; Laneve, P.; Colantoni, A.; Legnini, I.; Capauto, D.; Rosa, A.; Santis, R. de; Scarfò, R.; Peruzzi, G.; Lu, L.; Caffarelli, E.; Shneider, N. A.; Morlando, M.; Bozzoni, I. (2017). FUS affects circular RNA expression in murine embryonic stem cell-derived motor neurons. *Nature communications* 8, 14741. DOI: 10.1038/ncomms14741.
- Fang, Z.; Cui, X. (2011). Design and validation issues in RNA-seq experiments. *Briefings in bioinformatics* 12(3), 280–287. DOI: 10.1093/bib/bbr004.
- Farina, K. L.; Huttelmaier, S.; Musunuru, K.; Darnell, R.; Singer, R. H. (2003). Two ZBP1 KH domains facilitate beta-actin mRNA localization, granule formation, and cytoskeletal attachment. *The Journal of cell biology* 160(1), 77–87. DOI: 10.1083/jcb.200206003.
- Gebauer, F.; Schwarzl, T.; Valcárcel, J.; Hentze, M. W. (2021). RNA-binding proteins in human genetic disease. *Nature reviews. Genetics* 22(3), 185–198. DOI: 10.1038/s41576-020-00302-y.
- Geng, C.; Macdonald, P. M. (2006). Imp associates with squid and Hrp48 and contributes to localized expression of gurken in the oocyte. *Molecular and cellular biology* 26(24), 9508–9516. DOI: 10.1128/MCB.01136-06.
- Genz, C.; Fundakowski, J.; Hermesh, O.; Schmid, M.; Jansen, R.-P. (2013). Association of the yeast RNA-binding protein She2p with the tubular endoplasmic reticulum depends on membrane curvature. *The Journal of biological chemistry* 288(45), 32384–32393. DOI: 10.1074/jbc.M113.486431.
- Gerstberger, S.; Hafner, M.; Tuschl, T. (2014). A census of human RNA-binding proteins. *Nature reviews. Genetics* 15(12), 829–845. DOI: 10.1038/nrg3813.

- Git, A.; Allison, R.; Perdiguero, E.; Nebreda, A. R.; Houliston, E.; Standart, N. (2009). Vg1RBP phosphorylation by Erk2 MAP kinase correlates with the cortical release of Vg1 mRNA during meiotic maturation of *Xenopus* oocytes. *RNA* 15(6), 1121–1133. DOI: 10.1261/rna.1195709.
- Git, A.; Standart, N. (2002). The KH domains of *Xenopus* Vg1RBP mediate RNA binding and self-association. *RNA* 8(10), 1319–1333. DOI: 10.1017/s135583820202705x.
- Grabowski, P. J.; Zaug, A. J.; Cech, T. R. (1981). The intervening sequence of the ribosomal RNA precursor is converted to a circular RNA in isolated nuclei of tetrahymena. *Cell* 23(2), 467–476. DOI: 10.1016/0092-8674(81)90142-2.
- Gross, H. J.; Domdey, H.; Lossow, C.; Jank, P.; Raba, M.; Alberty, H.; Sanger, H. L. (1978). Nucleotide sequence and secondary structure of potato spindle tuber viroid. *Nature* 273(5659), 203–208. DOI: 10.1038/273203a0.
- Gruner, H.; Cortes-Lopez, M.; Cooper, D. A.; Bauer, M.; Miura, P. (2016). CircRNA accumulation in the aging mouse brain. *Scientific reports* 6, 38907. DOI: 10.1038/srep38907.
- Guo, J. U.; Agarwal, V.; Guo, H.; Bartel, D. P. (2014). Expanded identification and characterization of mammalian circular RNAs. *Genome biology* 15(7), 409. DOI: 10.1186/s13059-014-0409-z.
- Hafner, M.; Landthaler, M.; Burger, L.; Khorshid, M.; Hausser, J.; Berninger, P.; Rothballer, A.; Ascano, M.; Jungkamp, A.-C.; Munschauer, M.; Ulrich, A.; Wardle, G. S.; Dewell, S.; Zavolan, M.; Tuschl, T. (2010). Transcriptome-wide identification of RNA-binding protein and microRNA target sites by PAR-CLIP. *Cell* 141(1), 129–141. DOI: 10.1016/j.cell.2010.03.009.
- Hammer, N. A.; Hansen, T. V. O.; Byskov, A. G.; Rajpert-De Meyts, E.; Grondahl, M. L.; Bredkjaer, H. E.; Wewer, U. M.; Christiansen, J.; Nielsen, F. C. (2005). Expression of IGF-II mRNA-binding proteins (IMPs) in gonads and testicular cancer. *Reproduction* 130(2), 203–212. DOI: 10.1530/rep.1.00664.
- Hann, B. C.; Walter, P. (1991). The signal recognition particle in *S. cerevisiae*. *Cell* 67(1), 131–144. DOI: 10.1016/0092-8674(91)90577-1.
- Hanniford, D.; Ulloa-Morales, A.; Karz, A.; Berzoti-Coelho, M. G.; Moubarak, R. S.; Sanchez-Sendra, B.; Kloetgen, A.; Davalos, V.; Imig, J.; Wu, P.; Vasudevaraja, V.; Argibay, D.; Lilja, K.; Tabaglio, T.; Monteagudo, C.; ... Hernando, E. (2020). Epigenetic silencing of CDR1as drives IGF2BP3-mediated melanoma invasion and metastasis. *Cancer cell* 37(1), 55-70.e15. DOI: 10.1016/j.ccell.2019.12.007.
- Hansen, H. T.; Rasmussen, S. H.; Adolph, S. K.; Plass, M.; Krogh, A.; Sanford, J.; Nielsen, F. C.; Christiansen, J. (2015). *Drosophila* Imp iCLIP identifies an RNA assemblage coordinating F-actin formation. *Genome biology* 16, 123. DOI: 10.1186/s13059-015-0687-0.
- Hansen, T. B. (2018). Characterization of circular RNA concatemers. *Methods in molecular biology* 1724, 143–157. DOI: 10.1007/978-1-4939-7562-4_12.
- Hansen, T. B.; Jensen, T. I.; Clausen, B. H.; Bramsen, J. B.; Finsen, B.; Damgaard, C. K.; Kjems, J. (2013a). Natural RNA circles function as efficient microRNA sponges. *Nature* 495(7441), 384–388. DOI: 10.1038/nature11993.

- Hansen, T. B.; Kjems, J.; Damgaard, C. K. (2013b). Circular RNA and miR-7 in cancer. *Cancer research* 73(18), 5609–5612. DOI: 10.1158/0008-5472.CAN-13-1568.
- Hansen, T. B.; Wiklund, E. D.; Bramsen, J. B.; Villadsen, S. B.; Statham, A. L.; Clark, S. J.; Kjems, J. (2011). MiRNA-dependent gene silencing involving Ago2-mediated cleavage of a circular antisense RNA. *The EMBO journal* 30(21), 4414–4422. DOI: 10.1038/emboj.2011.359.
- Hansen, T. V. O.; Hammer, N. A.; Nielsen, J.; Madsen, M.; Dalbaeck, C.; Wewer, U. M.; Christiansen, J.; Nielsen, F. C. (2004). Dwarfism and impaired gut development in insulin-like growth factor II mRNA-binding protein 1-deficient mice. *Molecular and cellular biology* 24(10), 4448–4464. DOI: 10.1128/MCB.24.10.4448-4464.2004.
- Havin, L.; Git, A.; Elisha, Z.; Oberman, F.; Yaniv, K.; Schwartz, S. P.; Standart, N.; Yisraeli, J. K. (1998). RNA-binding protein conserved in both microtubule- and microfilament-based RNA localization. *Genes & development* 12(11), 1593–1598. DOI: 10.1101/gad.12.11.1593.
- Hentze, M. W.; Castello, A.; Schwarzl, T.; Preiss, T. (2018). A brave new world of RNA-binding proteins. *Nature reviews. Molecular cell biology* 19(5), 327–341. DOI: 10.1038/nrm.2017.130.
- Hermesh, O.; Jansen, R.-P. (2013). Take the (RN)A-train: localization of mRNA to the endoplasmic reticulum. *Biochimica et biophysica acta* 1833(11), 2519–2525. DOI: 10.1016/j.bbamcr.2013.01.013.
- Holden, P.; Horton, W. A. (2009). Crude subcellular fractionation of cultured mammalian cell lines. *BMC research notes* 2, 243. DOI: 10.1186/1756-0500-2-243.
- Holdt, L. M.; Stahringer, A.; Sass, K.; Pichler, G.; Kulak, N. A.; Wilfert, W.; Kohlmaier, A.; Herbst, A.; Northoff, B. H.; Nicolaou, A.; Gäbel, G.; Beutner, F.; Scholz, M.; Thiery, J.; Musunuru, K.; ... Teupser, D. (2016). Circular non-coding RNA ANRIL modulates ribosomal RNA maturation and atherosclerosis in humans. *Nature communications* 7, 12429. DOI: 10.1038/ncomms12429.
- Houseley, J. M.; Garcia-Casado, Z.; Pascual, M.; Paricio, N.; O'Dell, K. M. C.; Monckton, D. G.; Artero, R. D. (2006). Noncanonical RNAs from transcripts of the *Drosophila* muscleblind gene. *The Journal of heredity* 97(3), 253–260. DOI: 10.1093/jhered/esj037.
- Ho-Xuan, H.; Glažar, P.; Latini, C.; Heizler, K.; Haase, J.; Hett, R.; Anders, M.; Weichmann, F.; Bruckmann, A.; van den Berg, D.; Hüttelmaier, S.; Rajewsky, N.; Hackl, C.; Meister, G. (2020). Comprehensive analysis of translation from overexpressed circular RNAs reveals pervasive translation from linear transcripts. *Nucleic acids research* 48(18), 10368–10382. DOI: 10.1093/nar/gkaa704.
- Hsu, J. C.-C.; Reid, D. W.; Hoffman, A. M.; Sarkar, D.; Nicchitta, C. V. (2018). Oncoprotein AEG-1 is an endoplasmic reticulum RNA-binding protein whose interactome is enriched in organelle resident protein-encoding mRNAs. *RNA* 24(5), 688–703. DOI: 10.1261/rna.063313.117.
- Hu, S.; Wu, X.; Zhou, B.; Xu, Z.; Qin, J.; Lu, H.; Lv, L.; Gao, Y.; Deng, L.; Yin, J.; Li, G. (2014). IMP3 combined with CD44s, a novel predictor for prognosis of patients with

- hepatocellular carcinoma. *Journal of cancer research and clinical oncology* 140(6), 883–893. DOI: 10.1007/s00432-014-1639-x.
- Hu, X.; Peng, W.-X.; Zhou, H.; Jiang, J.; Zhou, X.; Huang, D.; Mo, Y.-Y.; Yang, L. (2020). IGF2BP2 regulates DANCR by serving as an N6-methyladenosine reader. *Cell death and differentiation* 27(6), 1782–1794. DOI: 10.1038/s41418-019-0461-z.
- Huang, H.; Weng, H.; Sun, W.; Qin, X.; Shi, H.; Wu, H.; Zhao, B. S.; Mesquita, A.; Liu, C.; Yuan, C. L.; Hu, Y.-C.; Hüttelmaier, S.; Skibbe, J. R.; Su, R.; Deng, X.; ... Chen, J. (2018). Recognition of RNA N6-methyladenosine by IGF2BP proteins enhances mRNA stability and translation. *Nature cell biology* 20(3), 285–295. DOI: 10.1038/s41556-018-0045-z.
- Huppertz, I.; Attig, J.; D'Ambrogio, A.; Easton, L. E.; Sibley, C. R.; Sugimoto, Y.; Tajnik, M.; König, J.; Ule, J. (2014). iCLIP: protein-RNA interactions at nucleotide resolution. *Methods* 65(3), 274–287. DOI: 10.1016/j.ymeth.2013.10.011.
- Hüttelmaier, S.; Zenklusen, D.; Lederer, M.; Dichtenberg, J.; Lorenz, M.; Meng, X.; Bassell, G. J.; Condeelis, J.; Singer, R. H. (2005). Spatial regulation of beta-actin translation by Src-dependent phosphorylation of ZBP1. *Nature* 438(7067), 512–515. DOI: 10.1038/nature04115.
- Itzhak, D. N.; Tyanova, S.; Cox, J.; Borner, G. H. (2016). Global, quantitative and dynamic mapping of protein subcellular localization. *eLife* 5. DOI: 10.7554/eLife.16950.
- Ivanov, A.; Memczak, S.; Wyler, E.; Torti, F.; Porath, H. T.; Orejuela, M. R.; Piechotta, M.; Levanon, E. Y.; Landthaler, M.; Dieterich, C.; Rajewsky, N. (2015). Analysis of intron sequences reveals hallmarks of circular RNA biogenesis in animals. *Cell reports* 10(2), 170–177. DOI: 10.1016/j.celrep.2014.12.019.
- Jambhekar, A.; McDermott, K.; Sorber, K.; Shepard, K. A.; Vale, R. D.; Takizawa, P. A.; DeRisi, J. L. (2005). Unbiased selection of localization elements reveals cis-acting determinants of mRNA bud localization in *Saccharomyces cerevisiae*. *Proceedings of the National Academy of Sciences of the United States of America* 102(50), 18005–18010. DOI: 10.1073/pnas.0509229102.
- Järvelin, A. I.; Noerenberg, M.; Davis, I.; Castello, A. (2016). The new (dis)order in RNA regulation. *Cell communication and signaling* 14, 9. DOI: 10.1186/s12964-016-0132-3.
- Jeck, W. R.; Sharpless, N. E. (2014). Detecting and characterizing circular RNAs. *Nature biotechnology* 32(5), 453–461. DOI: 10.1038/nbt.2890.
- Jeck, W. R.; Sorrentino, J. A.; Wang, K.; Slevin, M. K.; Burd, C. E.; Liu, J.; Marzluff, W. F.; Sharpless, N. E. (2013). Circular RNAs are abundant, conserved, and associated with ALU repeats. *RNA* 19(2), 141–157. DOI: 10.1261/rna.035667.112.
- Jeng, Y.-M.; Chang, C.-C.; Hu, F.-C.; Chou, H.-Y. E.; Kao, H.-L.; Wang, T.-H.; Hsu, H.-C. (2008). RNA-binding protein insulin-like growth factor II mRNA-binding protein 3 expression promotes tumor invasion and predicts early recurrence and poor prognosis in hepatocellular carcinoma. *Hepatology* 48(4), 1118–1127. DOI: 10.1002/hep.22459.
- Jia, M.; Gut, H.; Chao, J. A. (2018). Structural basis of IMP3 RRM12 recognition of RNA. *RNA* 24(12), 1659–1666. DOI: 10.1261/rna.065649.118.

- Johnson, N.; Vilardi, F.; Lang, S.; Leznicki, P.; Zimmermann, R.; High, S. (2012). TRC40 can deliver short secretory proteins to the Sec61 translocon. *Journal of cell science* 125(18), 4414. DOI: 10.1242/jcs.120626.
- Jønson, L.; Christiansen, J.; Hansen, T. V. O.; Vikeså, J.; Yamamoto, Y.; Nielsen, F. C. (2014). IMP3 RNP safe houses prevent miRNA-directed HMGA2 mRNA decay in cancer and development. *Cell reports* 7(2), 539–551. DOI: 10.1016/j.celrep.2014.03.015.
- Jønson, L.; Vikesaa, J.; Krogh, A.; Nielsen, L. K.; Hansen, T. v.; Borup, R.; Johnsen, A. H.; Christiansen, J.; Nielsen, F. C. (2007). Molecular composition of IMP1 ribonucleoprotein granules. *Molecular & cellular proteomics* 6(5), 798–811. DOI: 10.1074/mcp.M600346-MCP200.
- Jost, I.; Shalamova, L. A.; Gerresheim, G. K.; Niepmann, M.; Bindereif, A.; Rossbach, O. (2018). Functional sequestration of microRNA-122 from Hepatitis C Virus by circular RNA sponges. *RNA biology* 15(8), 1032–1039. DOI: 10.1080/15476286.2018.1435248.
- Kalinowski, F. C.; Brown, R. A. M.; Ganda, C.; Giles, K. M.; Epis, M. R.; Horsham, J.; Leedman, P. J. (2014). MicroRNA-7: A tumor suppressor miRNA with therapeutic potential. *The international journal of biochemistry & cell biology* 54, 312–317. DOI: 10.1016/j.biocel.2014.05.040.
- Kellogg, M. K.; Miller, S. C.; Tikhonova, E. B.; Karamyshev, A. L. (2021). SRPassing co-translational targeting: The role of the signal recognition particle in protein targeting and mRNA protection. *International journal of molecular sciences* 22(12). DOI: 10.3390/ijms22126284.
- Kjems, J.; Garrett, R. A. (1988). Novel splicing mechanism for the ribosomal RNA intron in the archaeobacterium *desulfurococcus mobilis*. *Cell* 54(5), 693–703. DOI: 10.1016/S0092-8674(88)80014-X.
- Kleaveland, B.; Shi, C. Y.; Stefano, J.; Bartel, D. P. (2018). A network of noncoding regulatory RNAs acts in the mammalian brain. *Cell* 174(2), 350-362.e17. DOI: 10.1016/j.cell.2018.05.022.
- Kloc, M.; Etkin, L. D. (1998). Apparent continuity between the messenger transport organizer and late RNA localization pathways during oogenesis in *Xenopus*. *Mechanisms of Development* 73(1), 95–106. DOI: 10.1016/S0925-4773(98)00041-0.
- Köhn, M.; Lederer, M.; Wächter, K.; Hüttelmaier, S. (2010). Near-infrared (NIR) dye-labeled RNAs identify binding of ZBP1 to the noncoding Y3-RNA. *RNA* 16(7), 1420–1428. DOI: 10.1261/rna.2152710.
- Korn, S. M.; Ulshöfer, C. J.; Schneider, T.; Schlundt, A. (2021). Structures and target RNA preferences of the RNA-binding protein family of IGF2BPs: An overview. *Structure* 29(8), 787–803. DOI: 10.1016/j.str.2021.05.001.
- Kos, A.; Dijkema, R.; Arnberg, A. C.; van der Meide, P. H.; Schellekens, H. (1986). The hepatitis delta (delta) virus possesses a circular RNA. *Nature* 323(6088), 558–560. DOI: 10.1038/323558a0.

- Kramer, M. C.; Liang, D.; Tatomer, D. C.; Gold, B.; March, Z. M.; Cherry, S.; Wilusz, J. E. (2015). Combinatorial control of *Drosophila* circular RNA expression by intronic repeats, hnRNPs, and SR proteins. *Genes & development* 29(20), 2168–2182. DOI: 10.1101/gad.270421.115.
- Kristensen, L. S.; Ebbesen, K. K.; Sokol, M.; Jakobsen, T.; Korsgaard, U.; Eriksen, A. C.; Hansen, T. B.; Kjems, J.; Hager, H. (2020). Spatial expression analyses of the putative oncogene ciRS-7 in cancer reshape the microRNA sponge theory. *Nature communications* 11(1), 4551. DOI: 10.1038/s41467-020-18355-2.
- Kristensen, L. S.; Hansen, T. B.; Venø, M. T.; Kjems, J. (2018a). Circular RNAs in cancer: opportunities and challenges in the field. *Oncogene* 37(5), 555–565. DOI: 10.1038/onc.2017.361.
- Kristensen, L. S.; Okholm, T. L. H.; Venø, M. T.; Kjems, J. (2018b). Circular RNAs are abundantly expressed and upregulated during human epidermal stem cell differentiation. *RNA biology* 15(2), 280–291. DOI: 10.1080/15476286.2017.1409931.
- Kwon, S.; Abramson, T.; Munro, T. P.; John, C. M.; Köhrmann, M.; Schnapp, B. J. (2002). UUCAC- and Vera-dependent localization of VegT RNA in *Xenopus* oocytes. *Current Biology* 12(7), 558–564. DOI: 10.1016/S0960-9822(02)00740-6.
- Lai, W. S.; Arvola, R. M.; Goldstrohm, A. C.; Blackshear, P. J. (2019). Inhibiting transcription in cultured metazoan cells with actinomycin D to monitor mRNA turnover. *Methods* 155, 77–87. DOI: 10.1016/j.ymeth.2019.01.003.
- Lambrianidou, A.; Sereti, E.; Soupsana, K.; Komini, C.; Dimas, K.; Trangas, T. (2021). mTORC2 deploys the mRNA binding protein IGF2BP1 to regulate c-MYC expression and promote cell survival. *Cellular signalling* 80, 109912. DOI: 10.1016/j.cellsig.2020.109912.
- Landthaler, M.; Gaidatzis, D.; Rothballer, A.; Chen, P. Y.; Soll, S. J.; Dinic, L.; Ojo, T.; Hafner, M.; Zavolan, M.; Tuschl, T. (2008). Molecular characterization of human Argonaute-containing ribonucleoprotein complexes and their bound target mRNAs. *RNA* 14(12), 2580–2596. DOI: 10.1261/rna.1351608.
- Lavenniah, A.; Luu, T. D. A.; Li, Y. P.; Lim, T. B.; Jiang, J.; Ackers-Johnson, M.; Foo, R. S.-Y. (2020). Engineered circular RNA sponges act as miRNA inhibitors to attenuate pressure overload-induced cardiac hypertrophy. *Molecular therapy* 28(6), 1506–1517. DOI: 10.1016/j.ymthe.2020.04.006.
- Lederer, M.; Bley, N.; Schleifer, C.; Hüttelmaier, S. (2014). The role of the oncofetal IGF2 mRNA-binding protein 3 (IGF2BP3) in cancer. *Seminars in cancer biology* 29, 3–12. DOI: 10.1016/j.semcancer.2014.07.006.
- Legnini, I.; Di Timoteo, G.; Rossi, F.; Morlando, M.; Briganti, F.; Sthandier, O.; Fatica, A.; Santini, T.; Andronache, A.; Wade, M.; Laneve, P.; Rajewsky, N.; Bozzoni, I. (2017). Circ-ZNF609 is a circular RNA that can be translated and functions in myogenesis. *Molecular cell* 66(1), 22–37.e9. DOI: 10.1016/j.molcel.2017.02.017.

- Lemm, I.; Ross, J. (2002). Regulation of c-myc mRNA decay by translational pausing in a coding region instability determinant. *Molecular and cellular biology* 22(12), 3959–3969. DOI: 10.1128/MCB.22.12.3959-3969.2002.
- Li, B.; Zhu, L.; Lu, C.; Wang, C.; Wang, H.; Jin, H.; Ma, X.; Cheng, Z.; Yu, C.; Wang, S.; Zuo, Q.; Zhou, Y.; Wang, J.; Yang, C.; Lv, Y.; ... Qin, W. (2021). circNDUFB2 inhibits non-small cell lung cancer progression via destabilizing IGF2BPs and activating anti-tumor immunity. *Nature communications* 12(1), 295. DOI: 10.1038/s41467-020-20527-z.
- Li, Q.; Wang, Y.; Wu, S.; Zhou, Z.; Ding, X.; Shi, R.; Thorne, R. F.; Zhang, X. D.; Hu, W.; Wu, M. (2019a). CircACC1 regulates assembly and activation of AMPK complex under metabolic stress. *Cell metabolism* 30(1), 157-173.e7. DOI: 10.1016/j.cmet.2019.05.009.
- Li, T.; Hu, P.-S.; Zuo, Z.; Lin, J.-F.; Li, X.; Wu, Q.-N.; Chen, Z.-H.; Zeng, Z.-L.; Wang, F.; Zheng, J.; Chen, D.; Li, B.; Kang, T.-B.; Xie, D.; Lin, D.; ... Xu, R.-H. (2019b). METTL3 facilitates tumor progression via an m6A-IGF2BP2-dependent mechanism in colorectal carcinoma. *Molecular cancer* 18(1), 112. DOI: 10.1186/s12943-019-1038-7.
- Li, X.-X.; Xiao, L.; Chung, H. K.; Ma, X.-X.; Liu, X.; Song, J.-L.; Jin, C. Z.; Rao, J. N.; Gorospe, M.; Wang, J.-Y. (2020). Interaction between HuR and circPABPN1 modulates autophagy in the intestinal epithelium by altering ATG16L1 translation. *Molecular and cellular biology* 40(6). DOI: 10.1128/MCB.00492-19.
- Li, Z.; Gilbert, J. A.; Zhang, Y.; Zhang, M.; Qiu, Q.; Ramanujan, K.; Shavlakadze, T.; Eash, J. K.; Scaramozza, A.; Goddeeris, M. M.; Kirsch, D. G.; Campbell, K. P.; Brack, A. S.; Glass, D. J. (2012). An HMGA2-IGF2BP2 axis regulates myoblast proliferation and myogenesis. *Developmental cell* 23(6), 1176–1188. DOI: 10.1016/j.devcel.2012.10.019.
- Liang, D.; Tatomer, D. C.; Luo, Z.; Wu, H.; Yang, L.; Chen, L.-L.; Cherry, S.; Wilusz, J. E. (2017). The output of protein-coding genes shifts to circular RNAs when the pre-mRNA processing machinery is limiting. *Molecular cell* 68(5), 940-954.e3. DOI: 10.1016/j.molcel.2017.10.034.
- Liang, D.; Wilusz, J. E. (2014). Short intronic repeat sequences facilitate circular RNA production. *Genes & development* 28(20), 2233–2247. DOI: 10.1101/gad.251926.114.
- Liao, B.; Hu, Y.; Brewer, G. (2011). RNA-binding protein insulin-like growth factor mRNA-binding protein 3 (IMP-3) promotes cell survival via insulin-like growth factor II signaling after ionizing radiation. *The Journal of biological chemistry* 286(36), 31145–31152. DOI: 10.1074/jbc.M111.263913.
- Liao, B.; Hu, Y.; Herrick, D. J.; Brewer, G. (2005). The RNA-binding protein IMP-3 is a translational activator of insulin-like growth factor II leader-3 mRNA during proliferation of human K562 leukemia cells. *The Journal of biological chemistry* 280(18), 18517–18524. DOI: 10.1074/jbc.M500270200.
- Lisowska, K. M.; Olbryt, M.; Dudaladava, V.; Pamuła-Piłat, J.; Kujawa, K.; Grzybowska, E.; Jarzab, M.; Student, S.; Rzepecka, I. K.; Jarzab, B.; Kupryjańczyk, J. (2014). Gene expression analysis in ovarian cancer - faults and hints from DNA microarray study. *Frontiers in oncology* 4(6), 1–11. DOI: 10.3389/fonc.2014.00006.

- Litke, J. L.; Jaffrey, S. R. (2019). Highly efficient expression of circular RNA aptamers in cells using autocatalytic transcripts. *Nature biotechnology* 37(6), 667–675. DOI: 10.1038/s41587-019-0090-6.
- Liu, C.-X.; Li, X.; Nan, F.; Jiang, S.; Gao, X.; Guo, S.-K.; Xue, W.; Cui, Y.; Dong, K.; Ding, H.; Qu, B.; Zhou, Z.; Shen, N.; Yang, L.; Chen, L.-L. (2019). Structure and degradation of circular RNAs regulate PKR activation in innate immunity. *Cell* 177(4), 865-880.e21. DOI: 10.1016/j.cell.2019.03.046.
- Liu, X.; Abraham, J. M.; Cheng, Y.; Wang, Z.; Wang, Z.; Zhang, G.; Ashktorab, H.; Smoot, D. T.; Cole, R. N.; Boronina, T. N.; DeVine, L. R.; Talbot, C. C.; Liu, Z.; Meltzer, S. J. (2018). Synthetic circular RNA functions as a miR-21 sponge to suppress gastric carcinoma cell proliferation. *Molecular therapy. Nucleic acids* 13, 312–321. DOI: 10.1016/j.omtn.2018.09.010.
- Livingstone, C. (2013). IGF2 and cancer. *Endocrine-related cancer* 20(6), R321-39. DOI: 10.1530/ERC-13-0231.
- Lunde, B. M.; Moore, C.; Varani, G. (2007). RNA-binding proteins: modular design for efficient function. *Nature reviews. Molecular cell biology* 8(6), 479–490. DOI: 10.1038/nrm2178.
- Ma, W.; Mayr, C. (2018). A membraneless organelle associated with the endoplasmic reticulum enables 3'UTR-mediated protein-protein interactions. *Cell* 175(6), 1492-1506.e19. DOI: 10.1016/j.cell.2018.10.007.
- Mancarella, C.; Pasello, M.; Manara, M. C.; Toracchio, L.; Sciandra, E. F.; Picci, P.; Scotlandi, K. (2018). Insulin-like growth factor 2 mRNA-binding protein 3 influences sensitivity to anti-IGF system agents through the translational regulation of IGF1R. *Frontiers in endocrinology* 9, 178. DOI: 10.3389/fendo.2018.00178.
- Mancarella, C.; Scotlandi, K. (2020). IGF2BP3 From Physiology to Cancer: Novel Discoveries, Unsolved Issues, and Future Perspectives. *Frontiers in cell and developmental biology* 7, 363. DOI: 10.3389/fcell.2019.00363.
- Mateescu, B.; Batista, L.; Cardon, M.; Gruosso, T.; Feraudy, Y. de; Mariani, O.; Nicolas, A.; Meyniel, J.-P.; Cottu, P.; Sastre-Garau, X.; Mechta-Grigoriou, F. (2011). miR-141 and miR-200a act on ovarian tumorigenesis by controlling oxidative stress response. *Nature medicine* 17(12), 1627–1635. DOI: 10.1038/nm.2512.
- Mateu-Regué, À.; Christiansen, J.; Bagger, F. O.; Winther, O.; Hellriegel, C.; Nielsen, F. C. (2019). Single mRNP analysis reveals that small cytoplasmic mRNP granules represent mRNA singletons. *Cell reports* 29(3), 736-748.e4. DOI: 10.1016/j.celrep.2019.09.018.
- Mayr, C.; Hemann, M. T.; Bartel, D. P. (2007). Disrupting the pairing between let-7 and hmg2 enhances oncogenic transformation. *Science* 315(5818), 1576–1579. DOI: 10.1126/science.1137999.
- McClatchey, A. I.; Yap, A. S. (2012). Contact inhibition (of proliferation) redux. *Current opinion in cell biology* 24(5), 685–694. DOI: 10.1016/j.ceb.2012.06.009.

- Meganck, R. M.; Liu, J.; Hale, A. E.; Simon, K. E.; Fanous, M. M.; Vincent, H. A.; Wilusz, J. E.; Moorman, N. J.; Marzluff, W. F.; Asokan, A. (2021). Engineering highly efficient backsplicing and translation of synthetic circRNAs. *Molecular therapy. Nucleic acids* 23, 821–834. DOI: 10.1016/j.omtn.2021.01.003.
- Memczak, S.; Jens, M.; Elefsinioti, A.; Torti, F.; Krueger, J.; Rybak, A.; Maier, L.; Mackowiak, S. D.; Gregersen, L. H.; Munschauer, M.; Loewer, A.; Ziebold, U.; Landthaler, M.; Kocks, C.; Le Noble, F.; ... Rajewsky, N. (2013). Circular RNAs are a large class of animal RNAs with regulatory potency. *Nature* 495(7441), 333–338. DOI: 10.1038/nature11928.
- Mesmin, B.; Maxfield, F. R. (2009). Intracellular sterol dynamics. *Biochimica et biophysica acta* 1791(7), 636–645. DOI: 10.1016/j.bbali.2009.03.002.
- Mohibi, S.; Chen, X.; Zhang, J. (2019). Cancer the'RBP'eutics-RNA-binding proteins as therapeutic targets for cancer. *Pharmacology & therapeutics* 203, 107390. DOI: 10.1016/j.pharmthera.2019.07.001.
- Mori, H.; Sakakibara, S.; Imai, T.; Nakamura, Y.; Iijima, T.; Suzuki, A.; Yuasa, Y.; Takeda, M.; Okano, H. (2001). Expression of mouse igf2 mRNA-binding protein 3 and its implications for the developing central nervous system. *Journal of neuroscience research* 64(2), 132–143. DOI: 10.1002/jnr.1060.
- Mueller-Pillasch, F.; Pohl, B.; Wilda, M.; Lacher, U.; Beil, M.; Wallrapp, C.; Hameister, H.; Knöchel, W.; Adler, G.; Gress, T. M. (1999). Expression of the highly conserved RNA binding protein KOC in embryogenesis. *Mechanisms of Development* 88(1), 95–99. DOI: 10.1016/s0925-4773(99)00160-4.
- Müller, S.; Appel, B. (2017). In vitro circularization of RNA. *RNA biology* 14(8), 1018–1027. DOI: 10.1080/15476286.2016.1239009.
- Müller, S.; Bley, N.; Glaß, M.; Busch, B.; Rousseau, V.; Misiak, D.; Fuchs, T.; Lederer, M.; Hüttelmaier, S. (2018). IGF2BP1 enhances an aggressive tumor cell phenotype by impairing miRNA-directed downregulation of oncogenic factors. *Nucleic acids research* 46(12), 6285–6303. DOI: 10.1093/nar/gky229.
- Müller, S.; Glaß, M.; Singh, A. K.; Haase, J.; Bley, N.; Fuchs, T.; Lederer, M.; Dahl, A.; Huang, H.; Chen, J.; Posern, G.; Hüttelmaier, S. (2019). IGF2BP1 promotes SRF-dependent transcription in cancer in a m6A- and miRNA-dependent manner. *Nucleic acids research* 47(1), 375–390. DOI: 10.1093/nar/gky1012.
- Munro, T. P.; Kwon, S.; Schnapp, B. J.; St Johnston, D. (2006). A repeated IMP-binding motif controls oskar mRNA translation and anchoring independently of *Drosophila melanogaster* IMP. *The Journal of cell biology* 172(4), 577–588. DOI: 10.1083/jcb.200510044.
- Murahashi, M.; Hijikata, Y.; Yamada, K.; Tanaka, Y.; Kishimoto, J.; Inoue, H.; Marumoto, T.; Takahashi, A.; Okazaki, T.; Takeda, K.; Hirakawa, M.; Fujii, H.; Okano, S.; Morita, M.; Baba, E.; ... Tani, K. (2016). Phase I clinical trial of a five-peptide cancer vaccine combined with cyclophosphamide in advanced solid tumors. *Clinical immunology* 166-167, 48–58. DOI: 10.1016/j.clim.2016.03.015.

- Nicastro, G.; Candel, A. M.; Uhl, M.; Oregioni, A.; Hollingworth, D.; Backofen, R.; Martin, S. R.; Ramos, A. (2017). Mechanism of β -actin mRNA recognition by ZBP1. *Cell reports* 18(5), 1187–1199. DOI: 10.1016/j.celrep.2016.12.091.
- Nielsen, F. C.; Nielsen, J.; Kristensen, M. A.; Koch, G.; Christiansen, J. (2002). Cytoplasmic trafficking of IGF-II mRNA-binding protein by conserved KH domains. *Journal of cell science* 115(Pt 10), 2087–2097.
- Nielsen, J.; Christiansen, J.; Lykke-Andersen, J.; Johnsen, A. H.; Wewer, U. M.; Nielsen, F. C. (1999). A family of insulin-like growth factor II mRNA-binding proteins represses translation in late development. *Molecular and cellular biology* 19(2), 1262–1270. DOI: 10.1128/MCB.19.2.1262.
- Nielsen, J.; Kristensen, M. A.; Willemoës, M.; Nielsen, F. C.; Christiansen, J. (2004). Sequential dimerization of human zipcode-binding protein IMP1 on RNA: a cooperative mechanism providing RNP stability. *Nucleic acids research* 32(14), 4368–4376. DOI: 10.1093/nar/gkh754.
- Nigro, J. M.; Cho, K. R.; Fearon, E. R.; Kern, S. E.; Ruppert, J.; Oliner, J. D.; Kinzler, K. W.; Vogelstein, B. (1991). Scrambled exons. *Cell* 64(3), 607–613. DOI: 10.1016/0092-8674(91)90244-S.
- Nishikawa, M.; Nojima, S.; Akiyama, T.; Sankawa, U.; Inoue, K. (1984). Interaction of digitonin and its analogs with membrane cholesterol. *Journal of biochemistry* 96(4), 1231–1239. DOI: 10.1093/oxfordjournals.jbchem.a134941.
- Noto, J. J.; Schmidt, C. A.; Matera, A. G. (2017). Engineering and expressing circular RNAs via tRNA splicing. *RNA biology* 14(8), 978–984. DOI: 10.1080/15476286.2017.1317911.
- Oleynikov, Y.; Singer, R. H. (2003). Real-time visualization of ZBP1 association with β -Actin mRNA during transcription and localization. *Current Biology* 13(3), 199–207. DOI: 10.1016/S0960-9822(03)00044-7.
- Olivier, C.; Poirier, G.; Gendron, P.; Boisgontier, A.; Major, F.; Chartrand, P. (2005). Identification of a conserved RNA motif essential for She2p recognition and mRNA localization to the yeast bud. *Molecular and cellular biology* 25(11), 4752–4766. DOI: 10.1128/MCB.25.11.4752-4766.2005.
- Palanichamy, J. K.; Tran, T. M.; Howard, J. M.; Contreras, J. R.; Fernando, T. R.; Sterne-Weiler, T.; Katzman, S.; Toloue, M.; Yan, W.; Basso, G.; Pigazzi, M.; Sanford, J. R.; Rao, D. S. (2016). RNA-binding protein IGF2BP3 targeting of oncogenic transcripts promotes hematopoietic progenitor proliferation. *The Journal of clinical investigation* 126(4), 1495–1511. DOI: 10.1172/JCI80046.
- Pamudurti, N. R.; Bartok, O.; Jens, M.; Ashwal-Fluss, R.; Stottmeister, C.; Ruhe, L.; Hanan, M.; Wyler, E.; Perez-Hernandez, D.; Ramberger, E.; Shenzis, S.; Samson, M.; Dittmar, G.; Landthaler, M.; Chekulaeva, M.; ... Kadener, S. (2017). Translation of circRNAs. *Molecular cell* 66(1), 9–21. DOI: 10.1016/j.molcel.2017.02.021.
- Panda, A. C.; De, S.; Grammatikakis, I.; Munk, R.; Yang, X.; Piao, Y.; Dudekula, D. B.; Abdelmohsen, K.; Gorospe, M. (2017). High-purity circular RNA isolation method (RPAD)

reveals vast collection of intronic circRNAs. *Nucleic acids research* 45(12), e116. DOI: 10.1093/nar/gkx297.

Patel, V. L.; Mitra, S.; Harris, R.; Buxbaum, A. R.; Lionnet, T.; Brenowitz, M.; Girvin, M.; Levy, M.; Almo, S. C.; Singer, R. H.; Chao, J. A. (2012). Spatial arrangement of an RNA zipcode identifies mRNAs under post-transcriptional control. *Genes & development* 26(1), 43–53. DOI: 10.1101/gad.177428.111.

Petkovic, S.; Müller, S. (2015). RNA circularization strategies in vivo and in vitro. *Nucleic acids research* 43(4), 2454–2465. DOI: 10.1093/nar/gkv045.

Pfafenrot, C.; Preußner, C. (2019). Establishing essential quality criteria for the validation of circular RNAs as biomarkers. *Biomolecular detection and quantification* 17, 100085. DOI: 10.1016/j.bdq.2019.100085.

Piwecka, M.; Glažar, P.; Hernandez-Miranda, L. R.; Memczak, S.; Wolf, S. A.; Rybak-Wolf, A.; Filipchyk, A.; Klironomos, F.; Cerda Jara, C. A.; Fenske, P.; Trimbuch, T.; Zywitzka, V.; Plass, M.; Schreyer, L.; Ayoub, S.; ... Rajewsky, N. (2017). Loss of a mammalian circular RNA locus causes miRNA deregulation and affects brain function. *Science* 357(6357). DOI: 10.1126/science.aam8526.

Rajaratnam, K.; Schnoor, M.; Richardson, R. M.; Rajagopal, S. (2019). How do chemokines navigate neutrophils to the target site: Dissecting the structural mechanisms and signaling pathways. *Cellular signalling* 54, 69–80. DOI: 10.1016/j.cellsig.2018.11.004.

Ravanidis, S.; Kattan, F.-G.; Doxakis, E. (2018). Unraveling the pathways to neuronal homeostasis and disease: Mechanistic insights into the role of RNA-binding proteins and associated factors. *International journal of molecular sciences* 19(8). DOI: 10.3390/ijms19082280.

Ray, D.; Kazan, H.; Cook, K. B.; Weirauch, M. T.; Najafabadi, H. S.; Li, X.; Gueroussov, S.; Albu, M.; Zheng, H.; Yang, A.; Na, H.; Irimia, M.; Matzat, L. H.; Dale, R. K.; Smith, S. A.; ... Hughes, T. R. (2013). A compendium of RNA-binding motifs for decoding gene regulation. *Nature* 499(7457), 172–177. DOI: 10.1038/nature12311.

Reid, D. W.; Nicchitta, C. V. (2015). Diversity and selectivity in mRNA translation on the endoplasmic reticulum. *Nature reviews. Molecular cell biology* 16(4), 221–231. DOI: 10.1038/nrm3958.

Richard, P.; Manley, J. L. (2009). Transcription termination by nuclear RNA polymerases. *Genes & development* 23(11), 1247–1269. DOI: 10.1101/gad.1792809.

Riley, K. J.; Steitz, J. A. (2013). The "Observer Effect" in genome-wide surveys of protein-RNA interactions. *Molecular cell* 49(4), 601–604. DOI: 10.1016/j.molcel.2013.01.030.

Ross, A. F.; Oleynikov, Y.; Kislauskis, E. H.; Taneja, K. L.; Singer, R. H. (1997). Characterization of a beta-actin mRNA zipcode-binding protein. *Molecular and cellular biology* 17(4), 2158–2165. DOI: 10.1128/MCB.17.4.2158.

Rosbach, O.; Hung, L.-H.; Khrameeva, E.; Schreiner, S.; König, J.; Curk, T.; Zupan, B.; Ule, J.; Gelfand, M. S.; Bindereif, A. (2014). Crosslinking-immunoprecipitation (iCLIP) analysis

- reveals global regulatory roles of hnRNP L. *RNA biology* 11(2), 146–155. DOI: 10.4161/rna.27991.
- Runge, S.; Nielsen, F. C.; Nielsen, J.; Lykke-Andersen, J.; Wewer, U. M.; Christiansen, J. (2000). H19 RNA binds four molecules of insulin-like growth factor II mRNA-binding protein. *The Journal of biological chemistry* 275(38), 29562–29569. DOI: 10.1074/jbc.M001156200.
- Rybak-Wolf, A.; Stottmeister, C.; Glažar, P.; Jens, M.; Pino, N.; Giusti, S.; Hanan, M.; Behm, M.; Bartok, O.; Ashwal-Fluss, R.; Herzog, M.; Schreyer, L.; Papavasileiou, P.; Ivanov, A.; Öhman, M.; ... Rajewsky, N. (2015). Circular RNAs in the mammalian brain are highly abundant, conserved, and dynamically expressed. *Molecular cell* 58(5), 870–885. DOI: 10.1016/j.molcel.2015.03.027.
- Salzman, J.; Chen, R. E.; Olsen, M. N.; Wang, P. L.; Brown, P. O. (2013). Cell-type specific features of circular RNA expression. *PLoS genetics* 9(9), e1003777. DOI: 10.1371/journal.pgen.1003777.
- Salzman, J.; Gawad, C.; Wang, P. L.; Lacayo, N.; Brown, P. O. (2012). Circular RNAs are the predominant transcript isoform from hundreds of human genes in diverse cell types. *PloS one* 7(2), e30733. DOI: 10.1371/journal.pone.0030733.
- Samanta, S.; Pursell, B.; Mercurio, A. M. (2013). IMP3 protein promotes chemoresistance in breast cancer cells by regulating breast cancer resistance protein (ABCG2) expression. *The Journal of biological chemistry* 288(18), 12569–12573. DOI: 10.1074/jbc.C112.442319.
- Samuels, T. J.; Järvelin, A. I.; Ish-Horowicz, D.; Davis, I. (2020). Imp/IGF2BP levels modulate individual neural stem cell growth and division through myc mRNA stability. *eLife* 9. DOI: 10.7554/eLife.51529.
- Sänger, H. L.; Klotz, G.; Riesner, D.; Gross, H. J.; Kleinschmidt, A. K. (1976). Viroids are single-stranded covalently closed circular RNA molecules existing as highly base-paired rod-like structures. *Proceedings of the National Academy of Sciences* 73(11), 3852–3856. DOI: 10.1073/pnas.73.11.3852.
- Schindelin, J.; Arganda-Carreras, I.; Frise, E.; Kaynig, V.; Longair, M.; Pietzsch, T.; Preibisch, S.; Rueden, C.; Saalfeld, S.; Schmid, B.; Tinevez, J.-Y.; White, D. J.; Hartenstein, V.; Eliceiri, K.; Tomancak, P.; ... Cardona, A. (2012). Fiji: an open-source platform for biological-image analysis. *Nature methods* 9(7), 676–682. DOI: 10.1038/nmeth.2019.
- Schmid, M.; Jaedicke, A.; Du, T.-G.; Jansen, R.-P. (2006). Coordination of endoplasmic reticulum and mRNA localization to the yeast bud. *Current Biology* 16(15), 1538–1543. DOI: 10.1016/j.cub.2006.06.025.
- Schneider, T.; Bindereif, A. (2017). Circular RNAs: Coding or noncoding? *Cell research* 27(6), 724–725. DOI: 10.1038/cr.2017.70.
- Schneider, T.; Hung, L.-H.; Aziz, M.; Wilmen, A.; Thaum, S.; Wagner, J.; Janowski, R.; Müller, S.; Schreiner, S.; Friedhoff, P.; Hüttelmaier, S.; Niessing, D.; Sattler, M.; Schlundt, A.; Bindereif, A. (2019). Combinatorial recognition of clustered RNA elements by the multidomain RNA-binding protein IMP3. *Nature communications* 10(1), 2266. DOI: 10.1038/s41467-019-09769-8.

Schneider, T.; Hung, L.-H.; Schreiner, S.; Starke, S.; Eckhof, H.; Rossbach, O.; Reich, S.; Medenbach, J.; Bindereif, A. (2016). CircRNA-protein complexes: IMP3 protein component defines subfamily of circRNPs. *Scientific reports* 6, 31313. DOI: 10.1038/srep31313.

Schreiner, S.; Didio, A.; Hung, L.-H.; Bindereif, A. (2020). Design and application of circular RNAs with protein-sponge function. *Nucleic acids research* 48(21), 12326–12335. DOI: 10.1093/nar/gkaa1085.

Sim, S.; Yao, J.; Weinberg, D. E.; Niessen, S.; Yates, J. R.; Wolin, S. L. (2012). The zipcode-binding protein ZBP1 influences the subcellular location of the Ro 60-kDa autoantigen and the noncoding Y3 RNA. *RNA* 18(1), 100–110. DOI: 10.1261/rna.029207.111.

Song, T.; Zheng, Y.; Wang, Y.; Katz, Z.; Liu, X.; Chen, S.; Singer, R. H.; Gu, W. (2015). Specific interaction of KIF11 with ZBP1 regulates the transport of β -actin mRNA and cell motility. *Journal of cell science* 128(5), 1001–1010. DOI: 10.1242/jcs.161679.

Sparanese, D.; Lee, C. H. (2007). CRD-BP shields c-myc and MDR-1 RNA from endonucleolytic attack by a mammalian endoribonuclease. *Nucleic acids research* 35(4), 1209–1221. DOI: 10.1093/nar/gkl1148.

Stagsted, L. V. W.; Nielsen, K. M.; Daugaard, I.; Hansen, T. B. (2019). Noncoding AUG circRNAs constitute an abundant and conserved subclass of circles. *Life science alliance* 2(3). DOI: 10.26508/lsa.201900398.

Starke, S.; Jost, I.; Rossbach, O.; Schneider, T.; Schreiner, S.; Hung, L.-H.; Bindereif, A. (2015). Exon circularization requires canonical splice signals. *Cell reports* 10(1), 103–111. DOI: 10.1016/j.celrep.2014.12.002.

Stepanenko, A. A.; Heng, H. H. (2017). Transient and stable vector transfection: Pitfalls, off-target effects, artifacts. *Mutation research. Reviews in mutation research* 773, 91–103. DOI: 10.1016/j.mrrev.2017.05.002.

Stöhr, N.; Köhn, M.; Lederer, M.; Glass, M.; Reinke, C.; Singer, R. H.; Hüttelmaier, S. (2012). IGF2BP1 promotes cell migration by regulating MK5 and PTEN signaling. *Genes & development* 26(2), 176–189. DOI: 10.1101/gad.177642.111.

Stöhr, N.; Lederer, M.; Reinke, C.; Meyer, S.; Hatzfeld, M.; Singer, R. H.; Hüttelmaier, S. (2006). ZBP1 regulates mRNA stability during cellular stress. *The Journal of cell biology* 175(4), 527–534. DOI: 10.1083/jcb.200608071.

Stoll, L.; Rodríguez-Trejo, A.; Guay, C.; Brozzi, F.; Bayazit, M. B.; Gattesco, S.; Menoud, V.; Sobel, J.; Marques, A. C.; Venø, M. T.; Esguerra, J. L. S.; Barghouth, M.; Suleiman, M.; Marselli, L.; Kjems, J.; ... Regazzi, R. (2020). A circular RNA generated from an intron of the insulin gene controls insulin secretion. *Nature communications* 11(1), 5611. DOI: 10.1038/s41467-020-19381-w.

Sun, L.; Fazal, F. M.; Li, P.; Broughton, J. P.; Lee, B.; Tang, L.; Huang, W.; Kool, E. T.; Chang, H. Y.; Zhang, Q. C. (2019). RNA structure maps across mammalian cellular compartments. *Nature structural & molecular biology* 26(4), 322–330. DOI: 10.1038/s41594-019-0200-7.

Suvasini, R.; Shruti, B.; Thota, B.; Shinde, S. V.; Friedmann-Morvinski, D.; Nawaz, Z.; Prasanna, K. V.; Thennarasu, K.; Hegde, A. S.; Arivazhagan, A.; Chandramouli, B. A.; Santosh, 120

- V.; Somasundaram, K. (2011). Insulin growth factor-2 binding protein 3 (IGF2BP3) is a glioblastoma-specific marker that activates phosphatidylinositol 3-kinase/mitogen-activated protein kinase (PI3K/MAPK) pathways by modulating IGF-2. *The Journal of biological chemistry* 286(29), 25882–25890. DOI: 10.1074/jbc.M110.178012.
- Szabo, L.; Salzman, J. (2016). Detecting circular RNAs: bioinformatic and experimental challenges. *Nature reviews. Genetics* 17(11), 679–692. DOI: 10.1038/nrg.2016.114.
- Taliaferro, J. M. (2019). Classical and emerging techniques to identify and quantify localized RNAs. *Wiley interdisciplinary reviews. RNA* 10(5), e1542. DOI: 10.1002/wrna.1542.
- Taniuchi, K.; Furihata, M.; Hanazaki, K.; Saito, M.; Saibara, T. (2014a). IGF2BP3-mediated translation in cell protrusions promotes cell invasiveness and metastasis of pancreatic cancer. *Oncotarget* 5(16), 6832–6845. DOI: 10.18632/oncotarget.2257.
- Taniuchi, K.; Furihata, M.; Saibara, T. (2014b). KIF20A-mediated RNA granule transport system promotes the invasiveness of pancreatic cancer cells. *Neoplasia* 16(12), 1082–1093. DOI: 10.1016/j.neo.2014.10.007.
- Ulshöfer, C. J.; Pfafenrot, C.; Bindereif, A.; Schneider, T. (2021). Methods to study circRNA-protein interactions. *Methods*. DOI: 10.1016/j.ymeth.2021.04.014.
- Valverde, R.; Edwards, L.; Regan, L. (2008). Structure and function of KH domains. *The FEBS journal* 275(11), 2712–2726. DOI: 10.1111/j.1742-4658.2008.06411.x.
- Vikesaa, J.; Hansen, T. V. O.; Jønson, L.; Borup, R.; Wewer, U. M.; Christiansen, J.; Nielsen, F. C. (2006). RNA-binding IMPs promote cell adhesion and invadopodia formation. *The EMBO journal* 25(7), 1456–1468. DOI: 10.1038/sj.emboj.7601039.
- Wächter, K.; Köhn, M.; Stöhr, N.; Hüttelmaier, S. (2013). Subcellular localization and RNP formation of IGF2BPs (IGF2 mRNA-binding proteins) is modulated by distinct RNA-binding domains. *Biological chemistry* 394(8), 1077–1090. DOI: 10.1515/hsz-2013-0111.
- Wada, T.; Becskei, A. (2017). Impact of methods on the measurement of mRNA turnover. *International journal of molecular sciences* 18(12). DOI: 10.3390/ijms18122723.
- Walter, P.; Blobel, G. (1981). Translocation of proteins across the endoplasmic reticulum. II. Signal recognition protein (SRP) mediates the selective binding to microsomal membranes of in-vitro-assembled polysomes synthesizing secretory protein. *The Journal of cell biology* 91(2 Pt 1), 551–556. DOI: 10.1083/jcb.91.2.551.
- Walter, P.; Ibrahimi, I.; Blobel, G. (1981). Translocation of proteins across the endoplasmic reticulum. I. Signal recognition protein (SRP) binds to in-vitro-assembled polysomes synthesizing secretory protein. *The Journal of cell biology* 91(2 Pt 1), 545–550. DOI: 10.1083/jcb.91.2.545.
- Wang, E. T.; Cody, N. A. L.; Jog, S.; Biancolella, M.; Wang, T. T.; Treacy, D. J.; Luo, S.; Schroth, G. P.; Housman, D. E.; Reddy, S.; Lécuyer, E.; Burge, C. B. (2012). Transcriptome-wide regulation of pre-mRNA splicing and mRNA localization by muscleblind proteins. *Cell* 150(4), 710–724. DOI: 10.1016/j.cell.2012.06.041.

- Wang, Y.; Wang, Z. (2015). Efficient backsplicing produces translatable circular mRNAs. *RNA* 21(2), 172–179. DOI: 10.1261/rna.048272.114.
- Wang, Z.; Ma, K.; Cheng, Y.; Abraham, J. M.; Liu, X.; Ke, X.; Wang, Z.; Meltzer, S. J. (2019). Synthetic circular multi-miR sponge simultaneously inhibits miR-21 and miR-93 in esophageal carcinoma. *Laboratory investigation* 99(10), 1442–1453. DOI: 10.1038/s41374-019-0273-2.
- Weidensdorfer, D.; Stöhr, N.; Baude, A.; Lederer, M.; Köhn, M.; Schierhorn, A.; Buchmeier, S.; Wahle, E.; Hüttelmaier, S. (2009). Control of c-myc mRNA stability by IGF2BP1-associated cytoplasmic RNPs. *RNA* 15(1), 104–115. DOI: 10.1261/rna.1175909.
- Weiner, A. J.; Choo, Q. L.; Wang, K. S.; Govindarajan, S.; Redeker, A. G.; Gerin, J. L.; Houghton, M. (1988). A single antigenomic open reading frame of the hepatitis delta virus encodes the epitope(s) of both hepatitis delta antigen polypeptides p24 delta and p27 delta. *Journal of virology* 62(2), 594–599. DOI: 10.1128/JVI.62.2.594-599.1988.
- Wesselhoeft, R. A.; Kowalski, P. S.; Anderson, D. G. (2018). Engineering circular RNA for potent and stable translation in eukaryotic cells. *Nature communications* 9(1), 2629. DOI: 10.1038/s41467-018-05096-6.
- Wesselhoeft, R. A.; Kowalski, P. S.; Parker-Hale, F. C.; Huang, Y.; Bisaria, N.; Anderson, D. G. (2019). RNA circularization diminishes immunogenicity and can extend translation duration in vivo. *Molecular cell* 74(3), 508–520.e4. DOI: 10.1016/j.molcel.2019.02.015.
- Westholm, J. O.; Miura, P.; Olson, S.; Shenker, S.; Joseph, B.; Sanfilippo, P.; Celniker, S. E.; Graveley, B. R.; Lai, E. C. (2014). Genome-wide analysis of Drosophila circular RNAs reveals their structural and sequence properties and age-dependent neural accumulation. *Cell reports* 9(5), 1966–1980. DOI: 10.1016/j.celrep.2014.10.062.
- Wheeler, E. C.; van Nostrand, E. L.; Yeo, G. W. (2018). Advances and challenges in the detection of transcriptome-wide protein-RNA interactions. *Wiley interdisciplinary reviews. RNA* 9(1), e1436. DOI: 10.1002/wrna.1436.
- Wilusz, J. E. (2018). A 360° view of circular RNAs: From biogenesis to functions. *Wiley interdisciplinary reviews. RNA* 9(4), e1478. DOI: 10.1002/wrna.1478.
- Wolfe, M. B.; Goldstrohm, A. C.; Freddolino, P. L. (2019). Global analysis of RNA metabolism using bio-orthogonal labeling coupled with next-generation RNA sequencing. *Methods* 155, 88–103. DOI: 10.1016/j.ymeth.2018.12.001.
- Yang, Y.; Fan, X.; Mao, M.; Song, X.; Wu, P.; Zhang, Y.; Jin, Y.; Yang, Y.; Chen, L.-L.; Wang, Y.; Wong, C. C.; Xiao, X.; Wang, Z. (2017). Extensive translation of circular RNAs driven by N6-methyladenosine. *Cell research* 27(5), 626–641. DOI: 10.1038/cr.2017.31.
- Yaniv, K.; Yisraeli, J. K. (2002). The involvement of a conserved family of RNA binding proteins in embryonic development and carcinogenesis. *Gene* 287(1-2), 49–54. DOI: 10.1016/S0378-1119(01)00866-6.
- Yoshitake, Y.; Fukuma, D.; Yuno, A.; Hirayama, M.; Nakayama, H.; Tanaka, T.; Nagata, M.; Takamune, Y.; Kawahara, K.; Nakagawa, Y.; Yoshida, R.; Hirose, A.; Ogi, H.; Hiraki, A.; Jono, H.; ... Shinohara, M. (2015). Phase II clinical trial of multiple peptide vaccination for

advanced head and neck cancer patients revealed induction of immune responses and improved OS. *Clinical cancer research* 21(2), 312–321. DOI: 10.1158/1078-0432.CCR-14-0202.

You, X.; Vlatkovic, I.; Babic, A.; Will, T.; Epstein, I.; Tushev, G.; Akbalik, G.; Wang, M.; Glock, C.; Quedenau, C.; Wang, X.; Hou, J.; Liu, H.; Sun, W.; Sambandan, S.; ... Chen, W. (2015). Neural circular RNAs are derived from synaptic genes and regulated by development and plasticity. *Nature neuroscience* 18(4), 603–610. DOI: 10.1038/nn.3975.

Zeng, W.-J.; Lu, C.; Shi, Y.; Wu, C.; Chen, X.; Li, C.; Yao, J. (2020). Initiation of stress granule assembly by rapid clustering of IGF2BP proteins upon osmotic shock. *Biochimica et biophysica acta. Molecular cell research* 1867(10), 118795. DOI: 10.1016/j.bbamcr.2020.118795.

Zhang, J. Y.; Chan, E. K.; Peng, X. X.; Tan, E. M. (1999). A novel cytoplasmic protein with RNA-binding motifs is an autoantigen in human hepatocellular carcinoma. *The Journal of experimental medicine* 189(7), 1101–1110. DOI: 10.1084/jem.189.7.1101.

Zhang, S.; Mo, Q.; Wang, X. (2019). Oncological role of HMGA2 (Review). *International journal of oncology* 55(4), 775–788. DOI: 10.3892/ijo.2019.4856.

Zhang, X.-O.; Wang, H.-B.; Zhang, Y.; Lu, X.; Chen, L.-L.; Yang, L. (2014). Complementary sequence-mediated exon circularization. *Cell* 159(1), 134–147. DOI: 10.1016/j.cell.2014.09.001.

Zhang, Y.; Xue, W.; Li, X.; Zhang, J.; Chen, S.; Zhang, J.-L.; Yang, L.; Chen, L.-L. (2016). The biogenesis of nascent circular RNAs. *Cell reports* 15(3), 611–624. DOI: 10.1016/j.celrep.2016.03.058.

Zhang, Y.; Zhang, X.-O.; Chen, T.; Xiang, J.-F.; Yin, Q.-F.; Xing, Y.-H.; Zhu, S.; Yang, L.; Chen, L.-L. (2013). Circular intronic long noncoding RNAs. *Molecular cell* 51(6), 792–806. DOI: 10.1016/j.molcel.2013.08.017.

Zhao, W.; Lu, D.; Liu, L.; Cai, J.; Zhou, Y.; Yang, Y.; Zhang, Y.; Zhang, J. (2017). Insulin-like growth factor 2 mRNA binding protein 3 (IGF2BP3) promotes lung tumorigenesis via attenuating p53 stability. *Oncotarget* 8(55), 93672–93687. DOI: 10.18632/oncotarget.21280.

7 Abbreviations

×g	times gravity
°C	degree Celsius
μ	micro
A	adenine
A	Ampere
aa	amino acid(s)
ACTB	β-actin mRNA
ADAR	double-stranded RNA-specific adenosine deaminase
Ago2	argonaute 2
amp	ampicillin
ANKRD17	ankyrin repeat domain-containing protein 17
APS	ammonium persulfate
as	antisense
ATG16L1	autophagy-related gene 16 like 1
BGH	bovine growth hormone
BSA	bovine serum albumin
BSJ	backsplicing junction
C	cytosine
CAMSAP1	calmodulin-regulated spectrin-associated protein 1
Cas9	CRISPR-associated protein 9
CD44	cluster of differentiation 44
CDR1as	cerebellar degeneration-related protein 1 antisense
CDS	coding sequence
ciRS-7	circular RNA sponge for miR-7
CLIP	crosslinking and immunoprecipitation
CMV	cytomegalovirus
CRD	coding region stability determinant
CRD-BP	CRD-binding protein
CRISPR	clustered regularly interspaced short palindromic repeats
ctr	control
CXCL5	C-X-C motif chemokine 5
cyt	cytosol
DHX9	ATP-dependent RNA helicase A
dIMP	<i>Drosophila</i> IMP
DMEM	Dulbecco's modified eagle's medium
DMPC	dimethyl pyrocarbonate
DMSO	dimethylsulfoxide
DNA	deoxyribonucleic acid
DNase	deoxyribonuclease
dNTPs	deoxynucleotide triphosphates
dsRNA	double-stranded ribonucleic acid
DTT	dithiothreitol

<i>E. coli</i>	<i>Escherichia coli</i>
EDTA	ethylenediaminetetraacetic acid
ElciRNA	exon-intron circRNA
ELTD1	epidermal growth factor, latrophilin, and 7 transmembrane domain-containing protein 1
EMSA	electrophoretic mobility shift assay
ER	endoplasmic reticulum
<i>et al.</i>	<i>et alii</i>
FBS	fetal bovine serum
FKBP10	FK506 binding protein 10
Flp	flippase
FRT	Flp recombination target
FTL	ferritin light chain
FUS	fused in sarcoma
fwd	forward
G	guanine
g	gram
GANAB	glucosidase II alpha subunit
GAPDH	glyceraldehyde-3-phosphate dehydrogenase
GOI	gene of interest
GST	glutathione S transferase
h	hour(s)
HDV	hepatitis delta virus
HMG2	high-mobility-group AT-hook protein 2
hnRNP	heterogeneous nuclear ribonucleoprotein
HuR	hu antigen R
iCLIP	individual-nucleotide resolution CLIP
IGF2	insulin-like growth factor 2
IgG	immunoglobulin G
IMP	insulin-like growth factor 2 mRNA binding protein
IP	immunoprecipitation
IPTG	isopropyl- β -D-thiogalactopyranosid
IRES	internal ribosome entry site
k.d.	knockdown
k.o.	knockout
kb	kilobases
KCl	potassium chloride
K _d	dissociation constant
KH	hnRNP K homology
KOC	KH domain containing protein overexpressed in cancer
l	litre
LAMA4	laminin subunit alpha-4
LB	lysogen broth
let-7	lethal-7

LIN28B	abnormal cell lineage 28 B
M	molar
m	milli
m ⁶ A	N ⁶ -methyladenosine
MBL	muscleblind
MCOLN2	mucolipin-2
MCS	multiple cloning site
MFSD1	major facilitator superfamily domain containing 1
MgCl ₂	magnesium chloride
min	minute(s)
miRNA	microRNA
MMP1	matrix metalloproteinase-1
MO	membrane organelle
mRNA	messenger RNA
mRNP	messenger ribonucleoprotein complex
mTOR	mammalian target of rapamycin
N	nuclear
n	nano
NaCl	sodium chloride
NaOH	sodium hydroxide
NFATC3	nuclear factor of activated T cells 3
NF- κ B	nuclear factor kappa B
nt	nucleotide(s)
PABPN1	nuclear poly(A)-binding protein 1
PAGE	polyacrylamide gel electrophoresis
PBS	phosphate-buffered saline
PCR	polymerase chain reaction
PIE	permuted-exon intron
PKR	protein kinase R
PNK	polynucleotide kinase
pol	polymerase
qPCR	quantitative PCR
RBD	RNA-binding domain
RBM	RNA-binding motif
RBP	RNA-binding protein
rev	reverse
RIG-I	retinoic acid-inducible gene I
RIP	RNA immunoprecipitation
RNA	ribonucleic acid
RNase	ribonuclease
RNA-seq	(next generation) RNA-sequencing
RNP	ribonucleoprotein complex
rpm	rounds per minute
RRM	RNA-recognition motif

rRNA	ribosomal RNA
RT	reverse transcription
RtcB	RNA 2',3'-cyclic phosphate and 5'-OH ligase
s	sense
SDS	sodium dodecyl sulfate
sec	seconds
SELEX	systematic evolution of ligands by exponential enrichment
SERPINB7	serine protease inhibitor B7
SIA	scaffold independent analysis
siRNA	small interfering RNA
snoRD U78	small nucleolar RNA U78
SOC	super optimal broth
SR	serine/arginine-rich
SRGN	serglycin
Sry	sex-determining region Y
ssRNA	single-stranded ribonucleic acid
T	thymine
TEMED	tetramethylethylenediamine
TNC	tenascin C
Tornado	twister-optimised RNA for durable overexpression
Tris	tris(hydroxymethyl)aminomethane
tRNA	transfer RNA
U	uracil
U	unit(s)
U6	small nuclear RNA U6
UTR	untranslated region
UV	ultra violet
V	Volt
v/v	volume per volume
Vera	VgLE binding and ER association
Vg1	vegetal 1
Vg1RBP	Vg1 RNA-binding protein
VgLE	Vg1 RNA localisation element
w/v	weight per volume
wt	wildtype
ZBP1	zipcode-binding protein 1
ZKSCAN1	zinc finger protein with KRAB and SCAN domains 1

8 Eidesstattliche Erklärung

Ich erkläre: Ich habe die vorgelegte Dissertation selbstständig und ohne unerlaubte fremde Hilfe und nur mit den Hilfen angefertigt, die ich in der Dissertation angegeben habe. Alle Textstellen, die wörtlich oder sinngemäß aus veröffentlichten Schriften entnommen sind, und alle Angaben, die auf mündlichen Auskünften beruhen, sind als solche kenntlich gemacht. Ich stimme einer evtl. Überprüfung meiner Dissertation durch eine Antiplagiat-Software zu. Bei den von mir durchgeführten und in der Dissertation erwähnten Untersuchungen habe ich die Grundsätze guter wissenschaftlicher Praxis, wie sie in der „Satzung der Justus-Liebig-Universität Gießen zur Sicherung guter wissenschaftlicher Praxis“ niedergelegt sind, eingehalten.

Friedberg, 30.11.2021

Corinna Jessica Ulshöfer